

Formability analysis of AA5052 alloy for Single-Point Incremental Hole Flanging process

A Thesis Submitted to
Nirma University
In Partial Fulfilment of the Requirements
For The Degree of

Doctor of Philosophy

in

Technology & Engineering

by

Mr. Rudreshkumar Makwana (17PTPHDE172)

Guided by

Dr. Kaushik M. Patel



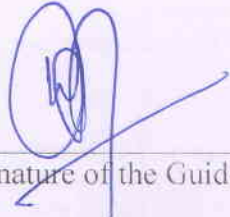
Mechanical Engineering Department
Institute of Technology, Nirma University
Ahmedabad-382481, Gujarat, India
August, 2023

**Nirma University
Institute of Technology**

Certificate

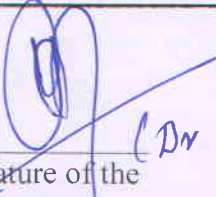
This is to certify that the thesis entitled **Formability analysis of AA5052 alloy for Single-point Incremental Hole Flanging process** has been prepared by **Makwana Rudreshkumar Dineshbhai** under my supervision and guidance. The thesis is his / her own original work completed after careful research and investigation. The work of the thesis is of the standard expected of a candidate for Ph.D. Programme in **Mechanical Engineering** and I recommend that it be sent for evaluation.

Date: 5/8/2023



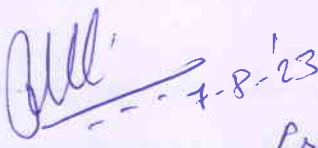
Signature of the Guide

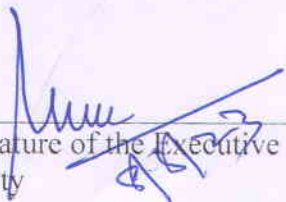
Forwarded Through:

(i) 

(Dr. K.M. Patel)
(i) Name and Signature of the
Head of the Department

(ii) P.v. Patel (P.v. Patel)
Name and Signature of the Dean - Faculty of Technology

(iii) Prof. Dr. P.N. Tekwami

Name and Signature of the Dean - Faculty of Doctoral Studies and Research

(iv) 

Name and Signature of the Executive Registrar
Nirma University

**Nirma University
Institute of Technology**

Declaration

I, **Makwana Rudreshkumar Dineshbhai**, registered as Research Scholar, bearing Registration No. **17TPHDE172** for Doctoral Programme under the Faculty of **Technology** of Nirma University do hereby declare that I have completed the course work, pre-synopsis seminar and my research work as prescribed under R. Ph.D. 3.5.

I do hereby declare that the thesis submitted is original and is the outcome of the independent investigations / research carried out by me and contains no plagiarism. The research is leading to the discovery of new facts / techniques / correlation of scientific facts already known. (Please tick whichever is applicable). This work has not been submitted to any other University or Body in quest of a degree, diploma or any other kind of academic award.

I do hereby further declare that the text, diagrams or any other material taken from other sources (including but not limited to books, journals and web) have been acknowledged, referred and cited to the best of my knowledge and understanding.

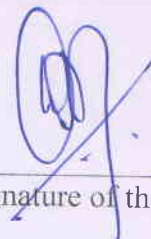
Date: **5/8/2023**



Signature of the student

I agree with the above declaration made by the student.

Date: **5/8/2023**



Signature of the guide

Enclosure - V

Specimen 'D'
Nirma University
Institute of Technology
Certificate

This is to certify that the thesis entitled **Formability Analysis of AA5052 Alloy for Single-point Incremental Hole Flanging Process** has been prepared by me, under the supervision and guidance of **Dr. K. M. Patel**. The thesis is my own original work completed after careful research and investigation. The work of the thesis is of the standard expected of a candidate for Ph.D. Programme. The final hard bound copy of the thesis is submitted after incorporating all the suggestions / corrections suggested by the referees.

Date: 20/01/2024



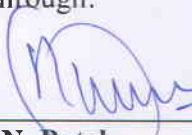
Rudreshkumar Makwana

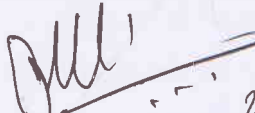
Date: 20/01/2024



Dr. K. M. Patel (Guide)

Forwarded Through:

(i)  24.01.2024
Dr. R. N. Patel
Dean - Faculty of Technology & Engineering

(ii)  25-1-24
Prof. (Dr.) P. N. Tekwani
Dean - Faculty of Doctoral Studies and Research

(iii)  20/1/24
Shri G. Ramachandran Nair
Executive Registrar, Nirma University

Acknowledgments

I express my earnest gratitude and sincere thanks to my research supervisor, Dr. K.M.Patel, Professor, Mechanical Engineering Department, Institute of Technology, Nirma University for his constant encouragement, inspiration and guidance without which the work could not have completed. I wish to acknowledge him for his moral support, careful reviews, technical comments, constructive criticism through all my research work and dissertation, and his highly appreciated instructions to continue my research and accomplish my goal.

I am thankful to Dr. B.A.Modi, Professor, Mechanical Engineering Department, for his continuous guidance, suggestions, directions and in depth reviews throughout the research work and dissertation, without which the research work could not have completed.

I would also like to thank members of my research progress committee, Dr. D.Ravikumar, Professor, Mechanical Engineering Department, IIT Delhi and Dr. H.K.Raval, Professor, Mechanical Engineering Department, Sardar Vallabhbhai National Institute of Technology, Surat for their valuable suggestions and insightful comments given during my progress seminars. I am also thankful to them for all the necessary help, constant encouragement and moral support throughout the research work.

I am grateful to the Management of Nirma University for giving permission to pursue Ph.D. and providing all necessary infrastructural facility and support. I am also thankful to Dr.R.N.Patel, Director, Institute of Technology, Nirma University for his constant encouragement and motivation throughout this work.

Many thanks are also extended to all my colleagues and all my friends at Mechanical Engineering Department, Institute of Technology, Nirma University for the thoughtful discussions I had with them and support received from them.

I express my thanks to all laboratory staff and technicians of Mechanical Engineering Department, especially, Mr. Dharmendra Naik, Mr. Jayesh D. Panchal and Mr. Abhijat Joshi for the warm-hearted help in my experimental work.

I acknowledge the financial support provided by Nirma University, in form of Minor Research Project grants sanctioned through letters NU/PhD/MRP/IT-ME/17-18/1093, NU/Ph.D/MRP/IT/2019-20, and NU/Ph.D/MRP/IT/2020-21.

I would like to thank the Almighty for giving me the opportunity to do the research work with good health and prosperity. Last, but not least, I place my deep sense of gratitude and thanks to my family and parents for their unconditional support and loving encouragement throughout my life.

Date:

Makwana Rudreshkumar D.

List of Figures

Figure 1.1 A hull of an aluminum boat under construction.....	2
Figure 1.2 A rectangular flange on the assembly cabin rear wall of an automobile	2
Figure 1.3 Schematic of SPIF.....	3
Figure 1.4 Schematic of single-stage SPIHF.....	4
Figure 2.1 Conventional flange forming	10
Figure 2.2 Schematic of setup for incremental sheet metal forming.....	12
Figure 2.3 (a) single point incremental forming (b) two-point incremental forming (c) incremental forming with partial die (d) incremental forming with full die	13
Figure 2.4 Parts formed by SPIF	14
Figure 2.5 Modeling and Manufacturing of Cranial plate using ISF	15
Figure 2.6 Procedure of single-point incremental forming	16
Figure 2.7 Setup of single-point incremental hole flanging	17
Figure 2.8 FFL and FLC on major strain-minor strain space	19
Figure 2.9 strain distribution on the wall of cylindrical flange formed by SPIF (a) Different precut hole diameters with tool radius 10 mm, (b) Minimum precut hole diameter that could be successfully formed into a flange, (c) failed flanges closest to success	22
Figure 2.10 (a) Different multi-step strategies, (b) Thickness distribution in DD and DU strategy.....	24
Figure 2.11 Different multistage strategies of SPIHF	25
Figure 2.12 (a) Novel tooling for SPIF, (b) New Featured Tool.....	27
Figure 2.13 Force trends during SPIF.....	32
Figure 2.14 Resultant force during the forming of truncated conical shape with different draw angles	32
Figure 2.15 Three-axis forces during forming of a truncated pyramid	33

Figure 2.16 Vertical and Horizontal forces acting during the single-stage cylindrical hole flanging using a non-rotating and rotating tool	34
Figure 2.17 Different regions to analyze strain distribution on the square flange	35
Figure 2.18 A complex shape flange and different regions on it.....	36
Figure 2.19 (a) Backward flange on a part, (b) Backward SPIHF	37
Figure 2.20 Multistage strategies for forming a straight cylindrical flange	38
Figure 2.21 Two-stage method of SPIHF	39
Figure 2.22 Geometric defects in SPIHF.....	42
Figure 3.1 Experimental Setup	47
Figure 3.2 SPIF tools	48
Figure 3.3 Experimental procedure to find the LFR	48
Figure 3.4 Single-stage and Multistage strategies used in this work.....	50
Figure 3.5 Circle grid engraved on the aluminum sheet.....	50
Figure 3.6 (a) Pointed anvil micrometer and (b) the marked locations on the flange	51
Figure 3.7 Height measurement by vernier height gauge.....	51
Figure 3.8 Flanges formed by SPIF tools with the diameter (a) 12 mm, (b) 10 mm, (c) 8 mm	53
Figure 3.9 Thickness distribution on the successfully formed flanges.....	54
Figure 3.10 Theoretical and Experimentally established FFL.....	55
Figure 3.11 (a) Flange formed in single-stage with a precut hole diameter 32 mm and failed flange with precut hole diameter 31 mm (b) crack on the failed flange.....	57
Figure 3.12 Strain plot for single and multi-stage flanges and theoretical Fracture Forming Limit line	58
Figure 3.13 Thickness distribution on flanges formed with the single-stage approach	58
Figure 3.14 Flanges formed with the multistage strategy with precut hole diameters 29mm, 28mm, and 27mm	59

Figure 3.15 Thickness distribution on flanges formed with the multistage strategy.....	60
Figure 3.16 Thickness distribution of the flange formed by single-stage and multistage....	61
Figure 3.17 Schematic showing tool-sheet contact zones	61
Figure 4.1 Procedure to study the effect of spindle speed on LFR.....	65
Figure 4.2 Flanges formed with different feed rate	67
Figure 4.3 (a)Thickness distribution, and (b) average thickness on formed flanges with the different feed rates	68
Figure 4.4 Flanges formed with different step depth.....	69
Figure 4.5 (a) Thickness distribution and (b) average thickness of formed flanges with different step depth	70
Figure 4.6 Damaged surface of AA5052-H32 sheet due to high values of process parameters	73
Figure 4.7 Flanges formed as per the L9 orthogonal array.....	75
Figure 4.8 Main effect plots- Thickness of flange.....	77
Figure 4.9 Main effect plots- Height of flange	77
Figure 4.10 Main effect plots- Surface roughness.....	78
Figure 4.11 Interaction plots- Thickness of flange.....	80
Figure 4.12 Interaction Plot for Heigh of the flange	80
Figure 4.13 Interaction plot for surface roughness	81
Figure 5.1 Tool path followed to form square flange in single-stage by SPIHF.....	84
Figure 5.2 Experimental setup for SPIHF of square flange.....	84
Figure 5.3 Terminology used to define LFR in forming of square flange	85
Figure 5.4 Critical zone on the square flange formed by SPIHF process	86
Figure 5.5 Failed and successfully formed flange by single-stage SPIHF	88
Figure 5.6 Strain distribution and critical zones of the flanges (PSL 44mm and PSL 45mm)	88

Figure 5.7 Flanges formed with a rotating SPIF tool	89
Figure 5.8 Strain distribution and critical zones of the flanges formed using rotating tool .	90
Figure 5.9 Square flanges formed from pre-cut square hole with PSL 44 mm and corner radius of 6,8 and 10 mm	91
Figure 5.10 Flanges formed from pre-cut square holes with different corner radius and strain distribution on them.....	92
Figure 6.1 Experimental setup of square SPIHF and VSPIHF tool	95
Figure 6.2 (a) Tool path for square flange forming (b) effective tool path in VSPIHF	96
Figure 6.3 (a) EBSD sample location, (b) Measurement area on the sample.....	97
Figure 6.4 Microstructures from EBSD tests for (a) non-deformed sheet (b) flange formed without tool rotation (c) flange formed with tool rotation (d) flange formed by VSPIHF...	99
Figure 6.5 (a) Thickness distribution on the flanges, (b) height of the flanges.....	101
Figure 6.6 Metal dust visible on the sheet and the tool head.....	102
Figure 6.7 Strain distribution on the flanges	102
Figure 6.8 (a) Stretch marks in the critical zone of the flanges, (b) edge bending.....	103
Figure 6.9 Surface texture of the flanges.....	104

List of Tables

Table 3.1 Chemical composition of AA1050 material used in the study	45
Table 3.2 Mechanical Properties of AA1050 material used in the study	46
Table 3.3 Chemical composition of AA5052-H32 material used in the study.....	46
Table 3.4 Mechanical properties of AA5052-H32 material used in the study	46
Table 3.5 LFR obtained by the three tools	52
Table 3.6 Height of the flanges formed with a precut hole diameter of 37 mm.....	54
Table 3.7 Details of experiments performed to establish FFL	56
Table 3.8 Results of experiments to find LFR.....	57
Table 3.9 Time required for flange forming	62
Table 4.1 Experimental details to study the effect of spindle speed	65
Table 4.2 Effect of spindle speed on LFR	66
Table 4.3 Experimental details to study the effect of feed rate	67
Table 4.4 Experimental details to study the effect of step depth.....	69
Table 4.5 Process parameters and their values	74
Table 4.6 Set of experiments as per L9 orthogonal array	74
Table 4.7 Summary of the responses of the flanges formed	76
Table 4.8 Best values and most effective parameters	79
Table 5.1 Results of experiments performed to find LFR	87
Table 6.1 Thickness along the flange	101
Table 6.2 Microhardness of the flange.....	104

Nomenclatures

ε_1 = Major Strain

ε_2 = Minor Strain

D = Damage function

σ_m = Hydrostatic stress

$\bar{\sigma}$ = Equivalent stress

r_{tool} = Radius of tool

t_f = Final thickness of sheet (after forming)

t_0 = Original thickness of sheet

α = half cone angle

D_f = Final flange diameter (inner surface)

D_i = Initial pre-cut hole diameter

\bar{y} = Mean Response

Abbreviations

ISF = Incremental Sheet metal Forming

SPIF = Single Point Incremental Forming

SPIHF = Single Point Incremental Hole Flanging

LFR = Limit Forming Ratio

FLC = Forming Limit Curve

FLD = Forming Limit Diagram

FFL = Fracture Forming Limit line

PCD = Pre-Cut hole Diameter

PSL = Pre-cut Square hole Length

Contents

Certificate	i
Abstract.....	ii
Declaration.....	iv
Acknowledgements.....	v
Contents	vii
List of Figures.....	xi
List of Tables	xv
Nomenclatures & Abbreviations	xvi
Chapter 1 Introduction	1
1.1 Sheet metal forming and applications of aluminium.....	1
1.2 Incremental Sheet-metal Forming and Hole Flanging.....	3
1.3 Motivation.....	5
1.4 Objectives of the present work	6
1.4.1 Development of setup and preliminary experiments	6
1.4.2 To investigate the Limit Forming Ratio, the thickness of the flange, the height of the flange, and strain distribution on the cylindrical flange in single-stage and multi-stage SPIHF	6
1.4.3 To study the effect of process parameters (spindle speed, feed rate, step depth) on the flange quality in single-stage SPIHF of the cylindrical flange.....	6
1.4.4 To obtain the experimental Fracture Forming Limit line for SPIHF.....	7
1.4.5 To investigate the formability of aluminum alloy in single-stage SPIHF of square flange	7
1.4.6 To improve the hardness of aluminum alloy by achieving grain refinement with a novel tool in single-stage SPIHF of the square flange	8

1.5 Organization of the Thesis	8
Chapter 2 Literature Review	10
2.1 Introduction to hole flanging process	10
2.2 Incremental sheet metal forming process, its applications, and hole flanging	11
2.2.1 Applications of incremental sheet metal forming.....	13
2.2.2 Implementation of SPIF for flange forming	15
2.3 Failure limits, strain distribution, and thickness distribution in SPIF and SPIHF.....	17
2.4 Tool shape and size in SPIF and SPIHF	26
2.5 Indicator of formability in hole flanging	28
2.6 Conventional hole flanging and SPIHF.....	30
2.7 Forces acting on the sheet metal during SPIF and SPIHF.....	31
2.8 Precut hole geometry and flange shape	34
2.9 Tool paths and strategies of SPIHF	36
2.10 Process parameters and their effects.....	39
2.10.1 Spindle speed.....	39
2.10.2 Feed rate.....	40
2.10.3 Step depth	40
2.11 Geometric Accuracy	41
2.12 Summary of literature review and objectives of the present work	42
Chapter 3 Development of setup and preliminary experiments	45
3.1 Material and Methods	45
3.1.1 Materials	45
3.1.2 Experimental setup	46
3.1.3 Limit Forming Ratio	47
3.1.4 Single-stage and multistage strategy of SPIHF	49

3.1.5 Strain measurement by circle grid method	49
3.1.6 Measurement of the thickness of the flange, the height of the flange, and the surface roughness on the inner surface of the flange.....	49
3.2 Results and discussion	52
3.2.1 Experiments to find LFR	52
3.2.2 Effect of single-stage and multistage strategies on the flange quality in SPIHF of the cylindrical flange	54
3.3 Summary.....	62
Chapter 4 Effect of process parameters on formability in single-stage SPIHF of the cylindrical flange.....	64
4.1 Experimental procedure.....	64
4.2 Preliminary experiments and their results	64
4.2.1 Effect of spindle speed.....	64
4.2.2 Effect of feed rate	66
4.2.3 Effect of step depth.....	69
4.3 Study of the effect of process parameters in single-stage SPIHF of cylindrical flange formed using AA5052-H32 sheet metal	71
4.3.1 Design of Experiments by Taguchi Method	71
4.3.2 Results and Discussion	75
4.4 Summary.....	81
Chapter 5 Formability in single-stage SPIHF of square flange	83
5.1 Materials and Methods	83
5.1.1 Experimental procedure to form square flange using single-stage SPIHF.....	83
5.1.2 Limit Forming Ratio in single-stage SPIHF of square flange	85
5.2 Results and Discussion	86
5.2.1 Failure of square flange and the critical zone.....	86

5.2.2 Formability with a non-rotating tool.....	87
5.2.3 Formability with a rotating tool.....	89
5.2.4 Effect of corner radius on Limit Forming Ratio.....	90
5.3 Summary.....	93
Chapter 6 Improvement in microhardness of AA5052-H32 material using an eccentric tool in single-stage SPIHF	95
6.1 Experimental Procedure.....	95
6.2 Results and Discussion	98
6.2.1 Microstructure.....	98
6.2.2 Thickness and height of flange.....	100
6.2.3 Surface roughness and microhardness.....	104
6.3 Summary.....	105
Chapter 7 Conclusions and Scope for the Future Work.....	106
7.1 Summary.....	106
7.2 Major Contributions of this Work	107
7.3 Scope for the future work	110
References.....	111
Publications from this research.....	121

Abstract

Single Point Incremental Forming technique is advantageous in terms of complex contour forming, high formability, and low-cost setup, especially in prototype manufacturing and job production of sheet metal parts. The technique has been implemented to perform the hole-flanging operation by researchers. The hole-flanging using Single Point Incremental Forming incorporates the advantages of the technique in the flange forming. The formability in the flange forming is analysed by measurement of the thickness of the flange, the height of the flange, and by finding the limit forming ratio. Moreover, the deformation mechanism is evaluated by analysing the strain distribution on the strain space diagram. Similar to the forming of conical and pyramidal shapes, the necking is suppressed in the Single Point Incremental Hole Flanging (SPIHF) too. However, due to the presence of the hole in the sheet metal, the strain distribution is different. The strain distribution also depends on the single-stage and multistage strategies used for the flange forming. The majority of the studies are on the multistage flange forming of conical or cylindrical flanges on the sheet of aluminum alloys, but the forming of flanges of other shapes may have different deformation mechanisms. A comparative study of the single-stage and multistage strategies has been studied and analysis has been presented in this thesis. Moreover, the square flange forming using the single-stage SPIHF has been analysed. Further, a novel tool is proposed to achieve grain refinement on the aluminium alloy during the SPIHF process and the experimental study has been carried out to analyse the effect of the use of proposed tool on the grain structure.

A fixture and tools have been developed to perform SPIHF using Vertical Machining Center. The detailed analysis of the formability of the AA5052 alloy in the hole-flanging using the Single Point Incremental Forming technique has been carried out being a potential material for marine and other industrial applications. In the preliminary experiments, the effect of the tool diameter on the Limit Forming Ratio (LFR) in SPIHF of AA1050 alloy has been studied. The large tool diameter (12 mm) resulted in better formability with higher LFR (1.81) as compared to small tool diameter (8 mm) which gave the lower LFR (1.56). Moreover, the experimental study has been carried out on the formability of AA5052 alloy in single-stage and multi-stage SPIHF. The LFR of 1.81 and 2.0 were obtained in the single-stage and the multi-stage strategies respectively, which shows that higher formability could be achieved in

the later. However, the stretching of the flange reduced when the larger tool was used. Further, the effect of process parameters (spindle speed, feed rate and step depth) on the flange quality was evaluated based on the Taguchi method. The results suggest that the step depth is the most effective parameter whereas the spindle speed and feed rate have a high interactive effect.

To establish the use of the Single-Point Incremental Forming method in forming flange shapes other than the cylindrical, the square shape flange forming has been carried out. In the available literature, it was performed using the multistage method. In this work, the single-stage method has been implemented for the same. The deformation modes on the flange have been analysed. The Limit Forming Ratio for the same has been defined and it has been obtained for the AA5052-H32 material using an experimental study. The non-rotating tool resulted in the Limit Forming Ratio of 1.26 which reduced to 1.20 when a rotating tool was used. Moreover, the effect of the corner radius of the pre-cut square hole on the formability has been evaluated by forming the flanges with three different pre-cut hole corner radius of 6 mm, 8 mm, and 10 mm. The higher corner radius increased the Limit Forming Ratio to 1.35. Further, to improve the hardness of the AA5052-H32 material, a novel tool has been proposed. The novel tool has its axis eccentric to the spindle axis and hence generated an alternate contact pattern during the forming process. The grain structure of the as-received material and the formed flanges has been analysed by Electron Back Scattered Diffraction (EBSD) measurement. The results showed that the rotating tool refined the grain structure of the material, moreover, the proposed eccentric tool increased the grain refinement. The strain hardening has been observed on the flange formed by the novel tool and the microhardness increased.

In summary, this work has provided a better understanding of the single-stage and multistage Single Point Incremental Hole Flanging of cylindrical shapes. Also, the implementation of the single-stage strategy to form a square flange has been evaluated and an attempt has been made to improve the process by proposing a novel tool which was used for strain hardening of AA5052-H32 material.

Keywords: Incremental Sheetmetal Forming, SPIF, hole-flanging, SPIHF, formability, FFL, Taguchi method, single-stage, square flange, grain refinement

Chapter 1 Introduction

In this chapter, an introduction to the sheet metal forming process, applications of aluminium, requirement, and introduction of advanced sheet metal forming techniques like single point incremental forming are presented. Motivation, the scope of work, and objectives are discussed. At last, the complete organization of the thesis is given.

1.1 Sheet metal forming and applications of aluminium

Sheet metal forming is a metal forming technique most widely used in the industry. According to a report of Global Market Trajectory & Analysis (“Sheet Metal Fabrication Services: Global Strategic Business Report” 2023), the global sheet metal fabrication industry will reach \$19.6 Billion by the year 2030. The sheet metal industry includes metal work on ferrous and non-ferrous metals. Aluminium offers advantages like high specific strength, good corrosion resistance, and good formability. The 1xxx series is used in general applications where as the 2xxx, 5xxx, 6xxx, and 7xxx aluminium alloys are a good choice for industrial applications because of their good strength and formability (Hirsch 2014; Zheng et al. 2018). According to the Aluminium Association (US), Aluminium alloys are most widely used in commercial aircraft, military cargo/transport aircraft, space shuttles, the automotive industry, the packaging industry, electronic appliances, and many more. Further, aluminium is recyclable which reduces environmental issues (Ashkenazi 2019).

Most of these applications of aluminium are in the form of sheet metal. An aluminium boat is shown in Fig.1.1, which is made of 5052 and 5083 aluminium alloys. In making such sheet metal parts various operations like stretch forming and stretch flanging are required. Stretch flanging is an operation in which a flange is formed on the edge of an existing hole, it is also known as hole-flanging. The hole-flange is formed for various purposes, to increase the strength of the edge, to provide support for fitting another part, and also to increase aesthetic appearance. A flange on the assembly cabin rear wall of an automobile is visible in Fig.1.2. The increasing use of aluminium in industries creates a requirement for various sheet metal

forming techniques. An industry like boat making requires job production to meet the customized requirements, on the other side, the applications in the space industry require prototyping to meet the complex designs. Such requirements impose a constraint both in terms of cost and time in manufacturing sheet metal parts. Conventional sheet metal forming requires high-cost equipment like punch and die, which takes time in designing and manufacturing. Hence, new sheet metal forming techniques like incremental forming requires to be explored.

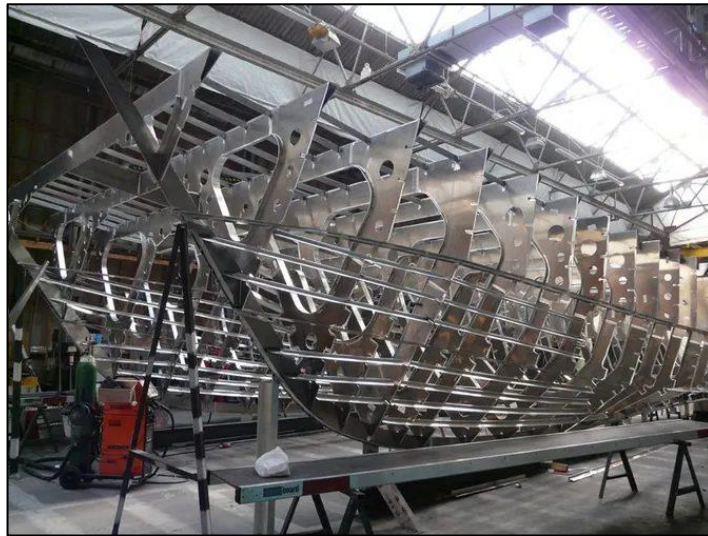


Figure 1.1 A hull of an aluminum boat under construction (courtesy- Aluminium Marine Consultants, United Kingdom)



Figure 1.2 A rectangular flange on the assembly cabin rear wall of an automobile (courtesy- ASAL products, Pune, India)

1.2 Incremental Sheet-metal Forming and Hole Flanging

The origin of Incremental Sheet-metal Forming (ISF) was marked with a patent filed by Edward Leszak which was granted in 1967 (Leszak 1967). The proposed setup comprised a roller tool that could be fed in a crossword direction to the axis of blank rotation. The sheet metal blank was mounted on a backing plate which was fixed on a turn table. The rotation of the turn table, and the downward and crossword movement of the tool, resulted in forming of the required shape.

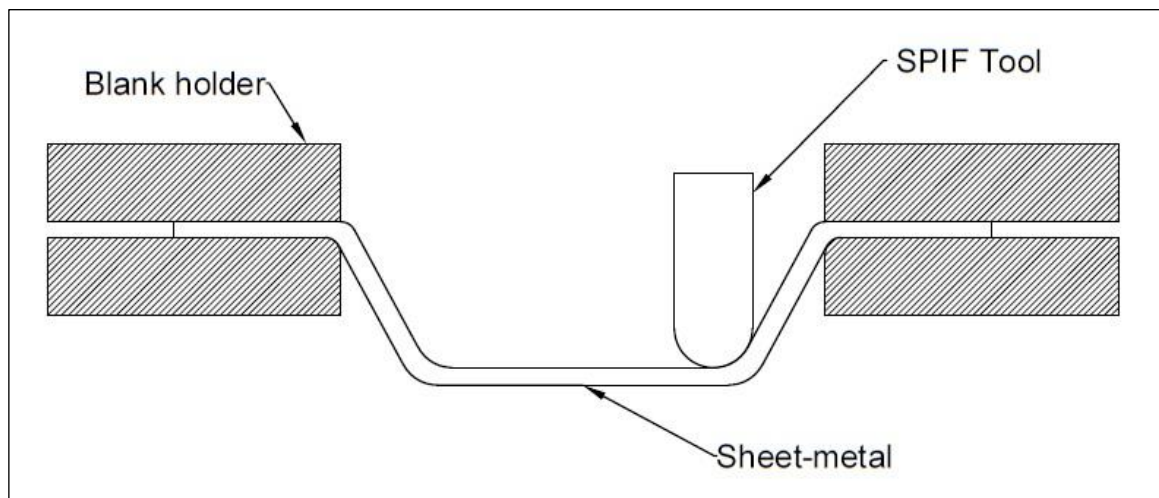


Figure 1.3 Schematic of SPIF

The principle of incremental forming was implemented to stretch form the sheet metal with a CNC machine (Dai, Wang, and Fang 2000). In this setup, the sheet metal was held on the work table of the CNC machine between a top plate and a backing plate with an opening at the centre as per the required shape i.e., to form square pyramidal part, the opening of a square shape was provided and to form a conical part, opening of a circular shape was provided. A tool with a hemispherical head was held in the spindle of the CNC machine. CNC programs were prepared as per the required shape and size of the part and through the program the tool was moved on the defined path. The motion of the tool included movement in the horizontal plane (X-Y) direction, and step depth in the downward (negative Z) direction. In this technique no die was used during the forming process, the shape was formed only with the help of the tool. This technique of ISF was later called Single Point Incremental Forming (SPIF). There are other techniques of ISF in which a support tool or a partial die is used, the

SPIF is a simple metal forming technique is a cost-effective alternative of conventional sheet metal forming. The schematic in Fig.1.3 shows the SPIF process. The principle of SPIF has been applied for hole-flanging and it has been explored by researchers since more than a decade. The process of hole flanging using SPIF is carried out on Vertical Maching Center (VMC). The process parameters like the spindle speed, feed rate and step depth affect the flange quality besides geometric parameters like tool diameter and friction (lubrication & coolant).

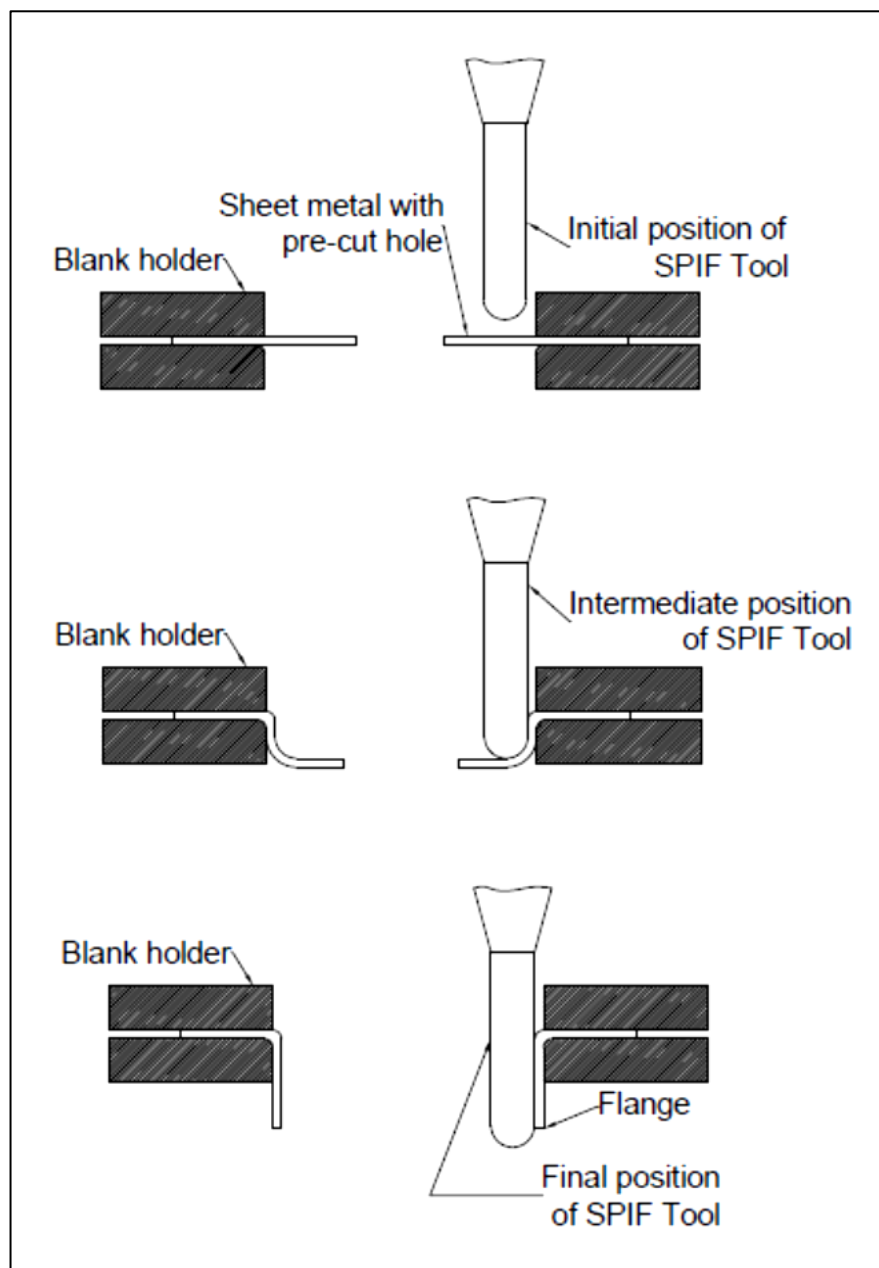


Figure 1.4 Schematic of single-stage SPIHF

It is possible to carry out SPIF process by a single-stage or by a multi-stage strategy. In the single-stage strategy, the tool is traversed on a path so that the required shape is formed in a single pass. In the multi-stage strategy, the final shape is obtained by a progressive forming which requires multiple passes. To implement the single-stage SPIF strategy for hole flanging, the tool is moved as per the schematic of “single-stage single-point incremental hole flanging” (SPIHF) process shown in Fig.1.4. In the forming of a circular flange through single-stage SPIHF, the tool is moved initially to the final diameter to be achieved and just above the sheet surface as shown in the figure. Then the tool is moved along the helical tool path hence the tool deforms the sheet incrementally. The pitch of the helix is decided as per step depth in every convolution. This action of the tool results in local deformation of the sheet and the flange is formed progressively. In the multi-stage SPIHF, the tool is moved similarly to the single-stage, but the final flange is achieved by forming small flanges of increasing size/angle. The multi-stage approach increases the formability; however, it increases the operation time also. The single-stage approach reduces the operation time to a great extent.

1.3 Motivation

SPIHF is a novel technique to form the flanges on existing holes. It adds up the advantages of SPIF to the hole-flanging process. Aluminium sheet-metal parts are widely used in the automotive, aerospace, and ship manufacturing industries. To implement the SPIHF process in the industry, it is required to study the formability achieved in the process. Most of the studies on hole flanging are focused on the circular flange either using a single-stage approach or a multi-stage approach. It is required to carry out a comparative study between both approaches to understand their advantages and limitations. It is also required to understand the effect of the process parameters on the flange quality so that appropriate process parameters can be selected. Further, looking at the various applications of hole flanging, it is required to study the formability of different shapes of flanges. Hence, the square flanging of aluminium sheet-metal requires attention. It is observed that flanges along the various contours cannot be produced successfully due to the prevailing mode of deformation. Hence, it is planned to carry out the strain analysis for square flange forming in the present research work. Limit Forming Ratio (LFR) which is one of the formability measures has already been defined for circular flanges. However, it is required to establish

the same for square flanges. Moreover, due to thinning during the flange forming, the flange becomes weak and hence, it is required to improve the strength of the same.

1.4 Objectives of the present work

Based on the research gaps found in the published literature, the following objectives have been identified for the present work.

1.4.1 Development of setup and preliminary experiments

The setup of SPIHF is developed and preliminary experiments are carried out to analyse the effect of tool diameter on the formability in single-stage SPIHF. The study has been performed on AA1050 sheet-metal as it is used in many general applications. Three SPIF tools with different diameters are used to form circular flanges in single-stage. A series of experiments are performed to find the Limit Forming Ratio for each tool. The thickness distribution on the flanges from the root towards the edge and the height of the flanges has been measured and analysed. Further, the effect of feed rate and step depth on the thickness and height of the flange has been analysed experimentally.

1.4.2 To investigate the Limit Forming Ratio, the thickness of the flange, the height of the flange, and strain distribution on the cylindrical flange in single-stage and multi-stage SPIHF

To understand the difference between the formability achieved by single-stage and multi-stage approaches, experimental investigations are carried out by forming flanges with both approaches. The experiments are performed on AA5052-H32 sheet-metal as it has applications in the automobile, aerospace, and shipbuilding industries. A series of experiments are performed with both approaches to find the Limit Forming Ratio in SPIHF to form the circular flange. The thickness of the flange and strain distribution on the flanges are measured and analysed. Comparative analysis for both approaches has been carried out.

1.4.3 To study the effect of process parameters (spindle speed, feed rate, step depth) on the flange quality in single-stage SPIHF of the cylindrical flange

To increase the effectiveness of the process, it is required to decrease the operation time. Hence, it is recommended that the flange forming should be carried out with a single-stage

approach. Further, to establish a clear understanding of the single-stage SPIHF, an experimental study has been performed to investigate the effect of process parameters on the flange quality. The Design of Experiments is carried out based on the Taguchi method. The L9 orthogonal array is used to prepare the list of experiments. Three levels of each process parameter i.e., spindle speed, feed rate, and step depth are considered. The thickness of the flange, the height of the flange, and the surface roughness of the flange are considered responses to define the quality of the flange. The thickness is measured along the axis of the flange using a digital pointed anvil micrometre. The height is measured using a vernier height gauge. The surface roughness is measured on the inside surface of the formed flange using a surface roughness tester. The results are analysed with the main effect plots of the S/N ratio, and the interactive effects of the parameters are analysed by interaction plots.

1.4.4 To obtain the experimental Fracture Forming Limit line for SPIHF

The formability limit for conventional sheet-metal forming is represented by a Forming Limit Curve obtained by standard test experiments. However, the formability limit in SPIF is represented by a Fracture Forming Limit line (FFL), as the necking is suppressed in this process. It is proposed in the current work that the FFL can be obtained by performing SPIHF experiments instead of conventional metal forming tests. Various circular and square flanges are formed and strain measurement has been carried out by the circle grid method to obtain the FFL. The same has been validated with the theoretical FFL.

1.4.5 To investigate the formability of aluminium alloy in single-stage SPIHF of square flange

There are various applications where a square flange is required on the sheet-metal part. It is required to study the forming of the same with SPIHF to establish the industrial use of the SPIF principle. Again, to reduce the operation time, the square flange should be formed with a single-stage approach. An experimental study has been carried out by forming a square flange using the principle of SPIHF. A new equation to find LFR for square flange has been proposed. The LFR for the AA5052-H32 material has been found by performing experiments to find the least pre-cut hole size which can be formed into a square flange of the required size without failure. Moreover, the effect of tool rotation on the LFR and the surface quality has been analysed by performing experiments with a non-rotating tool and a rotating tool.

Moreover, the pre-cut hole for square flanging is a square with a corner radius, which can affect the formability. Hence, the effect of the corner radius on the LFR has been analysed.

1.4.6 To improve the hardness of aluminium alloy by achieving grain refinement with a novel tool in single-stage SPIHF of the square flange

To further improve the utilization of SPIHF, a novel tool is proposed. The proposed tool is an eccentric SPIF tool that introduces low-frequency mechanical vibrations in the process. Experiments are performed to form square flanges with the novel tool. EBSD measurements are carried out to study the grain structures on the obtained flanges. Surface roughness is measured to check the flange quality. The Microhardness of the flanges is measured to check the improvement of the mechanical property with the use of the proposed tool.

1.5 Organization of the Thesis

Chapter 1 gives an introduction to the sheet-metal applications, SPIF and SPIHF process, and the use of aluminium alloys. This chapter also includes an overview of the motivation behind the current work, the research problem, the objectives of the research work, and the organization of the thesis.

Chapter 2 presents a comprehensive literature review of the research work published about SPIF and SPIHF in international journals, conferences, and books.

Chapter 3 explains the methodology to carry out an experimental study on forming a circular flange performed to find the effect of tool diameter on LFR, the thickness of the flange, and the height of the flange, and the analysis of the results obtained. A method to obtain the FFL experimentally by performing the SPIHF experiments has been discussed. Moreover, the results and analysis of a comparative experimental study on single-stage and multi-stage SPIHF are also included.

Chapter 4 presents a discussion about the preliminary experiments and their results. The design of experiments to study the effect of process parameters is presented. Also, the results and analysis of experimental investigations performed to understand the effect of spindle speed, feed rate, and step depth on the flange quality are discussed.

Chapter 5 covers the results and analysis of the experimental investigation on square flange forming using the SPIHF process. It includes the study of forces acting on the sheet-metal

during the process. The experimental results of the study on the effect of tool rotation on the LFR have also been presented. The results and discussion on the study of the effect of pre-cut corner radius on the LFR have also been included.

Chapter 6 is about the experimental study with a novel tool for SPIHF. The effect of the novel tool on the grain structure, surface roughness, and microhardness of the flanges has also been discussed.

Chapter 7 Summarises the research work carried out and conclusions drawn. It also covers the future scope of the work.

Chapter 2 Literature Review

This chapter aims to review the important work on SPIF and SPIHF reported by various researchers and to develop a basic understanding to find the research gaps. An extensive literature survey on Forming Limit Curve, Fracture Forming Limit line, Limit Forming Ratio, the effect of process parameters, force analysis, and single-stage, and multi-stage approaches have been presented. In addition, it includes the existing research gaps and frame work to carry out current research.

2.1 Introduction to hole flanging process

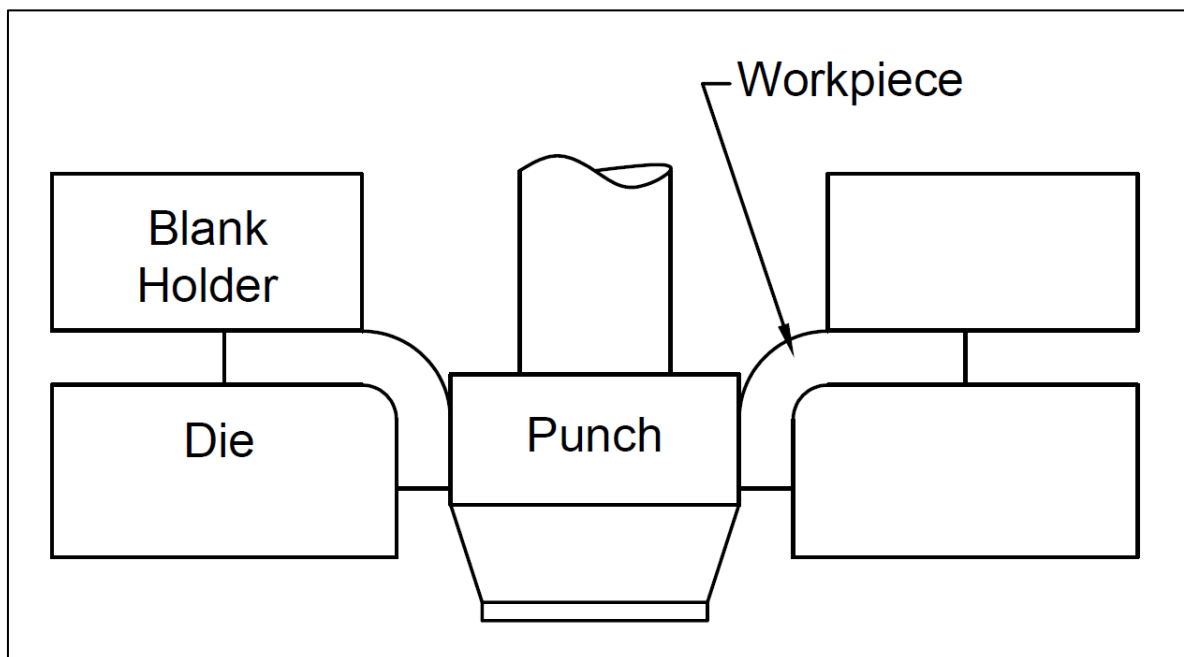


Figure 2.1 Conventional flange forming

Hole flanging is the process of forming a flange on sheet metal with a pre-existing hole on it. It is carried out to increase the strength of the hole edge or for assembling parts by joining processes such as spot welding (Lee et al. 2007). It also provides additional support for press fits or connections with tubes (Stachowicz 2008). The process has applications in the

automotive, aerospace, and shipbuilding industries (Cui and Gao 2010). Conventionally the hole-flanging process is performed by using a punch-die setup. The sheet is held on the die by a blank holder, and the punch is moved in the downward direction to form the sheet as per the shape of the die (Fig.2.1). A press is required to perform the conventional hole flanging process, also it is required to design punch and die as per the shape required after forming. To meet the investment of the setup, mass production in large batch sizes is demanded (Montanari et al.). To resolve this issue, SPIF can be implemented for hole flanging.

2.2 Incremental sheet metal forming process, its applications, and hole flanging

In 1967 a patent on incremental die-less forming was granted to Edward Leszak (Leszak 1967). In this patent, a new technique of forming conical shapes by using a ball/roller tool was presented. The application of the principle of die-less forming became feasible and easy to implement through the use of CNC machines (Dai, Wang, and Fang 2000; T. J. Kim and Yang 2000), and a major flow of research on the process which was called “Incremental Sheet metal Forming” (ISF) started in the first decade of the 21st century. The research requirement arose because of the changes in the market. It was observed that conventional sheet metal forming requires dies and it is suitable for large quantity production; however, due to the increase in customization and small batch production, the conventional forming process was required to be improved by introducing flexibility (Dai, Wang, and Fang 2000).

The schematic of the setup for the incremental sheet metal forming is shown in Fig.2.2. In the incremental sheet metal forming process, a tool is traversed on the sheet metal as per a predefined path with incremental steps. The sheet is held between two metal plates, which are generally called top and bottom plates. The incremental sheet metal forming has the advantages of simple and low-cost setup, simple tool geometry, and flexibility in changing tool paths by modification in the CNC program. It is possible to carry out the process by the single-point method and by the two-point method. In the single-point method, the forming is performed without using any die whereas, in the two-point method, two tools are used; other methods involve the use of a partial die or full die (H. Lu et al. 2017). The methods are shown by a schematic in Fig.2.3. The first method is Single Point Incremental Forming (SPIF), in which the tool is moved on a defined path without any support. The second method is Double

Point Incremental Forming, in which two tools are used. One tool is used to deform the sheet and the other one is used to give support from the other side. The third method uses a partial die, which is arranged below the sheet metal to be formed, and a SPIF tool which deforms the sheet metal on the die. One more such method is an incremental sheet metal forming using a full die. In this method, the tool traverses on the defined path, deforming the sheet as per the shape of the full die. The method of using the full die was implemented and a machine developed for incremental forming was utilized for the experimental work (Ceretti, Giardini, and Attanasio 2004). A tool with a hemispherical head was used to deform the Cu DHP sheet and AISI 304 sheet. The sheet metal forming was carried out using a die at the bottom. The whole process was initially simulated by FEM which was followed by experiments. It was observed that the CNC machine could be used successfully for forming the required shape. It was concluded that the technique could be applied to small batch production, rapid tooling, and flanging operation without die. The partial die method/full die method and the double point method have a little complex setup as compared to the single-point method, as in the single-point method no die or backing tool is required. Hence, the single-point method has remained the focus of most researchers. The process of incremental forming by using the single-point method is now widely known as SPIF.

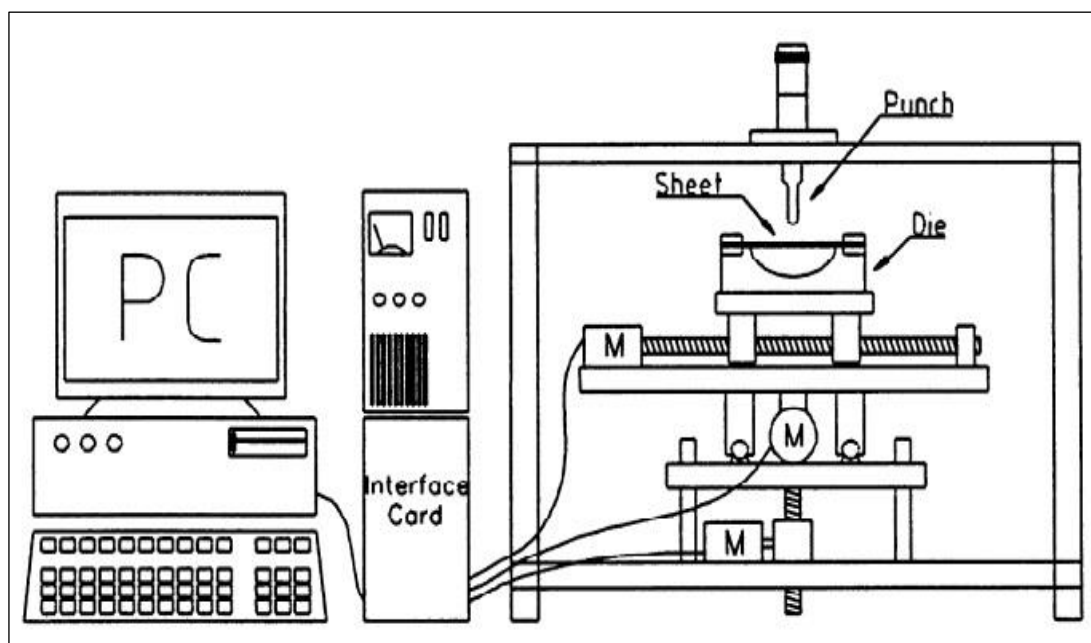


Figure 2.2 Schematic of setup for incremental sheet metal forming (T. J. Kim and Yang 2000)

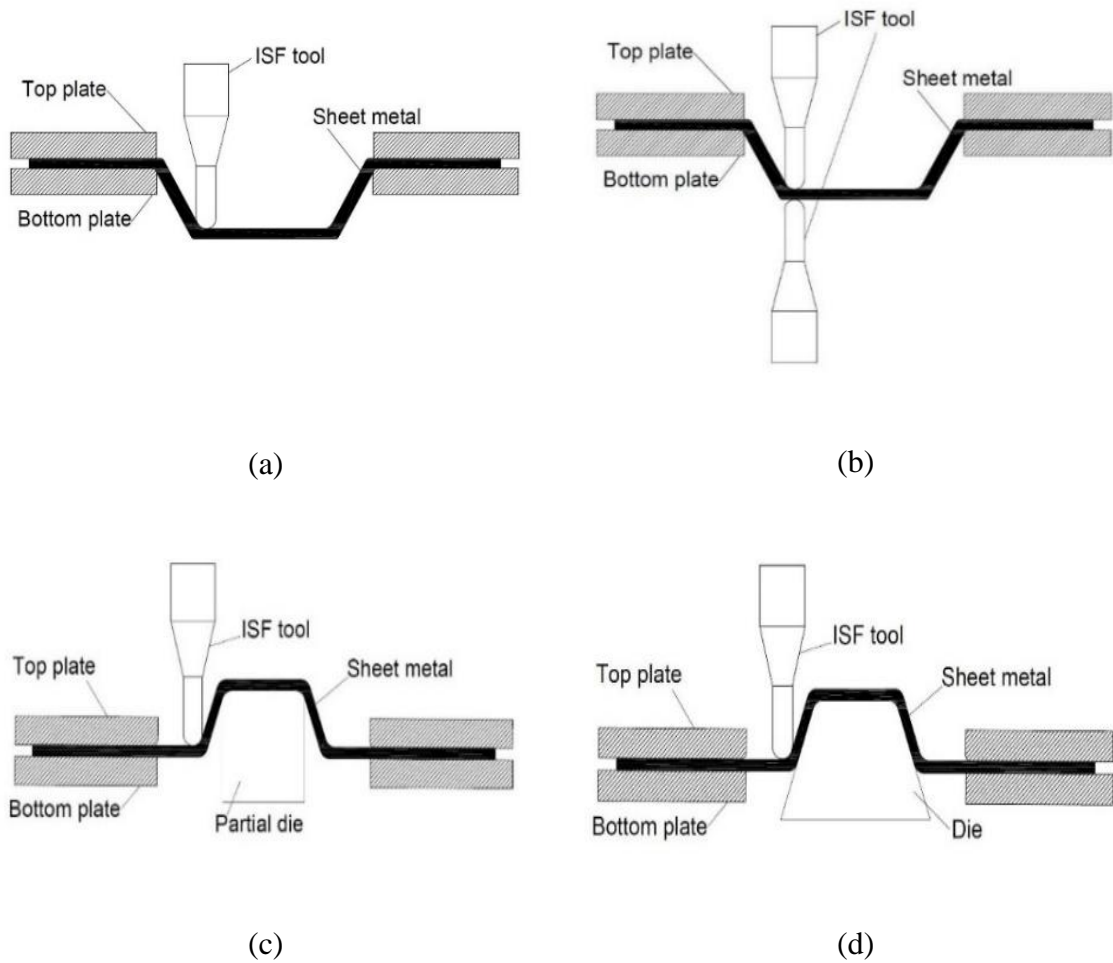


Figure 2.3 (a) single point incremental forming (b) two-point incremental forming (c) incremental forming with partial die (d) incremental forming with full die

2.2.1 Applications of incremental sheet metal forming

The various applications of SPIF has been reported in literature (Jeswiet et al. 2005). The viability of the SPIF process was demonstrated by forming various shapes shown in Fig.2.4. Moreover, different parts of the automobile as rapid prototypes were formed as reflectors of headlights, heat/noise shields used over exhaust manifolds, etc. Further, forming of other parts like a solar oven cavity, part of a gas tank, etc. was also reported. The solar oven cavity is usually made of fiberglass. The process of manufacturing it with fiberglass is time-consuming and laborious. If it is to be made from sheet metal, the die has to be used which is very expensive. It became possible to make the solar oven cavity from aluminum by implementing the SPIF process for the same.

Also, different parts used for medical applications like ankle support were reported to be formed by SPIF, the reverse engineering approach was used for the same. Moreover, the SPIF technique was applied to form an implant that resembles the articular surface of the knee joint (Oleksik et al. 2010). The implant was formed on titanium sheets and it was concluded that the SPIF could successfully be implemented to form such parts. Moreover, the application of SPIF to form cranial implants to be used in cranioplasty was explored in the research work (B. Lu et al. 2016). The cranial implant was formed on the titanium sheet using the incremental forming technique (Fig.2.5). The tool path was generated by CAD/CAM application using the reverse engineering approach. The tool path was simulated using FEA and the same was used for actual forming. It was observed that there was a geometrical difference between the FEA and actual forming, which was due to the spring back in the material. Although a more rigid methodology was required, the feasibility of SPIF to form such biomedical parts was proven. The application of SPIF to form automobile parts was demonstrated in a research work (Liuru, Yinmei, and Zhongmin 2015), in which a car fender was manufactured. In addition, the SPIF can also be performed by a robotic manipulator (Meier et al. 2009) which shows that the SPIF has processing flexibility also. The use of SPIF to form composite parts has also been attempted with promising results (Fiorotto, Sorgente, and Lucchetta 2010).

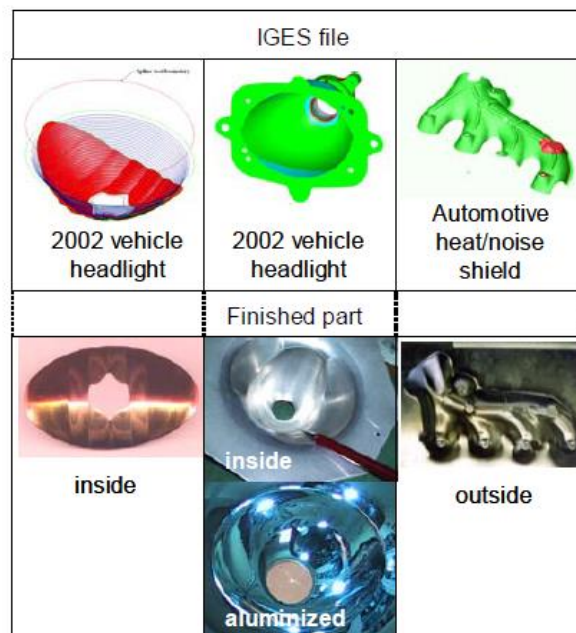


Figure 2.4 Parts formed by SPIF (Jeswiet et al.)

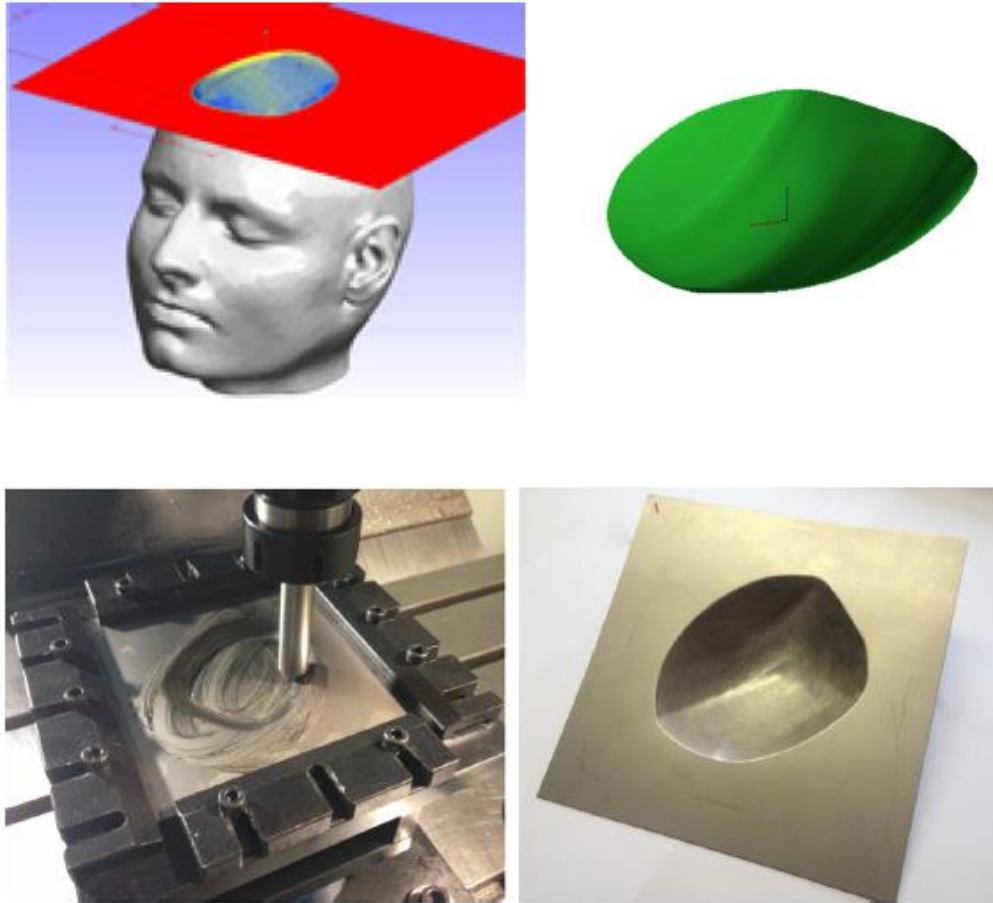


Figure 2.5 Modeling and Manufacturing of Cranial plate using ISF (B. Lu et al. 2016)

2.2.2 Implementation of SPIF for flange forming

The SPIF method has been implemented to perform hole flanging (Cui and Gao 2010), which can be called Single Point Incremental Hole Flanging (SPIHF) and it was observed that higher formability was achieved by the same. The setup of SPIHF is similar to the SPIF setup. However, it is required to cut a hole in the sheet before the flange forms. The procedure of SPIHF is shown in Fig.2.6.

In SPIHF, the sheet metal is first held between the top and bottom plates of the fixture. Then, a hole of the required diameter is cut by an end mill cutter. The SPIF tool is then traversed on the planned tool path to form the flange. An experimental setup used for SPIHF is shown in Fig.2.7. The SPIHF has been performed mostly on aluminum alloys, however, it was also used to form flanges on materials like Polyethelyn terephthalate (PET) and Polycarbonate (PC) (Silva, Martinho, and Martins 2013). It was observed that straight flange forming was

possible on PET but flange with a wall angle of more than 70° was not possible on PC. The PET exhibits more resistance to the growth of the crack and the plastic deformation takes place easily compare to PC. This is because the PET has a semi-crystalline structure with repetitive polymer chains, also the fracture toughness is higher. The study demonstrates the feasibility of forming straight wall flange on the PET material using the SPIHF process.

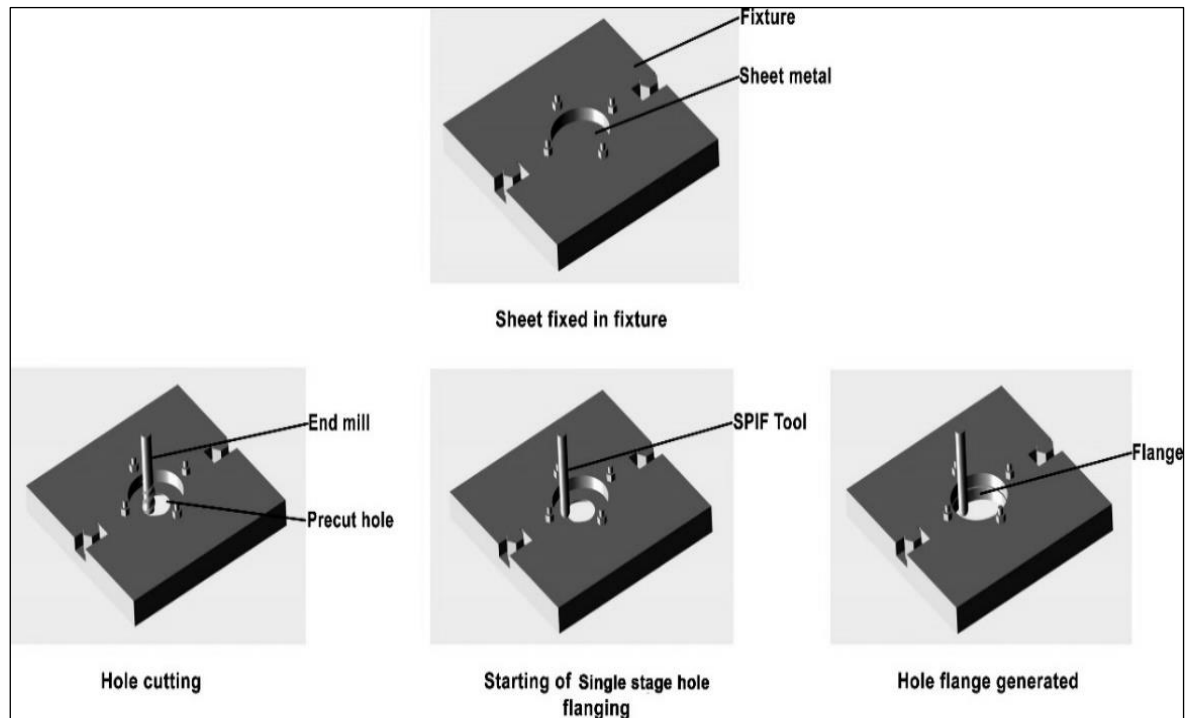


Figure 2.6 Procedure of single-point incremental forming

The SPIHF can also be implemented to form flanges on the thin-walled tube as demonstrated in the experimental work (Yang et al. 2014). The flanges were formed on the 316L stainless steel tubes with a thickness of 0.5 mm. The flange forming was carried out on an existing hole on the tube. Here, as the flange protrusion was required on the outer side, the backward flange forming technique was implemented. The backward flange forming could be performed with two strategies. In the first strategy a conventional SPIF tool was used, the tool was inserted inside the existing hole with certain inclination and then it was moved in the upward direction to form the flange. In the second method, a bar tool with a tapered shoulder was used for the flanging operation, initially the tool was inserted inside the existing hole by keeping it straight and then it was moved in the upward direction to form the flange. The flange forming was performed progressively in multiple stages. The literature shows

that it is feasible and advantageous to implement the SPIF principle for hole flanging on metal and polymeric materials.

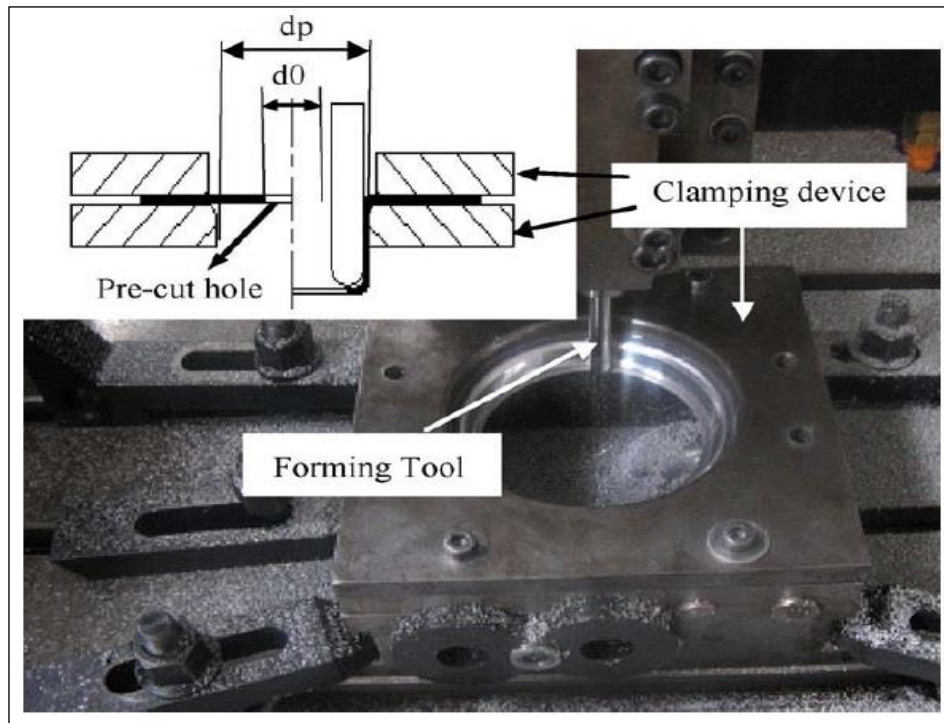


Figure 2.7 Setup of single-point incremental hole flanging (Cui and Gao 2010)

2.3 Failure limits, strain distribution, and thickness distribution in SPIF and SPIHF

The deformation mechanism in incremental sheet metal forming is different than conventional forming. The deformation takes place through the incremental movement of the tool and is confined near the contact area between the tool and the sheet (Shim and Park 2001). The formability of a material is generally represented by a Forming Limit Curve (FLC) on principal strain space (ϵ_1, ϵ_2). The necking of material is responsible for the failure in conventional forming. To plot the failure limit, conventional forming tests are carried out to deform the material and strain values are measured at the necking zone (Martínez-Donaire, García-Lomas, and Vallellano 2014; Shim and Park 2001; M. Borrego et al. 2016; Holmberg, Enquist, and Thilderkvist 2004). These strain values are then plotted on principal strain space and a curve is fitted through them which is named FLC. Further, the strain values at the crack give the Fracture Forming Limit line (FFL). FLC and FFL for a material can be obtained by

Bulge tests, Nakajima tests, and Hemispherical dome tests in which the material is deformed by a punch and die into various shapes followed by strain measurements in the necking zone and near the fracture. An attempt was made to obtain the FLC by performing tensile tests (Holmberg, Enquist, and Thilderkvist 2004). The experiments were performed on two materials, mild steel, and high-strength steel. Special grip wedges were used to grip the sheet metal specimen. The test was stopped when the crack opened to half the specimen width. It was observed that the left-hand side of the FLC could be obtained by the tensile tests, however, the right-hand side could not be determined. The literature suggests that there is a scope to establish an easier method to obtain the FLC.

To understand the formability of the SPIF, an experimental study was carried out (Filice, Fratini, and Micari 2002), and strains on the part formed by SPIF were measured by the circle grid method. It was observed that the FLC of SPIF was different than the FLC of conventional forming and it was represented by a line on the principal strain space with a slope of -1. Further, SPIF experiments were performed to form a pyramidal shape, octagonal cone shape, and bucket shape (Park and Kim 2003). It was observed in the study that forming objects with sharp corners was difficult and failure took place at the corner with biaxial tension. It was also shown that the FLC is different for conventional metal forming and SPIF. The formability of aluminum 3003 sheets in SPIF was analyzed (Jeswiet, Hagan, and Szekeres 2002) by performing experiments to form pyramidal and conical shapes with different wall angles. The largest angle which could be formed by the SPIF was 72° . Further, the value of strength co-efficient K was found by performing tensile tests on the formed parts with different wall angles of 20° , 30° , 40° , 50° and 60° . During the forming of these parts, an orange peel effect was observed in all the specimens, also the strain hardening exponent was not constant for the forming of different wall angle. It was observed that severe plastic deformation could be carried out by SPIF and hence the formability increased to a great extent. To understand the failure mechanism in SPIF, an analytical model based on membrane analysis was developed (Silva, Skjoedt, et al. 2008). It was concluded by the analysis that the meridional tensile stresses were responsible for the crack in SPIF and not the shear stress. Further analysis of the failure limit in SPIF was carried out in an experimental study (Silva, Skjoedr, et al. 2008). The AA1050-H111 sheets of 1 mm thickness were deformed to form a truncated conical shape by a tool with a hemispherical head. It was observed that the deformation took place with uniform thinning which indicated that there

was no necking on the sheet metal unlike the conventional metal forming. Moreover, the FLC plotted by strain measurement at the necking on the sheet metal was not relevant to the failure in SPIF. It was evident that the FFL should be employed to show the failure limit (Fig.2.8). The FLC is obtained by connecting the failure points on the sheet after necking. When the necking is because of biaxial or uniaxial stretching, the deformation is suffered by the sheet in two directions whereas in case of plane strain condition, the deformation occurs along a single direction. Because of this, in case of plane strain condition the failure takes place at lower strain value which is observed as a dip on the FLC. In case of SPIF, the necking is suppressed hence in all the deformation modes, the fracture takes place after continuous thinning. Hence, there is no dip at the plane strain mode as observed on the FLC.

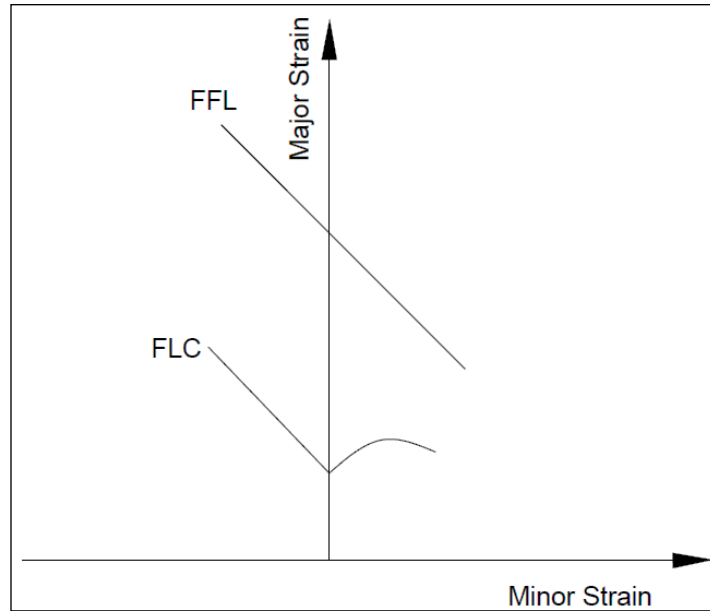


Figure 2.8 FFL and FLC on major strain-minor strain space

The damage function (equation 2.1) was used to derive the equation 2.2 assuming the Tresca yield criterion, to find the slope of FFL for SPIF.

$$D = \int_0^{\bar{\epsilon}_f} f\left(\frac{\sigma_m}{\bar{\sigma}}\right) d\bar{\epsilon} \quad (2.1)$$

$$\frac{\epsilon_1^{biaxial} - \epsilon_2^{plane\ strain}}{\epsilon_2^{biaxial} - 0} = \frac{5(r_{tool}/t) - 2}{3(r_{tool}/t) + 6} \quad (2.2)$$

It was noted that for the values of (r_{tool}/t) in the range of 2 to 10, the slope of the FFL varied between -0.7 to -1.3. By this, a confirmation about expressing the FFL by $\varepsilon_1 + \varepsilon_2 = q$, was achieved. For plane strain condition it can be expressed by $\varepsilon_t = -q$. It is in close agreement with the FFL of conventional forming, in which the line is represented with a slope of -1. Further, experimental investigations in this direction were carried out (Isik et al. 2014). It was discussed that q could be represented by $-\ln(1 - R_f)$, where the critical thickness reduction $R_f = (t_f - t_0)/t_f$. Hence, by measuring the thickness at crack on the failed part with plane strain condition, a point on the major strain axis can be plotted and a line with a slope of -1 passing through the point represents the theoretical FFL. Further, pyramidal and conical shapes were formed on AA1050-H111 sheets by the SPIF process, and strain values near the crack on the failed components were measured. These values were then plotted on the strain space and a line was interpolated through them to get the FFL. The slope of the obtained FFL was '-0.70' and it was in agreement with the FFL obtained by conventional forming tests. Hence, it was shown that the FFL can be conveniently obtained by SPIF tests instead of conventional forming tests.

The formability of AISI304 sheet material was evaluated (Gabriel Centeno et al. 2014) by performing stretch-bending and SPIF. The formability in stretch-bending was observed to be 30% higher than the FLC whereas the enhancement was 150% above the FLC in the case of SPIF. It was also observed that the fracture strain points in stretch-bending were near the FFL obtained by the Nakazima tests whereas in SPIF the fracture strain points were above the FFL.

The formability in SPIF can further be increased by additional features, for example, a setup for heat-assisted SPIF was developed and analyzed the effect of temperature on the formability (Ambrogio et al. 2009). The experimental study was performed on AZ31Magnesium alloy sheet material. The FFL was obtained by experiments performed on a sheet heated to 200° C and another sheet heated to 300°C. Increased formability was obtained when the sheet material was heated to a higher temperature. The method was called "Warm Incremental Forming".

The SPIF and SPIHF processes are different because, in the latter, a pre-cut hole exists on the sheet metal. To understand the failure criterion in the SPIHF, an experimental study was

carried out (G. Centeno et al. 2012). The experiments were performed to form conical and cylindrical flanges on AA1050-H111 sheets with 1 mm thickness. A multi-stage strategy was used, in which flanges were formed in multiple stages with increasing angles. The strain on the two formed conical flanges (with a pre-cut hole diameter of 40 mm and 52 mm) was analyzed. The strain behavior on the flange with a smaller pre-cut hole diameter remained the same as in the SPIF of the sheet without a hole, crack appeared with the circumferential orientation because of in-plane stretching due to meridional stress. The sheet with the pre-cut hole of 52 mm diameter did not fail, the strain behavior was influenced by the existing hole on it. The deformation took place through the combination of in-plane stretching and bending in the vicinity of the hole. The first mode of deformation (in-plane stretching) happened near the root of the flange, whereas the second mode of deformation (bending) took place at the hole edge. There was a progressive transition from the first to the second mode during the process. Further, cylindrical flanges were formed by the multi-stage strategy and it was observed that the strain behavior was similar to the conical flange. A critical pre-cut hole diameter was found, any pre-cut hole diameter less than that could not result in a successful flange. The strain values obtained in the multistage cylindrical hole flanging were analyzed as reported in a literature (Montanari et al.). In the experimental work on AA1050-H111, the FFL was obtained by performing the tensile test and hydraulic bulge tests. The experiments were then performed to form straight cylindrical flange with multistage approach. The wall angle was increased in each stage. Strain values were measured after each stage of forming and finally a strain envelope was plotted on the major strain vs minor strain space. It was observed that in the SPIHF, the strain paths growth was linear upto the maximum achievable strain values unlike the tensile test, elliptical bulge test and biaxial circular tests. This strain behavior confirmed that there was no necking during the SPIHF. Further, the strain distribution on the cylindrical flange formed by SPIHF was carried out (M. Borrego et al. 2016). The strain distribution was analyzed from the root of the flange to the edge of the flange, the same is shown in Fig.2.9. On the successfully formed flange, the major strain was observed to be in the axial direction and increasing till the mid-height of the flange, the deformation mode was biaxial stretching. Thereafter, the major strain reduced and direction changed to circumferential, the deformation mode changed from equibiaxial stretching to unidirectional tension at the edge. The strain evolutions on the FLD appeared to be a loop.

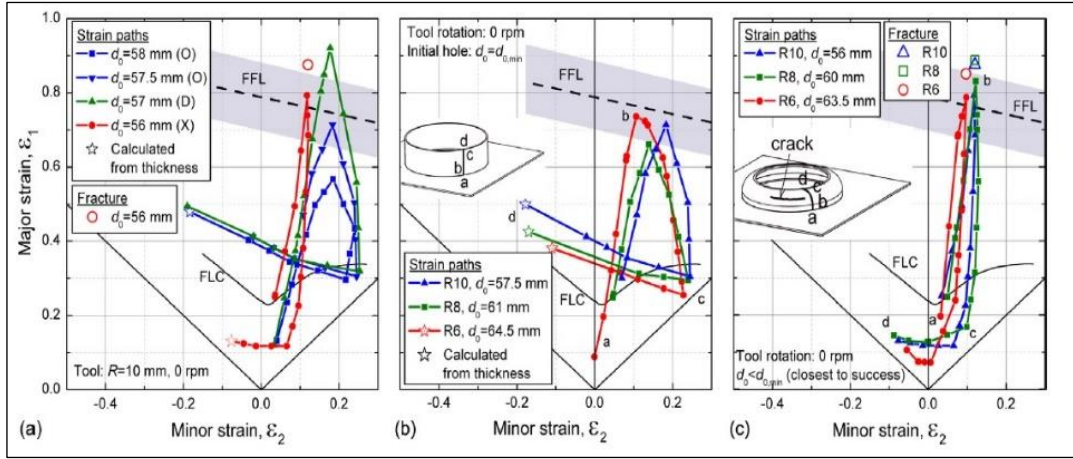


Figure 2.9 strain distribution on the wall of cylindrical flange formed by SPIF (a) Different precut hole diameters with tool radius 10 mm, (b) Minimum precut hole diameter that could be successfully formed into a flange, (c) failed flanges closest to success (M. Borrego et al. 2016)

The crack with circumferential orientation was observed on the failed flanges, with strain values in the 10% zone of the FFL obtained by the Nakazima tests. The Nakazima tests are commonly used testing method to obtain the FLC which has been used by many researchers (Gabriel Centeno et al. 2014; Martínez-Donaire, García-Lomas, and Vallellano 2014; Bayati et al. 2021). To analyze the micro void growth on the deformed sheet in SPIF, a study on the stress triaxiality was performed by (Martínez-Donaire et al. 2019). The stress triaxiality (η) is defined as a ratio of hydrostatic stress (σ_m) to equivalent stress ($\bar{\sigma}$). It was noted that low-stress triaxiality results in low void growth. The stress triaxiality in Nakazima tests was compared to the hole flanging by single-stage SPIF. For the comparison, the average stress triaxiality values and the displacement of the tool in the Z direction were plotted for both (SPIF and Nakazima test). The average stress triaxiality is given by the equation (2.3). When the value reaches the critical value of micro void growth, the fracture takes place.

$$\bar{\eta} = \frac{1}{\bar{\epsilon}} \int_0^{\bar{\epsilon}} \frac{\sigma_m}{\bar{\sigma}} d\bar{\epsilon} \quad (2.3)$$

It was observed that average stress triaxiality was less than half in SPIF compared to the Nakajima tests, which explains the enhancement in formability. Moreover, it was concluded that the FFL is different for conventional forming and SPIF. It was also observed that on the

part formed by SPIF, the void growth was more at the outer surface than the inner. This was the reason that cracks appeared on the outer surface of the failed flanges.

The thickness distribution on the flange wall depends on various factors like the strategy of flanging (single-stage/multistage), The size and shape of the tool, the step depth, the spindle speed, and the feed rate. The wall thickness of the part formed by SPIF could be predicted by the sine law of shear forming. The sine law is represented by an equation (equation 2.4) as given in the literature (Kobayashi, Hall, and Thomsen 1961), where in t_f is the thickness of wall after forming, t_0 is initial thickness of sheet and α is the wall angle. The equation was given for the spinning operation to form a conical shape.

$$t_f = t_0 \sin \alpha \quad (2.4)$$

To study the wall thickness in SPIF, an experimental study was carried out (Young and Jeswiet 2004). The experiments with a single pass and double pass were performed to form a conical shape and thickness distribution on the wall was analyzed. The results showed that the wall thickness on the cone varies from the root to the flat end (in a truncated conical shape) or apex (in a full cone shape). The results of the single pass SPIF showed that there was a reduction in thickness from the root towards the end; initially at the nearby area of the root, then there was a more or less uniform thickness till the edge and it reduced again near the edge. The deformation near the root happened due to bending whereas on the wall it was due to shearing. On the conical shape with a high wall angle of 70° , Failure on the sheet occurred at a distance of 15mm from the root. A sharp thinning band was observed in this zone which could not be predicted by the sine law. Further, experiments were performed by a double pass method, in which a conical shape with a low wall angle value was formed in the first pass. It was followed by a second pass in which a high-angle wall was formed. It was observed that the thickness distribution became less uniform compared to what was obtained by a single-pass method. Moreover, thickness more than predicted by the sine law was obtained at some places on the wall. In other studies on the truncated conical shape forming by SPIF, it was observed that the thickness decreased continuously from the top to the bottom and the thickness at the bottom remained higher than that at the wall (Skjoedt et al. 2008; Essa and Hartley 2011; Mirnia et al. 2014; Pandre et al. 2021; T. J. Kim and Yang

2000). The reason behind the continuous reduction in thickness is the continuous stretching of the material by the stepwise downward movement of the tool.

Further, experiments were performed to form the conical parts by single-step and multi-step methods (Duflou et al. 2008). Two intermediate steps were added in the multi-step method to form the required shape. The higher thickness on the wall of the part formed by multi-step was observed, whereas the thicker base on the part formed by the single-step method was observed. The distribution of the thickness was similar to that reported earlier. Another study on multi-stage SPIF was performed (Skjoedt et al. 2010), in which multi-step strategies were implemented to form a part with a vertical wall. In the first step of both strategies, a conical shape was formed. Now, all intermediate steps and the final step were performed by moving the tool either in an upward direction or in a downward direction (Fig.2.10(a)). First, the part was formed by a two-step method which was called DD (both steps formed with downward tool motion) and DU (first step downward and second step upward tool motion). It was observed that the thickness distribution in both the strategy was different (Fig.2.10(b)). The DD strategy was similar to single-step SPIF. However, in the DU strategy with the tool moving in the upward direction, more thinning was observed at the center part. Moreover, experiments with two different four-step strategies (DDDU, and DUDD) were performed which shows that the latter gives higher thinning. In another experimental study (Hirt et al. 2004) based on the multistage SPIF of pyramidal shape, it was observed that the thinning on the wall was less than the predicted value by the ‘sine law’.

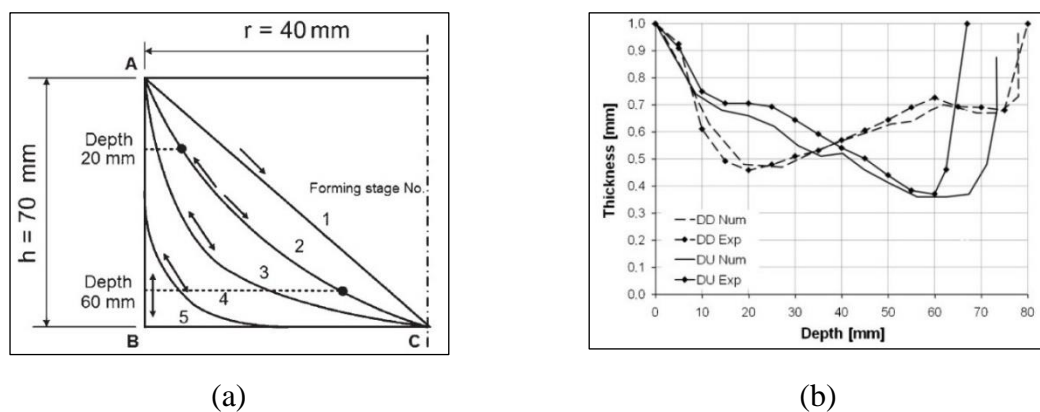


Figure 2.10 (a) Different multi-step strategies, (b) Thickness distribution in DD and DU strategy (Skjoedt et al. 2010)

An experimental study on the multistage hole flanging using SPIF was carried out (Cui and Gao 2010). Three different multi-stage strategies (Fig.2.11) were used to form a straight wall flange, 1) forming of straight flanges with increasing diameter, 2) forming intermediate conical flanges with increasing angles, and final flange with a straight wall, and 3) a combination of the first and second strategy.

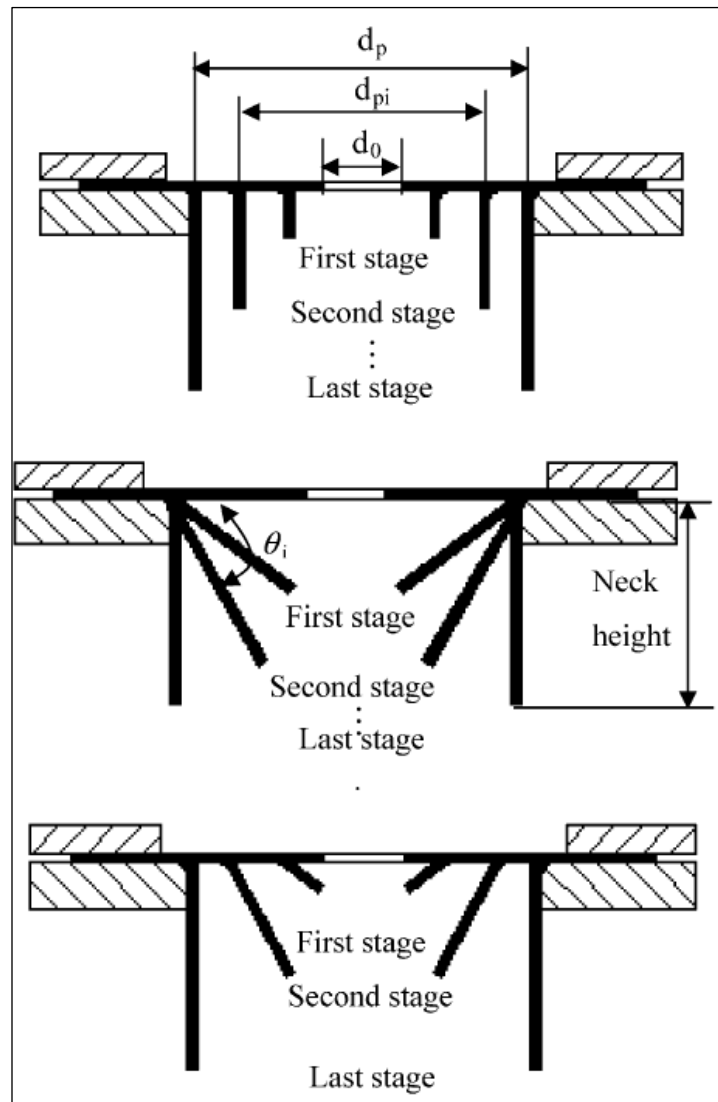


Figure 2.11 Different multistage strategies of SPIHF (Cui and Gao 2010)

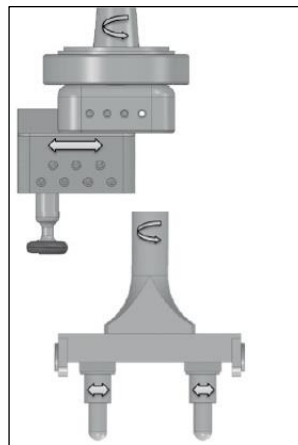
The thickness on the flange formed with the first strategy remained stable near the root of the flange, decreased in the middle zone, remained stable in the upper zone, and again decreased at the edge of the flange. The failure took place at the edge of the flange. The thickness on the flange formed with the second strategy decreased from the root to the mid zone, then

increased towards the edge, and finally decreased a little at the edge. The failure took place at the mid-height of the wall. The thickness distribution on the flange formed with the third strategy showed a gradual decrease from the root to the upper zone near the edge and decreased a little at the edge. In all the strategies, it was observed that better thickness was obtained when more stages were implemented to get the final shape. The thickness distribution on the flange may vary depending on the single-stage or multi-stage strategy of SPIF used for the forming. To analyze the thickness distribution in the single-stage hole flanging process, an experimental study was done (M. Borrego et al. 2016). The distribution was having a wavy profile similar to the multistage strategy, in which the thickness was reduced from the root to the mid-height of the flange and then increased till the edge. Although the profile of thickness distribution was similar in both strategies, better distribution was obtained by multistage (Skjoedt et al. 2010). However, a single-stage strategy forms the flange in a considerably low time. To obtain a better thickness distribution in less time, a two-stage strategy was proposed (D. Morales-Palma et al. 2017). It was shown that by introducing an intermediate stage, homogenization in the thickness distribution could be obtained.

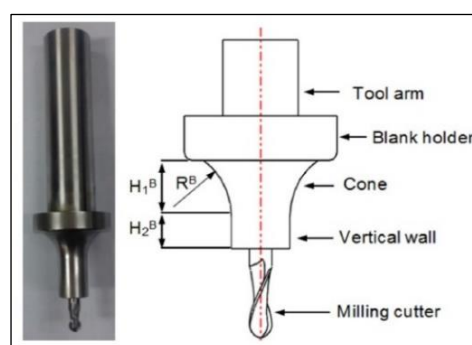
2.4 Tool shape and size in SPIF and SPIHF

In most of the research work on SPIF, the sphere head tool is used to deform the sheet metal. However, in many cases, a tool with a rotating ball attached at the end is used which is called a ball tool. In the ball tool, the ball can rotate freely during the forming and hence increases the friction. An experimental study on formability in SPIF showed that when the ball tool is used, the increased friction delays the occurrence of cracks (Y. H. Kim and Park 2002). However, it was also observed that too high friction cracks the sheet. Not only the shape of the tool, but the size of the tool also affects the geometrical accuracy and formability. The flat end tool and spherical head tool were used to form a conical shape and a comparative study was done (Kumar et al. 2019), the results showed that the spherical head tool gave better formability. The recommended size of the SPIF tool was suggested in a research work (G. Hussain et al. 2013). It was reported that for AA2024-O sheet material, the tool with a radius equal to two times its sheet thickness offered the highest suitability which can differ for different materials. In another study (Ghulam Hussain 2014), it was observed that the pillow at the bottom of the part formed by SPIF increased when a smaller tool with a radius

less than two times the thickness of the sheet was used. Moreover, the defects in the sheet increased and resulted in early failure. It was also reported (Jeswiet et al. 2005) that the forming forces increased when the larger diameter tool was used, hence formability increased with smaller tool size. However, different results are reported by various researchers. The effect of tool radius on the formability was analyzed in the experimental study using Al1060 and Al6061 sheet materials (Su et al. 2021). It was observed for the tool radius of 4mm, 5mm, and 6mm, that a higher wall angle was formed for a higher tool radius. The thinning increased and a higher forming limit was observed on the FLD when the bigger tool was used. Similar results were observed in an experimental study (Kumar et al. 2019), it was shown that formability was high for the tool with a larger diameter.



(a)



(b)

Figure 2.12 (a) Novel tooling for SPIF (Bambach, Voswinckel, and Hirt 2014), (b) New Featured Tool (Cao et al. 2016)

A new tooling setup was proposed to improve the geometrical accuracy of cylindrical flange formed by SPIF (Bambach, Voswinckel, and Hirt 2014). It was observed that when the conventional SPIF approach was used to form the flange, due to spring back the 90° wall angle was not formed, and the wall angle remained in the range of 82.5° to 83.5°. The proposed approach involved two tools simultaneously to form the flange (Fig.2.12(a)) which was overbent so that a 90° wall angle could be achieved. A new feature tool was developed to obtain uniform thickness distribution on the flange formed by SPIF (Cao et al. 2016). The tool comprised a milling cutter to cut the pre-cut hole on the sheet metal, a cylindrical section, and a hyperbolic section as shown in Fig.2.12(b). After cutting the pre-cut hole, the tool was moved from the inward to the outward direction to form the flange. It was observed that the flange formed by the newly featured tool was having uniform thickness distribution compared to the conventional SPIF tool. Also, the hole expansion ratio increased by 130%.

2.5 Indicator of formability in hole flanging

The available literature on hole flanging is about either cylindrical or square hole flanging. Few studies on complex flange shapes are available. An indicator of formability in hole flanging gives an idea about whether the required flange can be formed successfully without failure or not. To use the FFL for predicting the successful flange forming, it is required to perform strain measurement either by experiments or by FEA. In both cases, it is required to perform complex strain analysis. Hence, a simple indicator is a must to provide information about the formability and failure limit. It is evident from the literature (Chen et al. 2019; Cui and Gao 2010; G. Centeno et al. 2012; M. Borrego et al. 2016; Huang and Chien 2001), that flange forming depends on the pre-cut hole size. In an experimental study (Cui and Gao 2010), the effect of the pre-cut hole size was determined. Experiments were performed with different pre-cut hole diameter to form the cylindrical flange of 65 mm diameter. The results show that there is a specific diameter of pre-cut hole which can be defined as a critical pre-cut hole diameter. The pre-cut hole with a diameter greater than the critical diameter can be successfully deformed into the flange (of a specific diameter) without failure, and the pre-cut hole with a diameter less than the critical diameter fails before the flange is formed. The value of the critical pre-cut hole diameter varies and depends on the material, thickness of sheet, tool size and strategies used for forming. Flange. An indicator considering the final flange diameter and initial pre-cut hole diameter has been used to define the flange formability.

A hole expansion test has been used to test the hole flangability of the material which was represented by a “Hole Expansion Ratio” (Lee et al. 2007) calculated by equation 2.5.

$$\text{HER} = \frac{D_f - D_o}{D_o} \times 100 \quad (2.5)$$

Where D_f is the inside diameter of the flange at fracture in a hole expansion test, and D_o is the initial diameter of the hole. HER has been also represented by a fraction (Stachowicz 2008; Besong, Buhl, and Bambach 2019), which is the ratio of the final flange diameter to the initial diameter of the hole (equation 2.6).

$$\text{HER} = \frac{D_f}{D_o} \quad (2.6)$$

Further, the limiting criteria for flanging are defined as Limit Forming Ratio (LFR) (Silva, Bay, and Martins 2016; Petek and Kuzman 2012). The LFR is calculated by equation 2.7.

$$\text{LFR} = \left(\frac{D_f}{D_o} \right)_{\max} \quad (2.7)$$

The LFR can be calculated by performing a series of experiments either by considering a constant initial hole diameter and varying the final flange diameter or by a constant final flange diameter and varying the initial hole diameter. For example, an LFR of 1.46 is defined for AA7075-O sheets with 1.6 mm thickness based on experimental work carried out by varying the initial pre-cut hole diameter to form a cylindrical flange with an inside diameter of 95.8 mm (M. Borrego et al. 2016). The least pre-cut hole diameter which could be formed into a successful flange without failure was considered as D_f . It was also observed that, the minimum pre-cut hole to form the flange slightly decreased when a rotating tool (with 1000 rpm) was used. However, the difference was very small and was attributed to the intrinsic dispersion in the experimental tests and measures. The effect of tool radius was also evaluated and the results show that the LFR increased with increase in the tool radius. Further, it is observed that there is an inconsistency in the LFR measurement because with increase in tool radius, it should be decreasing whereas it increased as per the experimental results. This was attributed to the fact that LFR only accounts for the maximum strain at the hole edge, which is not the responsible strain in the SPIF. Hence, it was suggested that the non-dimensional flange height (h/d_f) should be used to indicate the formability.

2.6 Conventional hole flanging and SPIHF

Conventional hole flanging is carried out by a punch-die setup on the press. Unlike the local deformation in SPIHF, the deformation takes place on the whole contact area. Moreover, the failure is observed at the edge of the flange by unidirectional tension after necking (Huang and Chien 2001; Lee et al. 2007). The initial condition of the hole edge is also an important factor affecting formability. The effect of hole processing on the formability in hole flanging of hot rolled steel sheets was analyzed (Lee et al. 2007), two different processing conditions were considered; In the first process, the hole was made by punching and in the second process the hole was made by reaming. It was observed that higher formability was achieved on the hole made by reaming. Further, the flange formability was analyzed in an experimental study (Stachowicz 2008) performed on forming of deep-drawing steel sheets. It was observed that in conventional hole flanging, the flange formability depends on the punch geometry. Higher formability was achieved by the conical punch as compared to the cylindrical punch. It was also observed that formability improves with the higher strain hardening exponent and higher plastic anisotropy factor.

Further, the comparison between the formability limits of conventional forming and SPIF was given with an experimental investigations on AA1050-H111 sheet metal and Titanium grade 2 sheet metal (Silva et al. 2013). The FLC and FFL for the two materials were obtained by conventional forming tests. The fracture strain values for truncated conical shape formed by SPIF were plotted on the major-minor strain space and it was observed that the values were in good agreement with the FFL. Moreover, cylindrical flanges were formed by SPIHF and the conventional forming process. The hole flanging of Titanium grade 2 sheets resulted in earlier fracture than the conventional hole flanging process. Similar results were obtained for AISI304 material (Montanari et al.). It was observed that the pre-cut hole diameter which could not be formed into the flange in SPIHF was possible to form into a flange without a crack in conventional forming. Another comparative study between stretch bending and SPIF was carried out on AISI 304 steel sheet metal (Gabriel Centeno et al. 2014). Cylindrical tools (20 mm and 10 mm diameters) were used to deform the sheet with stretch bending, and SPIF tools (20 mm, 10 mm, and 6 mm diameters) were used to deform the sheets with incremental sheet metal forming. It was observed that higher formability was achieved by SPIF. A comparative study between the conventional hole flanging and SPIHF in terms of the

geometric accuracy of the flange was carried out using cold-rolled mild steel sheets (Voswinckel, Bambach, and Hirt 2015). It was observed that SPIHF offered high formability as compared to conventional hole flanging. However, a bulge was formed on the flange in SPIHF which reduced the geometric accuracy. An adaptive blank holder was used to resolve the problem of bulge formation. A study on the strain analysis on the flanges formed by SPIHF and conventional press work on AA7075-O material was performed (Marcos Borrego et al. 2020). The results showed that more stretching in the meridional direction occurred at the mid-zone of the flange formed by SPIHF, whereas the conventionally formed flange was shorter. However, the latter was having more uniform thickness distribution. The LFR of 1.55 and 1.57 was obtained by conventional forming and SPIHF respectively, which shows only a slight increase in the formability. However, the height of the flange increased by 37% and thinning by 100% in SPIHF.

Mostly the research works on SPIHF has been carried out on aluminum alloys, steel, and titanium sheet metals, however, studies are available on SPIHF of polymer materials like Polyethylene Terephthalate (PET) also (Valentino A.M. Cristino et al. 2015; Silva, Martinho, and Martins 2013). These results suggest that for polymer materials, higher formability is observed compared to conventional forming.

It is clear from this literature about the comparison between conventional forming and SPIHF that the claim of higher formability in SPIHF is not true for all materials. In ductile materials like aluminum, the necking is suppressed in SPIHF and the FFL remains at a distance from the FLC, hence higher formability is achieved. But in the materials like titanium and AISI304 steel, the same is not true. Hence, the advantage of high formability by SPIF and SPIHF is material dependent.

2.7 Forces acting on the sheet metal during SPIF and SPIHF

The forming forces acting on the sheet material during the SPIF process were analyzed in an experimental study (Ambrogio, Filice, and Micari 2006). Two deformation mechanisms are acting during the SPIF that is bending and stretching. The force trend showed that the force increases with the progress in the forming process, achieves a peak, and then varies as per different forming conditions. The bending remained the dominating mechanism until the peak in the force, after which stretching of the material began.

The trend of force after the peak could have three different variations as shown in Fig.2.13. if the wall angle is small, a steady state curve (SSc) was observed. The effect of material thinning was compensated by strain hardening. 2) if low-strength materials are deformed with high parameter values, then a polynomial curve (Pnc) was observed. After the peak, a low negative gradient was observed due to the large thinning. After a certain depth, an equilibrium between stretching and strain hardening was achieved and a steady forming force was observed. 3) if the material formability is low or the forming conditions are extreme, a monotonically decreasing curve (MDc) was observed. After the peak, equilibrium conditions were not achieved and the material failed.

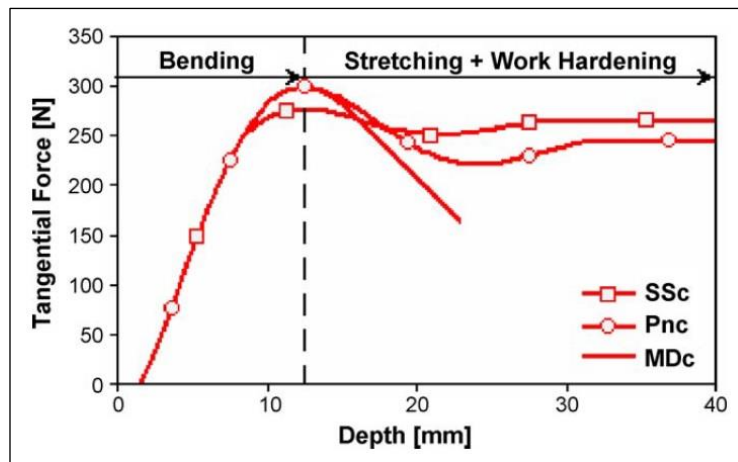


Figure 2.13 Force trends during SPIF

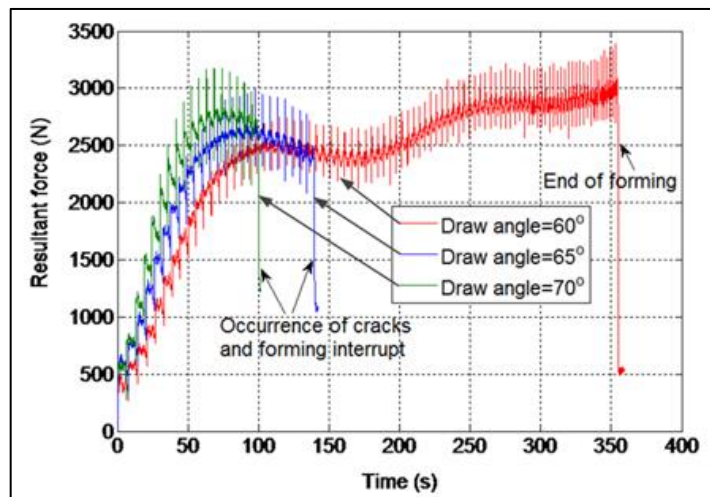


Figure 2.14 Resultant force during the forming of truncated conical shape with different draw angles (Liu, Li, and Meehan 2013)

There is an influence of the draw angle, the sheet thickness, and the step-down size (step-depth), on the forming forces. The same was evaluated in an experimental study on AA 7075-O sheet material (Liu, Li, and Meehan 2013). The force measurement was done by a sensor mounted on the SPIF tool. To study the effect of the draw angle, truncated cones were formed with different draw angles (60° , 65° , and 70°) using a sheet with 1.6 mm thickness. The truncated cone with a 60° draw angle was formed successfully, and the sheet failed for the other draw angles. It is observed in Fig.2.14 that for the truncated cones with 65° and 70° , the force increased initially, a peak was achieved and cracks appeared and then the force decreased. The maximum force value increased as the draw angle increased, also the crack happened earlier for the higher draw angle. For the draw angle of 60° , the force increased initially, then decreased, and again increased a little till the end of the forming. The effect of the sheet thickness and the step-down size was evaluated by forming a pyramidal shape on three sheets with different thicknesses (1.02 mm, 1.60 mm, and 2.54 mm), with three step-down sizes (0.5 mm, 1.0 mm, and 1.5 mm). The results showed (Fig.2.15) that the vertical forming force increased with an increase in sheet thickness and the same has been observed with an increase in the step-down size.

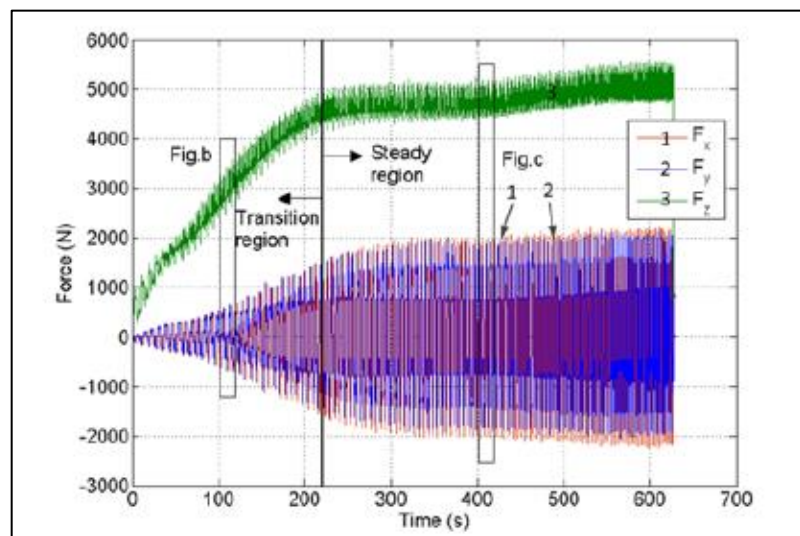


Figure 2.15 Three-axis forces during forming of a truncated pyramid(Liu, Li, and Meehan 2013)

The forming forces acting during the single-stage cylindrical hole flanging were evaluated in an experimental study (M. Borrego et al. 2016). The forces acting during the forming by a

non-rotating tool and a rotating tool were measured and analyzed. The non-rotating tool was locked and not able to rotate freely during the forming process. It is observed in Fig.2.16 that the vertical force is higher than the horizontal force for the non-rotating tool and the rotating tool both. Also, the force decreases when the rotating tool is used. Initially, the vertical force increases, and then after achieving a peak, it decreases and reaches zero at the end of the flange forming.

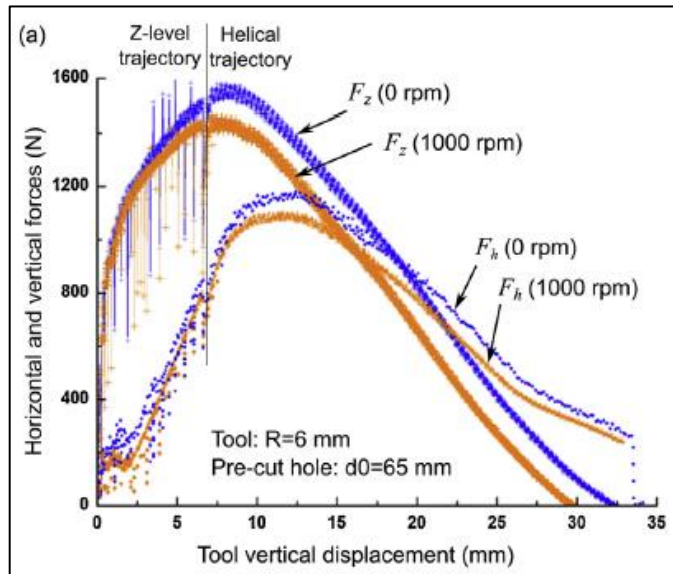


Figure 2.16 Vertical and Horizontal forces acting during the single-stage cylindrical hole flanging using a non-rotating and rotating tool (M. Borrego et al. 2016)

2.8 Precut hole geometry and flange shape

Most of the hole flanging studies are about forming a flange on a circular hole. The shape of the hole flange wall is majorly either conical or straight (G. Centeno et al. 2012; V. A. Cristino et al. 2014; Silva, Martinho, and Martins 2013). Few studies are performed on the flange forming on a square hole (V. A.M. Cristino et al. 2015) or complex hole shape (Silva, Bay, and Martins 2016). In their experimental study, square flanges were formed with a multistage strategy (V. A.M. Cristino et al. 2015). Different pre-cut hole sizes and corner radii were used in the experiments. The deformation mechanism was analyzed by measuring strain values after each stage of forming using a circle grid. The strain distribution was analyzed at different places on the formed flange as shown in Fig.2.17.

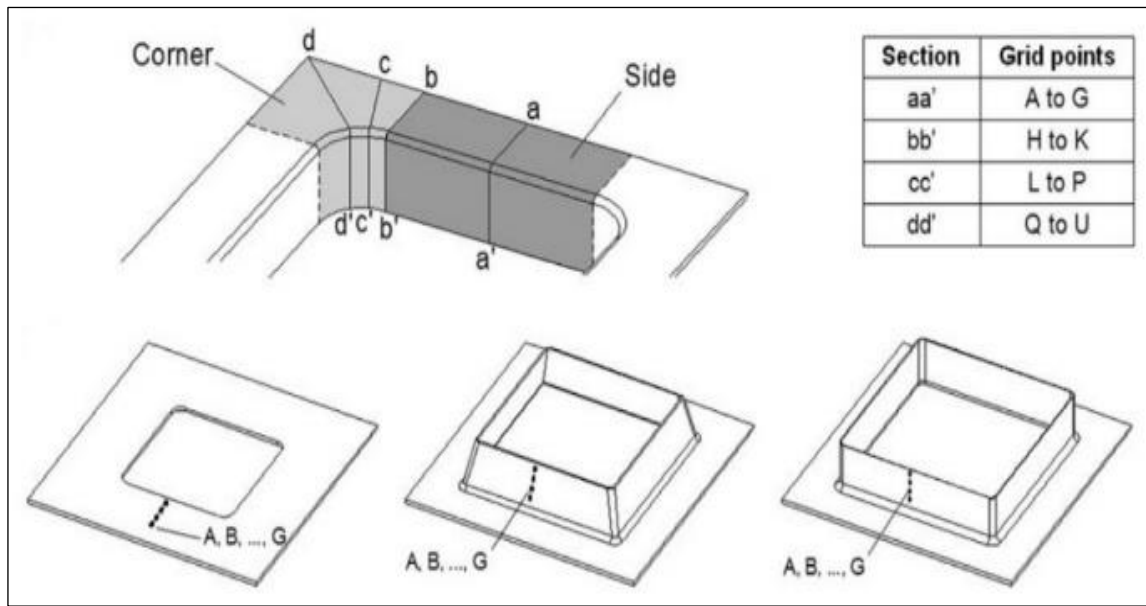


Figure 2.17 Different regions to analyze strain distribution on the square flange (V. A.M. Cristino et al. 2015)

The thickness reduction at the middle of the wall on the successfully formed flange was 27% with strain values far below the FFL and a high thickness reduction of 52% was observed in the surrounding of dd' with biaxial strain condition, Further, high thickness reduction of 61% was observed along cc'. The failure was observed when the precut hole size was such small (short square length/small corner radius) that could not withstand the high amount of stretching. On the failed flange, it was observed that the crack was between the cc' and dd'. It appeared in the meridional direction and open to the edge, which shows that high circumferential stress was responsible for the failure. A thickness reduction of 82% was observed near the crack. The strain plots revealed that the failure was due to the combined effect of high uniaxial tension at the cc' and high biaxial stretching at the middle of the flange at dd'. Moreover, the flange could be formed with straight walls (wall angle of 90°) for a larger corner radius but not with a smaller corner radius. In another study by (Silva, Bay, and Martins 2016), a complex shape flange (on a precut hole with a combination of a square and a circular flange) shown in Fig.2.18 was formed by multistage strategy. It was observed that the straight flange (90° wall) could not be formed successfully and the flange failed for a wall angle of more than 80°. The strain analysis showed that the flange failed at the middle of the corner for smaller radius values and at the merging of the straight wall and round corner for the larger radius values.

It is clear from the discussion above that the strain modes are different in square flange forming and cylindrical flange forming. However, in both cases, it was observed that the necking was suppressed. Moreover, it was concluded that the failure can be prevented by changing the length and/or corner radius of the precut hole.

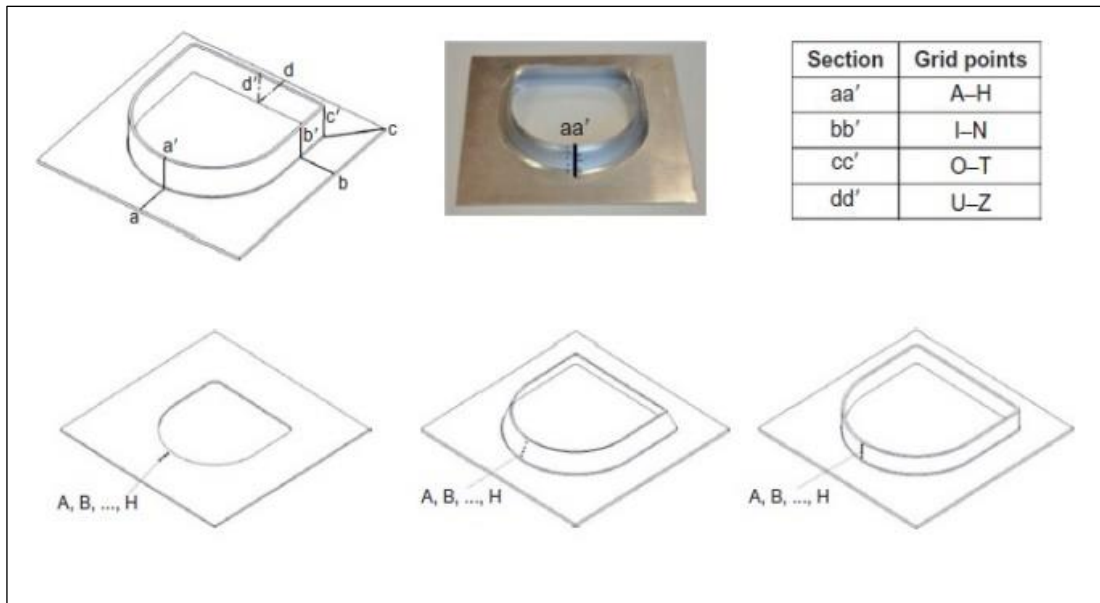


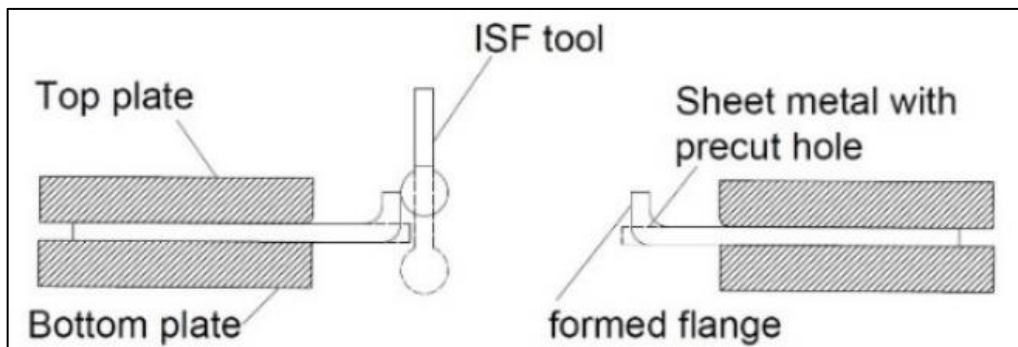
Figure 2.18 A complex shape flange and different regions on it (Silva, Bay, and Martins 2016)

2.9 Tool paths and strategies of SPIHF

The process of hole flanging can be carried out in a forward or backward direction. In forward hole flanging, the SPIF tool is moved in the downward direction incrementally to form a flange whereas, in backward hole flanging, a ball tool is moved in the upward direction incrementally such that the flange is formed at the top of the sheet (Petek and Kuzman 2012). It is required to use the backward hole flanging technique to form flanges on parts like the one shown in Fig.2.19. Further, the hole flanging can be carried out using a multi-stage strategy (Cui and Gao 2010; Yan et al. 2021) and a single-stage strategy. Various methods of multistage strategy (Fig.2.20) as explained in section 2.3 were implemented. Sets of experiments with different precut hole diameters were performed to find the LFR for the three multistage strategies. It was concluded that forming the final flange by increasing the diameter (Strategy 1 in Fig.2.20) in every stage, gives the highest LFR.



(a)



(b)

Figure 2.19 (a) Backward flange on a part (Petek and Kuzman 2012), (b) Backward SPIHF

A single-stage method of forming a straight flange is also explored by researchers (M. Borrego et al. 2016; Martínez-Donaire et al. 2019; Besong et al. 2020; Martínez-Donaire et al. 2017). The advantage of the single-stage method is that it decreases the forming time as well as the complexity of the tool path. There are two possible tool paths to form a straight cylindrical flange. The first tool path is a helical tool path, in which the tool is initially moved to a required position such that it just touches the top surface of the sheet. Then, the tool continuously travels in the downward direction following a helical path with a defined step depth. The second tool path is a circular tool path with linear increments in step depth. In this case, initially, the SPIF tool is kept just above the sheet at a required position. Then the tool is traversed in the downward direction for a distance equal to the step depth followed by traveling on a circular path. Once the tool comes back to the initial position, it is again traversed downward to take the step depth. This motion is repeated to form the flange. The drawback of the circular tool path is that the vertical force in the downward direction

increases suddenly while the tool goes down for the step depth distance (M. Borrego et al. 2016), which also leaves a scratch mark at the place of step depth. Because of these reasons, the helical tool path is recommended.

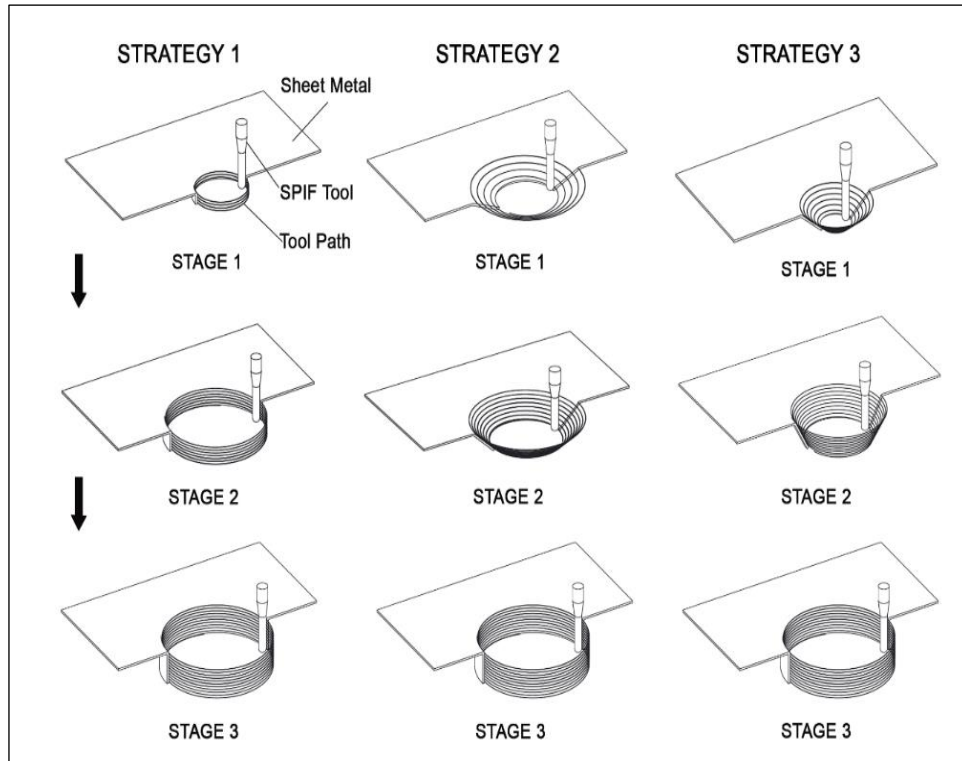


Figure 2.20 Multistage strategies for forming a straight cylindrical flange

As discussed in section 2.4, it is observed that a multi-stage strategy results in higher formability and better thickness distribution as compared to the single-stage method. To reduce the trade-off and improve the formability and thickness distribution with less process time than the multi-stage method, a two-stage flanging method was proposed (Domingo Morales-Palma et al. 2018; D. Morales-Palma et al. 2017). It was observed by analysing the thickness distribution on the flange formed by single-stage that high thinning took place at the middle of the flange, which was called the critical zone. While forming the flange when the tool reaches the middle, it has to overcome the resistance of the flat undeformed portion of the sheet metal. Hence, the material is stretched radially, which is responsible for high thinning. The two-stage method involved an intermediate stage with the shape shown in Fig.2.21, which reduced the pressure on the sheet in the middle zone and resulted in better thickness distribution.

Most of the research work on SPIHF has been carried out using a single-point incremental forming method, however, a Double Sided Incremental Forming (DSIF) method has been also implemented (Zhang et al. 2016). In the DSIF, a supporting tool traverses on the back side of the sheet-metal which acts as a blank holder. In this method, the front blank holder is not required. The DSIF can be carried out using the three different strategies. These strategies are similar to the strategies shown in Fig 2.20, the difference is the support provided by a tool at the back of the blank. With the DSIF method, the process becomes more flexible.

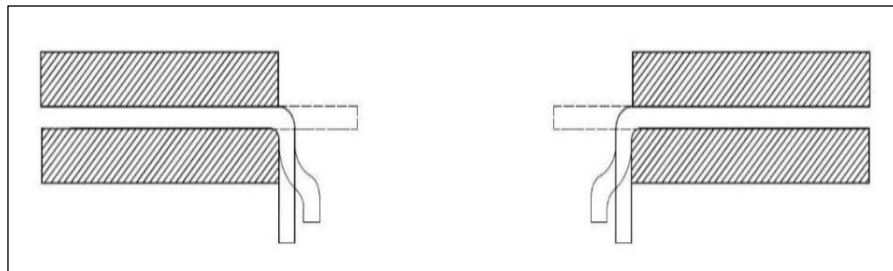


Figure 2.21 Two-stage method of SPIHF (D. Morales-Palma et al. 2017)

2.10 Process parameters and their effects

The process parameters involved in the SPIF and SPIHF process are tool size, tool rotation speed (spindle speed), feed rate, and step depth. The quality of the flange is represented by thickness distribution along the flange, the surface finish of the internal surface of the flange, and geometric accuracy.

2.10.1 Spindle speed

The SPIF and SPIHF can be performed by a non-rotating tool and a rotating tool both. When the rotating tool was used in SPIF, the friction between the sheet and the tool increased which increased the formability (Y. H. Kim and Park 2002). The tool rotation also affects the tangential force (Eyckens et al. 2010). It was observed that both the vertical force and horizontal force decreased when a rotating tool was used (Durante et al. 2009). Further, it was also observed that when the tool rotation speed was increased (up to 600 rpm) the temperature increased by three times compared to the case of the non-rotating tool. Similar observations were also made in other experimental studies (Kumar et al. 2019; Khalatbari et al. 2015; Yoganjaneyulu, Sathiya Narayanan, and Narayanasamy 2018), the high spindle speed

resulted in increased formability. Moreover, it is logical that the tool rotation affects the surface quality of the part formed. It was observed that a better surface finish was obtained when a rotating tool was used. The rotating tool decreased the forming force in SPIF and it was marked as an important factor for the formability (Gabriel Centeno et al. 2014). Further, the tool rotation also has effect on the hardness of the sheet material. In an experimental study (Najm et al. 2021), it was observed that the rotating tool stretched the sheet material in a cold working condition. The cold working deforms the grain structure of the sheet material and increased the hardness. The effect of spindle speed in cylindrical hole flanging by SPIF was analyzed in an experimental study (M. Borrego et al. 2016). The results revealed that the rotating SPIF tool (1000 rpm) gave better thickness distribution than the non-rotating SPIF tool. The rotating SPIF tool reduced friction and increased the temperature of the sheet and hence the forming forces reduced. Further, it also resulted in a better surface finish of the inside flange surface.

2.10.2 Feed rate

The feed rate in SPIF is the speed at which the tool traverses. It affects the processing time; a higher feed rate decreases the processing time to a great extent. Moreover, S.Najm et al (Najm et al. 2021) have reported that as the feed rate increased the hardness of the material increased in SPIF. In a parametric study, it was observed that feed rate was the least effective parameter to surface roughness (Baruah, Pandivelan, and Jeevanantham 2017). In another study, it was concluded that the feed rate had no undesirable effect on SPIF (Khalatbari et al. 2015). However, in an experimental study on SPIF of platinum sheet material (G. Hussain, Gao, and Hayat 2009), it was observed that a very high feed rate is unfavorable.

2.10.3 Step depth

In the case of the helical tool path, the step depth is the pitch of the helix and in the case of the circular tool path, it is the distance the tool travels in the downward direction at the end of each circular pass. It is the most influential parameter in the SPIF (G. Hussain, Gao, and Hayat 2009). It was observed in a research work (Y. H. Kim and Park 2002) that for three values of step depth (0.1 mm, 0.3 mm, and 0.5 mm), the high step depth resulted in high formability. The same observations were reported in another literature also (Liu, Li, and Meehan 2013) in the SPIF of truncated pyramidal shape, it was also observed that the vertical forming force increases with an increase in step depth. However, it was reported in a study

that higher step depth reduced the formability and increased surface roughness (Jeswiet et al. 2005). Also, in an experimental study (Khalatbari et al. 2015), it was observed that high step depth resulted in an intensification of forming forces. Hence, smaller step depth offered higher formability. Similar results were reported in another literature as well (Kumar et al. 2019), for step depths of 0.2 mm, 0.5 mm, and 0.8 mm.

2.11 Geometric Accuracy

The geometric accuracy of the part formed by the SPIF has been a challenge. The SPIF tool path is generally defined from the geometric information specified by the CAD model. If the tool path is followed without any correction, the tool tries to deform the sheet as per the desired shape. However, this would only be possible if the material would be deformed by pure plastic deformation. It is well understood that elastic deformation causes the spring back effect and introduces inaccuracy. A solution was proposed, in which initially the part was formed by the SPIF method following the CAD model (Hirt et al. 2004). Then, the part was measured by the Coordinate Measuring Machine, and from these measurements, the corrected coordinate values were defined. The coordinate values obtained by this method were then used to deform the metal to get the desired shape. A method was proposed to evaluate the spring back experimentally (Vahdati, Sedighi, and Khoshkish 2010). It was concluded in their study that the spring back can be reduced by high spindle speed, high feed rate, larger tool, thicker sheet, and smaller step depth. A study on the geometric error in the SPIF of the truncated cone shape was carried out (Essa and Hartley 2011). Three major geometric deviations were observed which were the bending of the sheet at the top, spring back at the bottom of the wall, and pillow effect at the bottom flat surface center. Different strategies were suggested to improve the geometric accuracy, which included a corrected tool path and the use of a support tool. It was observed that by providing support, the spring back could be reduced. Also, an extended tool path was implemented, in which the tool was traversed on the bottom flat surface. The extended tool path reduced the pillow effect.

The geometric accuracy in hole flanging is an important parameter representing the flange quality, it is defined by the closeness of the formed flange shape with the desired shape of the flange. For straight-hole flanging, the straightness of the flange wall represents geometric accuracy. For cylindrical flange, it can be quantified by measurement of the internal and

external diameter of the flange at regular intervals along the flange height or by performing a 3D scanning of the flange and comparing the same with the desired profile.

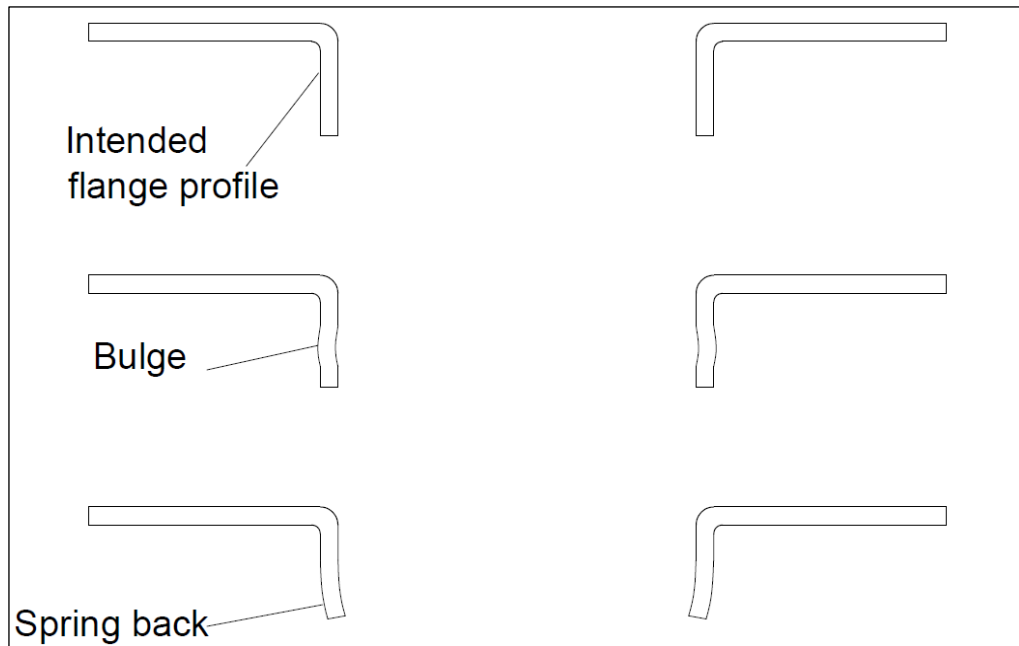


Figure 2.22 Geometric defects in SPIHF

2.12 Summary of literature review and objectives of the present work

SPIHF is a novel and cost-effective technique to form flanges of different shapes on sheet metal parts. The deformation of the sheet material in SPIHF takes place without necking. Hence, the FFL gives the correct representation of the formability instead of FLC. In ductile materials like aluminum, the FFL for SPIHF remains far from the FLC for conventional forming; which shows that higher formability than conventional hole flanging is achieved by the SPIHF. However, for some materials (Titanium), the FFL is not very far from the FLC. This shows that higher formability in SPIHF is material dependent. The deformation in SPIHF takes place locally in the vicinity of the tool similar to the conventional SPIF. However, due to the presence of a precut hole, the strain distribution is different than what is observed on the conical or pyramidal shapes formed by SPIF. It was shown in literature (Martínez-Donaire et al. 2019) that the FFL for SPIF and SPIF was different. Hence, a method to obtain FFL for SPIHF should be established.

The majority of the literature on cylindrical hole flanging is carried out using the multistage method which increases the operation time. A detailed study on single-stage SPIHF (cylindrical flange forming) is available (M. Borrego et al. 2016), however, there is no comparative study between the multistage and single-stage SPIHF on a common material. It is required to carry out a such study to understand the advantages and limitations of both approaches. Further, most of the available studies on the SPIHF are focused on the cylindrical hole flanging, there are few studies carried out on square and complex shape flange forming. In the available literature about square flange forming(V. A.M. Cristino et al. 2015), the multistage method was used. However, the same could be done by a single-stage method to reduce the operation time. Hence, a detailed study on the single-stage square hole flanging should be carried out. Moreover, the use of a high feed rate should be explored to reduce the operation time. The Limit Forming Ratio, strain distribution, and thickness distribution should be analyzed to study the formability. Further, the effect of the corner radius on the formability should be evaluated. As observed in the literature, tool rotation has a major effect on the surface roughness and formability, hence, the same should be studied for the single-stage square hole flanging.

As discussed, the SPIF and SPIHF are advantageous for ductile materials like aluminum. Aluminium sheet metal has wide industrial applications as mentioned in Chapter 1. Hence, the application of SPIHF for aluminum sheets should be explored. However, the strength of the aluminium parts has a limitation in comparison to steel. The grain refinement of the material increases the hardness and because of this reason, many research works have been carried out on different methods of achieving grain refinement. The grain refinement in SPIF can be obtained by implementing ultrasonic vibrations, but the complexity of the setup takes away the key advantage of SPIF which is a simple setup. The methods of achieving grain refinement by mechanically induced vibrations are explored by researchers. However, still, there is a scope to improve the method and also a detailed analysis of the strain distribution, thickness distribution, height of the flange, and surface quality of the flange is required. Moreover, the implementation of a mechanically induced vibration technique in a single-stage SPIHF should be explored.

To analyse the formability of aluminum alloy in single-stage SPIHF of the cylindrical and square flange, the following research objectives have been addressed in this study.

1. To study the effect of tool diameter on the Limit Forming Ratio, thickness, and height of cylindrical flange in single-stage SPIHF.
2. To investigate the Limit Forming Ratio, the thickness of the flange, the height of the flange, and strain distribution on the cylindrical flange in single-stage and multi-stage SPIHF.
3. To study the effect of process parameters (spindle speed, feed rate, step depth) on the flange quality in single-stage SPIHF of the cylindrical flange.
4. To obtain the experimental Fracture Forming Limit line for SPIHF.
5. To investigate the formability of aluminium alloy in single-stage SPIHF of the square flange.
6. To improve the hardness of aluminium alloy by achieving grain refinement with a novel tool in single-stage SPIHF of the square flange.

The next chapters will give details of the research work carried out to achieve the above-mentioned objectives.

Chapter 3 Development of setup and preliminary experiments

In this chapter, the methodology to carry out an experimental study on the effect of tool diameter on the Limit Forming Ratio, thickness, and height of flange has been described for SPIHF of cylindrical flange. Moreover, the results are analyzed. Further, the results and analysis of a comparative study between single-stage and multistage SPIHF of cylindrical flange have been presented.

3.1 Material and Methods

This section describes the details of the material used in the study, their mechanical properties, and methods adopted to perform the experimental study.

3.1.1 Materials

To initiate the experimental study, it was decided to use the general grade aluminium material. Hence, the preliminary experiments were conducted using AA1050 sheet metal with 1.5 mm thickness. The chemical composition of the material is shown in table 3.1 and its mechanical properties are shown in table 3.2. It is a metal with 99.5 % aluminum, which is used in applications like food containers, chemical processing plant equipment, architectural work, light reflectors, etc.

Table 3.1 Chemical composition of AA1050 material used in the study

Si	Fe	Cu	Mn	Mg	Zn	Ti	Cr	Ni	Pb	Al
0.120	0.170	0.004	0.041	0.041	0.027	0.012	0.002	0.004	0.001	Balance

It is well known that AA5052-H32 alloy is used in marine applications where various forming operations including flange forming are required (example: parts of a boat hull shown in Fig.1.1). Hence the further experimental study was carried out on AA5052-H32 sheet metal with 1.5 mm thickness. It is an aluminum-magnesium alloy with high corrosion resistance

and good strength. The chemical composition of the alloy is shown in table 3.3 and its mechanical properties are shown in table 3.4.

Table 3.2 Mechanical Properties of AA1050 material used in the study

Orientation with the Rolling direction	Yield Strength (N/mm ²)	Ultimate Tensile Strength (N/mm ²)	Elongation %
0°	134.200	148.267	11.0
45 °	134.185	151.225	11.2
90 °	135.449	148.148	11.7

Table 3.3 Chemical composition of AA5052-H32 material used in the study

Si	Fe	Cu	Mn	Mg	Zn	Cr	others	Al
0.25	0.4	0.1	0.1	2.8	0.1	0.15	0.15	Balance

Table 3.4 Mechanical properties of AA5052-H32 material used in the study

Orientation with the Rolling direction	Yield Strength (N/mm ²)	Ultimate Tensile Strength (N/mm ²)	Elongation %
0°	196.45	265.17	14.38
45 °	194.67	254.79	14.1
90 °	197.38	271.80	14.6

3.1.2 Experimental setup

The experimental setup for SPIHF includes a top holding plate and a bottom holding plate between which the sheet metal is held firmly. These steel plates were clamped to the work table of the Vertical Machining Center as shown in Fig.3.1.

An opening with the required shape of the flange was provided on both the holding plates i.e., if a cylindrical or conical flange was to be formed then a circular opening was provided, and if a square or pyramidal flange was to be formed then a square opening was provided. A hemispherical-headed tool was used to deform the sheet. Three such tools with diameters 8mm, 10mm, and 12mm (Fig.3.2) were used to analyse the effect of the tool diameter. The tools were made of EN31 material which was hardened and tempered.

3.1.3 Limit Forming Ratio

The Limit Forming Ratio (LFR) for cylindrical hole flange is defined as described in section 2.5. The LFR could be found by performing a series of experiments either by varying the precut hole diameter to form a flange with a fixed diameter or by varying the final flange diameter keeping the precut hole diameter fixed.

In this work, the LFR was obtained by varying the precut hole diameter to form a successful flange of 58 mm diameter (Fig.3.3). The least precut hole diameter which could be formed to a straight cylindrical flange without any failure was considered to be the critical diameter and the LFR was calculated considering the same. To find the effect of tool diameter on the LFR, experiments with three different tools (ϕ 8 mm, ϕ 10mm, and ϕ 12 mm) were performed to form the flange in a single stage following the experimental procedure explained above. The experiments were performed with a non-rotating tool, a feed rate of 300 mm/min, and a step depth of 0.5 mm.

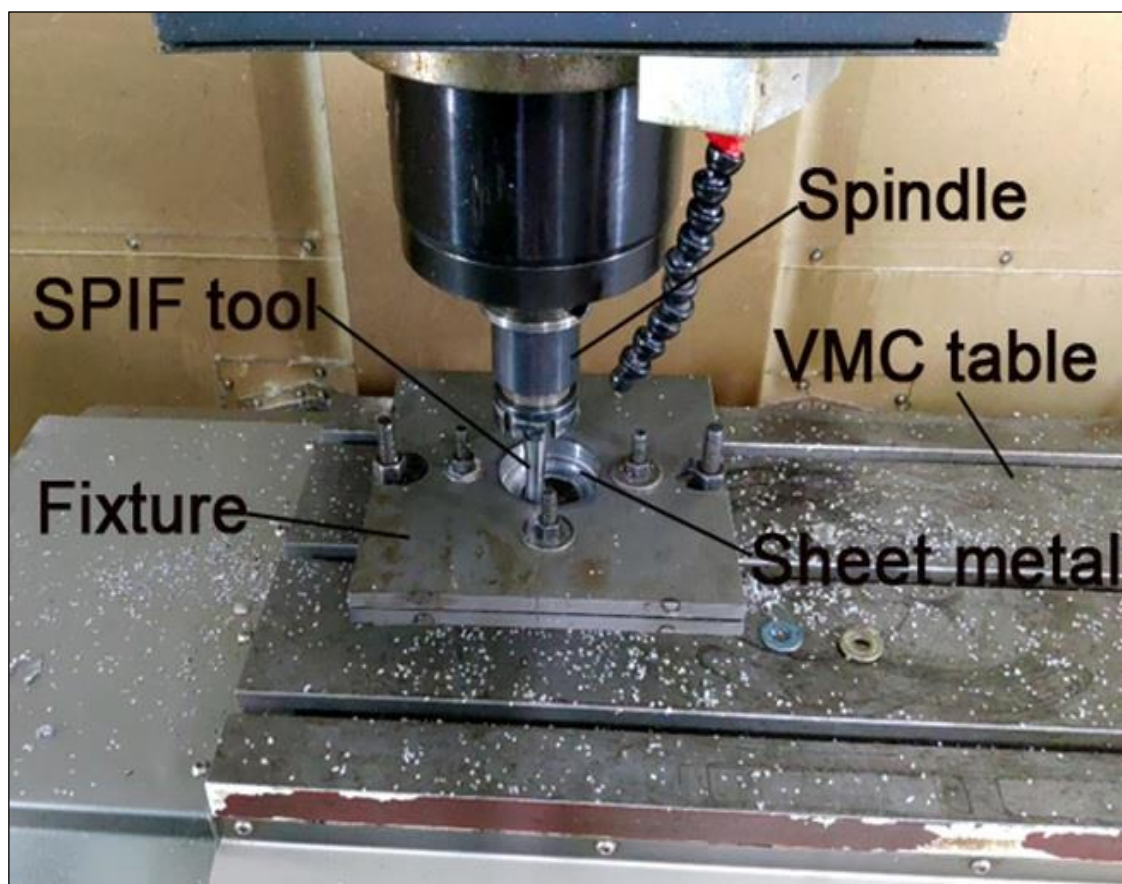


Figure 3.1 Experimental Setup

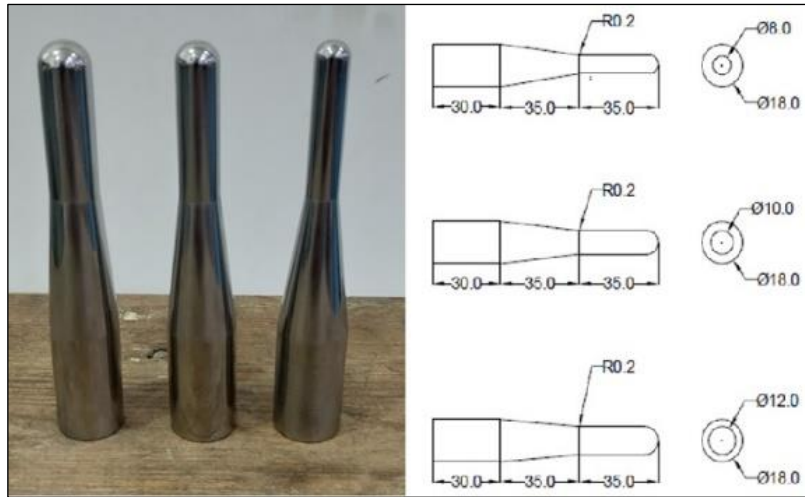


Figure 3.2 SPIF tools

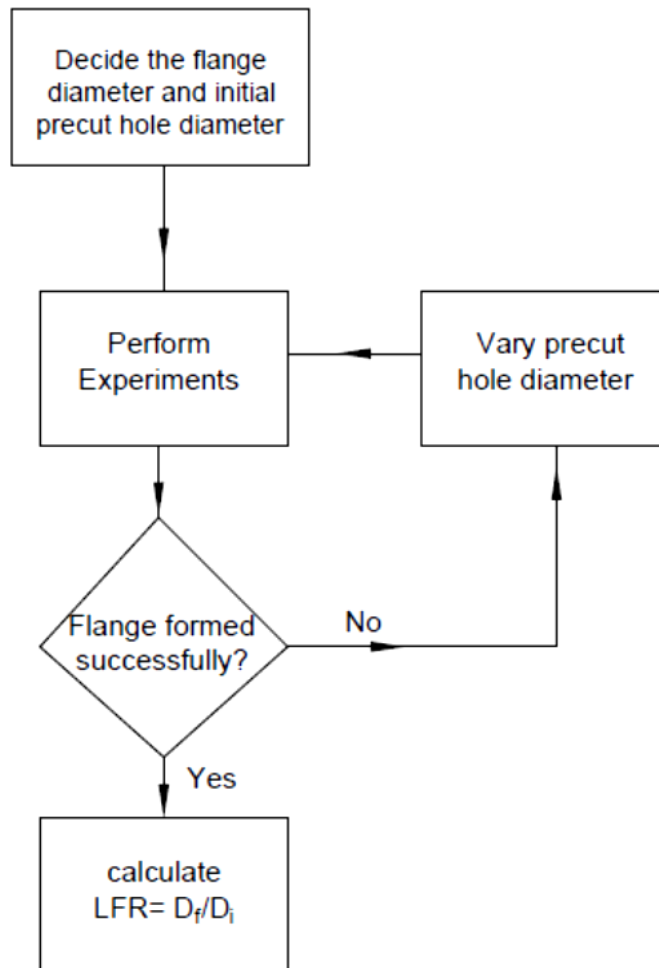


Figure 3.3 Experimental procedure to find the LFR

3.1.4 Single-stage and multistage strategy of SPIHF

The single-stage and multistage strategy of SPIHF is explained in section 2.8. In this work, a similar single-stage strategy was used in which the tool was initially moved to the X and Y coordinate values as per the required final flange diameter and to the Z value so that the tool remains just above the surface of the sheet metal. Then, the tool was traversed on a helical path to form the cylindrical flange. Also, a multistage strategy was used to form the same cylindrical flange. The best strategy out of the three as discussed in section 2.8, was selected. The single-stage and multistage strategies used in this work are shown in Fig.3.4.

3.1.5 Strain measurement by circle grid method

The measurement of strain was required to analyze the deformation of sheet material. The circle grid method was used for the same. A grid of circles with a 1 mm diameter (Fig.3.5) was engraved on the aluminum sheets by laser engraving before the SPIHF process. After the forming process, the circles deformed to the ellipses were used to measure the strain value. The major axis length of an ellipse was used to calculate the major strain and the minor axis length to calculate the minor strain. The measurements were carried out by a microscope connected with an image analyzer software. The following equation was used to calculate the strain values.

$$\text{Major /Minor Strain} = \frac{\text{Major/Minor Axis length}-\text{Circle Diameter}}{\text{Circle Diameter}} \quad (3.1)$$

3.1.6 Measurement of the thickness of the flange, the height of the flange, and the surface roughness on the inner surface of the flange

To analyze the thinning of the sheet during the flange-forming process, it was required to measure the thickness of the flange and the height of the flange. The thickness of the flange was measured at four locations on the flange as shown in Fig.3.6 and the average values were considered. To understand the thinning on the flange, the thickness distribution was obtained by measuring the thickness along the flange from the root of the flange to the edge, at an interval of 1 mm. To take accurate readings, a digital pointed anvil micrometre was used. The minimum thickness obtained by the measurement was considered to calculate the thinning percentage.

The height of the flange was measured by a vernier height gauge (Fig.3.7). The readings were taken at four points on the edge of the flange and the average value was defined as the height of the flange. To analyze the surface quality of the formed flange, the surface roughness on the inner surface of the flange was measured by a surface roughness tester Mututoyo SJ-210 with least count of 0.001 μm . The Ra values were measured at four places on the surface and the average value was considered.

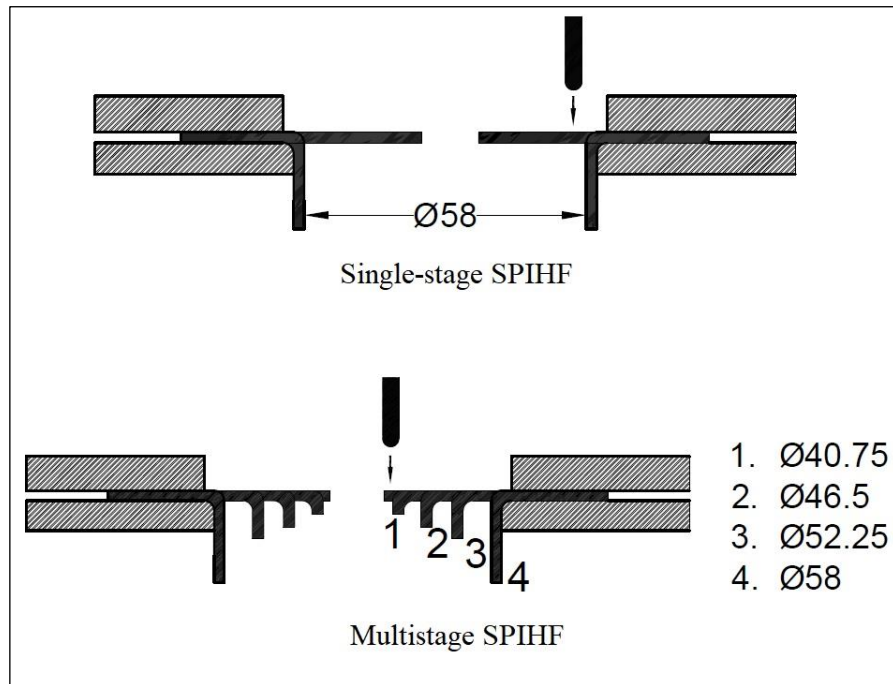


Figure 3.4 Single-stage and Multistage strategies used in this work

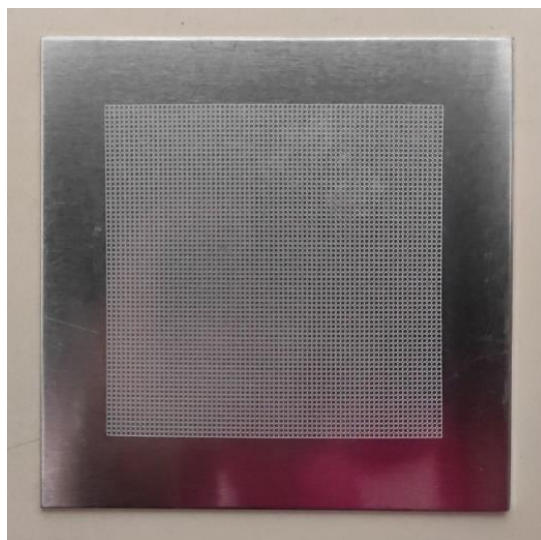
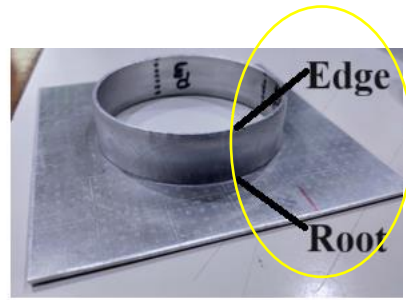


Figure 3.5 Circle grid engraved on the aluminum sheet



(a)



(b)

Figure 3.6 (a) Pointed anvil micrometer and (b) the marked locations on the flange



(a)



(b)

Figure 3.7 (a) Height measurement by vernier height gauge, (b) surface roughness measurement

3.2 Results and discussion

The results obtained by following the methodology explained in the previous section are analyzed and presented in this section.

3.2.1 Experiments to find LFR

To find the LFR in SPIHF of the AA1050 sheet material, experiments were performed as explained in section 3.1.3 with three tools of different diameters (8 mm, 10 mm, and 12 mm). The thickness and the height of the flanges with the critical precut hole diameter were measured. The least precut hole diameter which could be formed into a successful flange without failure was found for each of the three tools. It was observed for the tool of 8 mm diameter (T_8) that the flange with a precut hole diameter of 37 mm could be formed into the flange but the flange with a precut hole diameter of 36 mm failed before the straight cylindrical flange could be formed. Similarly, for the tools of 10 mm (T_{10}) and 12 mm diameter (T_{12}), the critical precut hole diameter was 34 mm and 32 mm respectively. The flanges formed by these tools are shown in Fig.3.8.

As per the definition of LFR given in section 2.5, the LFR for the three tools was calculated. It was found to be 1.56, 1.70, and 1.81 for the T_8 , T_{10} , and T_{12} respectively as summarised in table 3.6. It was observed that higher formability was obtained by the tool with a larger diameter. This can be attributed to the larger contact area between the tool and the sheet in the case of a large-diameter tool. Due to the increased area, the amount of local deformation in the contact zone was reduced. Hence, the stretching of the material was less and bending was the dominating mechanism of deformation.

Table 3.5 LFR obtained by the three tools

Tool diameter (mm)	Critical precut hole diameter (mm)	Limit Forming Ratio
12	32	1.81
10	34	1.70
8	37	1.56
*Critical precut hole diameter is the least diameter which can be		

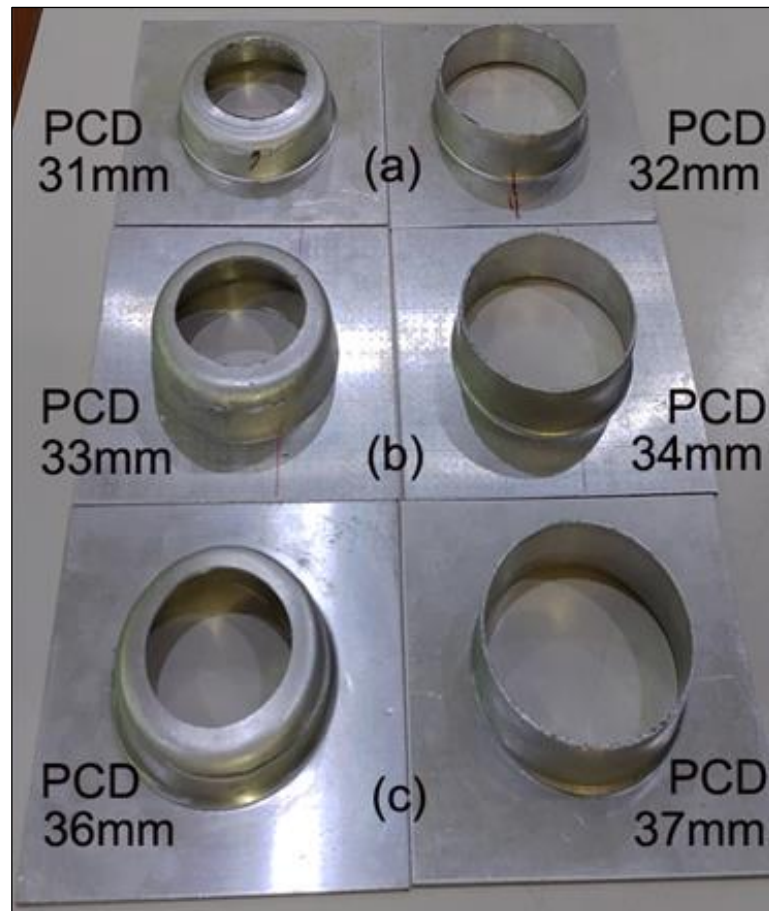


Figure 3.8 Flanges formed by SPIF tools with the diameter (a) 12 mm, (b) 10 mm, (c) 8 mm

The thickness distribution on the successfully formed flanges is shown in Fig.3.9. It is observed from the plots that, the thickness on the flange reduced from the root to the middle zone of the flange, and then increased towards the edge. The distribution of thickness was similar to what was observed in the literature (Cui and Gao 2010; Borrego et al. 2016). The resistance to the flow of the material in the flat zone was responsible for higher thinning in the middle zone. Due to the resistance, the stretching of the material was high in the middle zone. As soon as the flat portion was deformed, the stretching of the material reduced, and hence in the lower zone of the flange higher thickness was achieved. It is visible in the plot that thickness of the flange was more when the larger tool was used, which shows that the highest stretching took place when the tool T_8 was used. It is clear now that small tool delays the deformation of the flat portion and hence stretching in the middle zone increases as

discussed above. High stretching causes higher thinning and early failure of the flange, which explains the increased LFR.

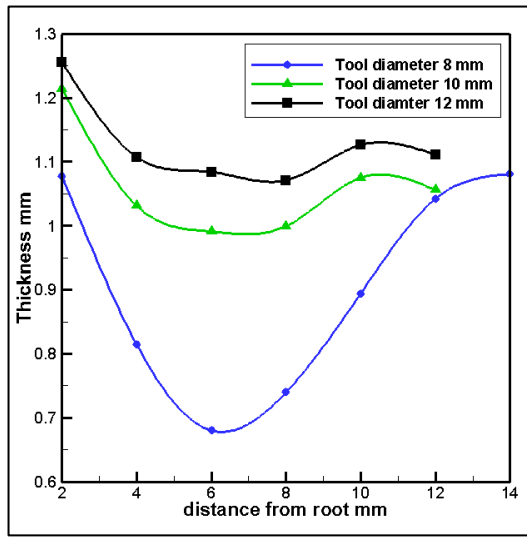


Figure 3.9 Thickness distribution on the successfully formed flanges

To check whether a similar trend was observed for the flange height, three flanges with a common pre-cut hole diameter of 37 mm were formed by the three tools. The results are shown in Table 3.7. It is observed that the smaller tool formed the longest flange and the larger tool formed the shortest flange. The results are following the observations about the thinning as discussed above. Higher stretching by the smaller tool forms the long flange and vice versa.

Table 3.6 Height of the flanges formed with a pre-cut hole diameter of 37 mm

Tool diameter (mm)	8	10	12
flange height (mm)	14.78	13.17	12.28

Further, to understand the effect of single-stage and multistage strategies on the flange quality, experiments were performed and the results and discussion are presented in the next section.

3.2.2 Effect of single-stage and multistage strategies on the flange quality in SPIHF of the cylindrical flange

To analyze the effect of the forming strategy, an experimental study was performed on AA5052 sheet metal. The results are discussed in this section.

3.2.2.1 Fracture Forming Limit line

The failure in SPIF and SPIHF can be predicted by FFL as discussed in section 2.3. The theoretical FFL can be established by finding a major strain value near the crack on a component that failed with plane strain mode using equation 3.2 (Isik et al. 2014).

$$\varepsilon_1 + \varepsilon_2 = q \quad (3.2)$$

In this equation $q = -\ln(1 - R_f)$, where $R_f = (t_f - t_0)/t_f$. The value of R_f can be obtained by measuring the initial thickness of the sheet and the thickness of the crack. As the failure with plane strain mode is to be considered, the minor strain value will be zero. Hence, the major strain value (ε_1) will be equal to the value of q .

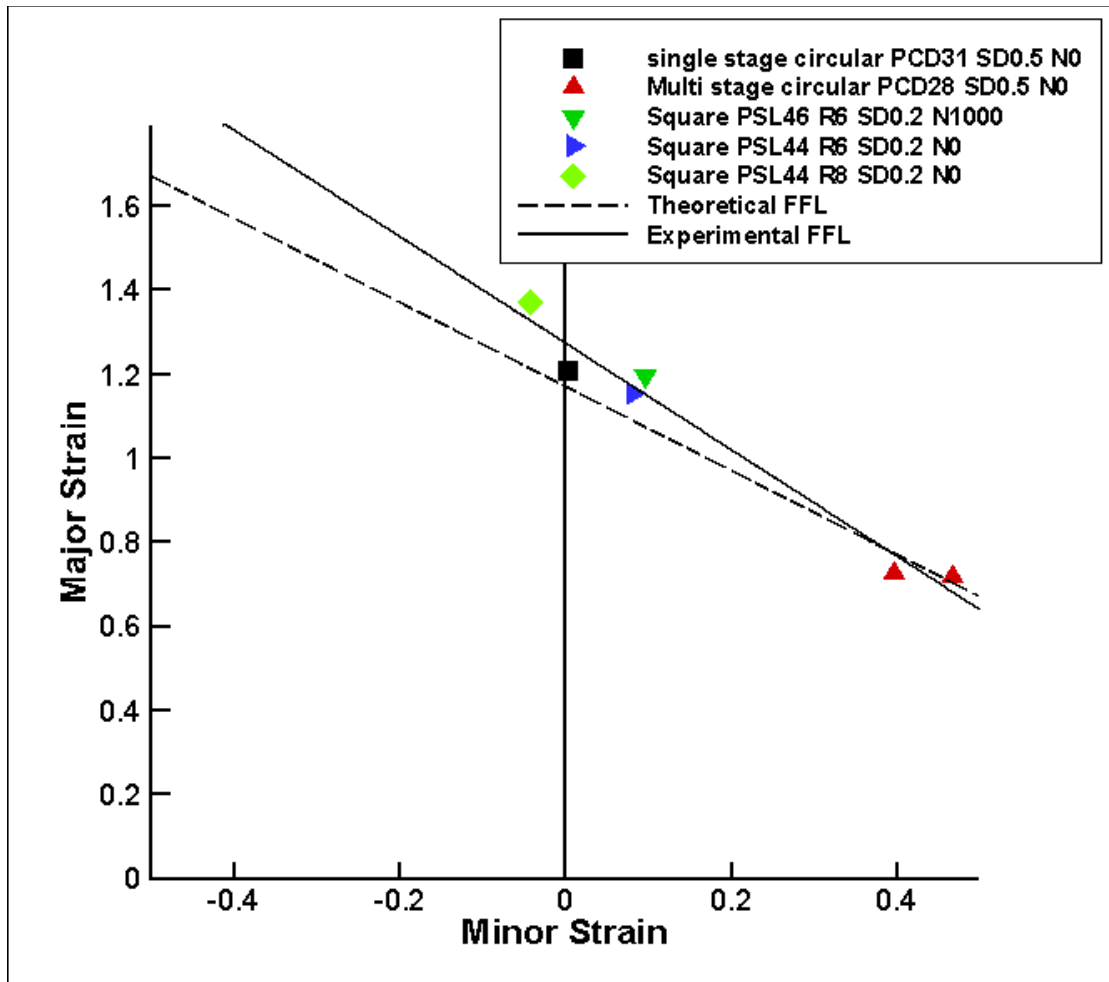


Figure 3.10 Theoretical and Experimentally established FFL

Table 3.7 Details of experiments performed to establish FFL

Shape of the flange	Strategy used	Rotating tool/
Cylindrical with PCD 31mm, SD 0.5 mm	Single-stage	Non-rotating tool
Cylindrical with PCD 28mm, SD 0.5 mm	Multistage	Non-rotating tool
Square with PSL46mm & corner radius 6 mm,	Single-stage	Rotating tool, N1000
Square with PSL44 mm & corner radius 6 mm,	Single-stage	Non-rotating tool
Square with PSL44 mm & corner radius 8 mm,	Single-stage	Non-rotating tool

In the current work, a cylindrical flange was formed with a single-stage strategy which failed with plane strain mode. The thickness was measured at the crack and based on that the major strain value was obtained as explained above. A line with a slope of '-1' was plotted on the major strain vs minor strain space, passing through the ϵ_1 value. This line is the theoretical FFL, it is shown in Fig.3.10.

To establish the FFL by the experimental method, different flanges were formed with various conditions. The cylindrical flanges were formed by single-stage and multi-stage methods, the square flanges were formed with different pre-cut hole corner radii and with a non-rotating tool as well as a rotating tool. The details of the experiments are shown in Table 3.7. After performing the experiments strain values were measured near the crack on the respective flanges and the same were plotted on the major strain-minor strain space. A line was fitted through these points which is considered as an experimentally established FFL (Fig.3.10) in the work presented further. It was observed that when the flange was formed by the multi-stage method, the failure occurred due to high biaxial stretching. This was because, the final flange was formed by expanding the flange in every stage incrementally. Hence the sheet experiences deformation in stages, in which the part of sheet which experienced high longitudinal stretching further undergoes circumferential strain in the next stage. Thus, the failure took place with high bi-directional stretching. Whereas, the part of sheet at the mid height of the flange undergoes high longitudinal strain in the single-stage strategy which results into failure because of plane strain condition.

3.2.2.2 Limit Forming Ratio in single-stage and multistage SPIHF

To find the LFR in both the forming strategy, experiments were performed by following the tool path as explained in section 3.1.4. The final flange diameter was kept at 58 mm whereas

precut hole diameter was varied by a decrement of 1 mm, starting from 35 mm until the sheet failed. The feed rate of 3000 mm/min and step depth of 0.5 mm was used with a non-rotating tool in all experiments.

The experimental results to find LFR in the single-stage are summarized in table 3.8. During the single-stage strategy, circular straight flanges were successfully formed for pre-cut hole diameters of 35 mm to 32 mm, but the sheet with a precut hole diameter of 31 mm failed during forming. So, the smallest diameter by which a straight flange was obtained by single-stage SPIHF is 32 mm and an LFR of 1.81 is achieved. The formed flanges (both failed and successfully formed) are shown in Fig.3.11 (a) & (b). The strain points are shown in Fig.3.12. The strain values in the lower part of the flange formed from precut hole diameter of 32 mm were in the zone of biaxial tension and in the upper part of the flange the values were in the plane strain condition. The thickness of this flange (Fig.3.13) decreased from the root of the flange to the middle and then it increased towards the edge of the flange.

Table 3.8 Results of experiments to find LFR

PCD (mm)	35	34	33	32	31	30	29	28	27
Flange formation- single-stage	S	S	S	S	F	--	--	--	--
Flange formation- multi-stage	S	S	S	S	S	S	S	F	F

*S- Successful straight flange formed, F- Sheet failed before forming a straight flange

For the flange formed from precut hole diameter of 31 mm, initially, the strain values were in the zone of uniaxial tension and then shifted to plane strain which led to failure. The thickness of the flange decreased from the root towards the middle, the thinning of 66% took place when the sheet failed because of high unidirectional stretching in the longitudinal direction and a horizontal crack appeared on the flange.



(a)

(b)

Figure 3.11 (a) Flange formed in single-stage with a precut hole diameter 32 mm and failed flange with precut hole diameter 31 mm (b) crack on the failed flange

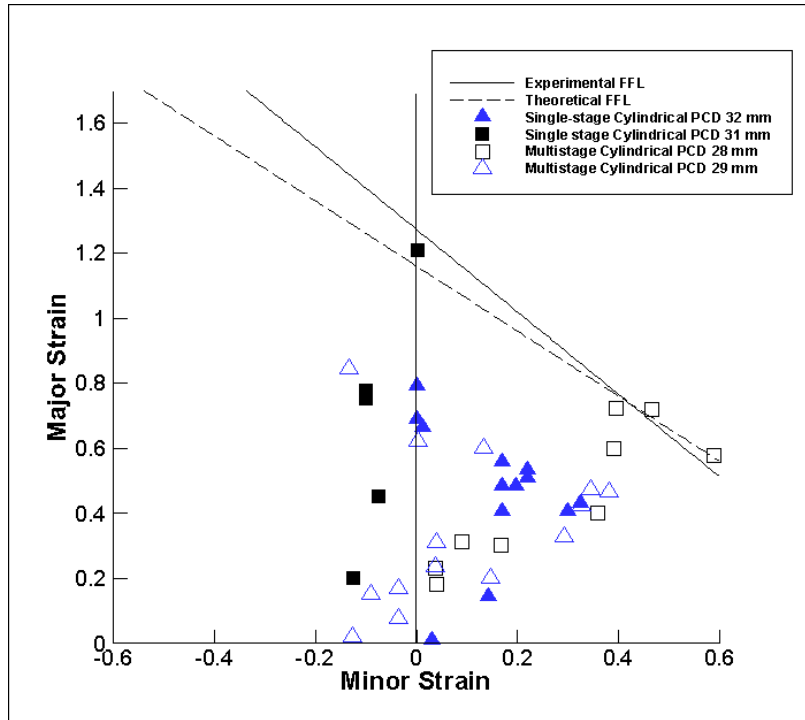


Figure 3.12 Strain plot for single and multi-stage flanges and theoretical Fracture Forming Limit line

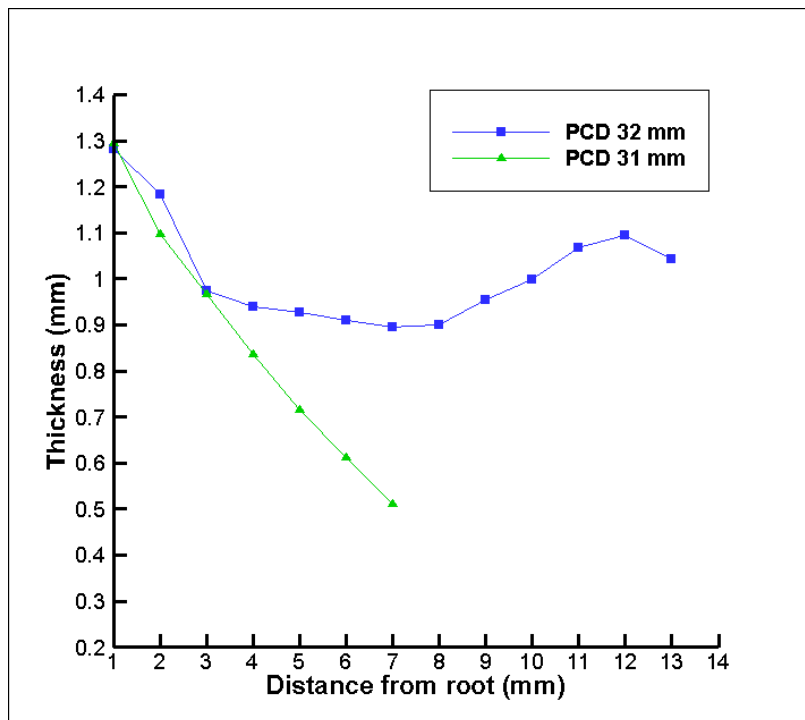


Figure 3.13 Thickness distribution on flanges formed with the single-stage approach

In the multi-stage strategy, successful flanges were formed for pre-cut hole diameters of 35 mm to 29 mm, whereas the sheet with a pre-cut hole diameter of 28 mm failed at the edge of the flange. Moreover, the sheet with a pre-cut hole diameter of 27 mm failed before the straight flange was formed. The flanges are shown in Fig.3.14. The strain values on the flanges are plotted on the major strain – minor strain space as shown in Fig.3.12.

The flange with a pre-cut hole diameter of 27 mm could not be formed into a straight flange successfully, and it failed with a horizontal crack. The thickness distribution on the flange as visible in Fig.3.15 shows that the thickness reduced continuously and reached the critical thinning of 66% which caused the failure. It was observed on the flange with a pre-cut hole diameter of 28mm that the deformation occurred with a biaxial stretching. The strain values increased from the root to the edge of the flange, and finally, the crack appeared at the edge. The thickness reduced from the root of the flange to the midheight and then became stable in the upper zone. In the end, the thickness reduced again and reached the critical value at the edge, so the failure occurred. The flange with a pre-cut hole diameter of 29 mm was successfully formed. It was observed that the flange was deformed with biaxial stretching initially and then near the edge with plane strain mode. The highest strain value was at the edge which remained far below the FFL and hence it did not fail. The thickness reduced from the root to the mid-height but then as the strain condition changed to plane strain mode, the thinning was less, and hence more thickness was observed on the upper zone. The thickness reduced further near the edge, however, the lowest thickness did not reach the critical value and hence the flange did not fail. As per the results, LFR obtained by multi-stage is 2.0. This shows that by multi-stage strategy there was an increase of 11 % in the formability.



Figure 3.14 Flanges formed with the multistage strategy with pre-cut hole diameters 29mm, 28mm, and 27mm

The geometry of the flanges was observed to analyze the geometric accuracy. It was observed on the flange formed by the single-stage strategy that at the mid-height of the flange a bulge formed. The reason behind the bulge formation was a lack of support and excessive stretching in zone B (Fig.3.17) of the flange as explained in section 3.2.1. The resistance to the flow of material in the flat zone (zone A) during the flange forming was responsible for excessive stretching in the midzone (zone B). This was not observed in the multistage approach because the edge of the precut hole was deformed in the first stage itself, hence there was no flat zone on the flange during the forming.

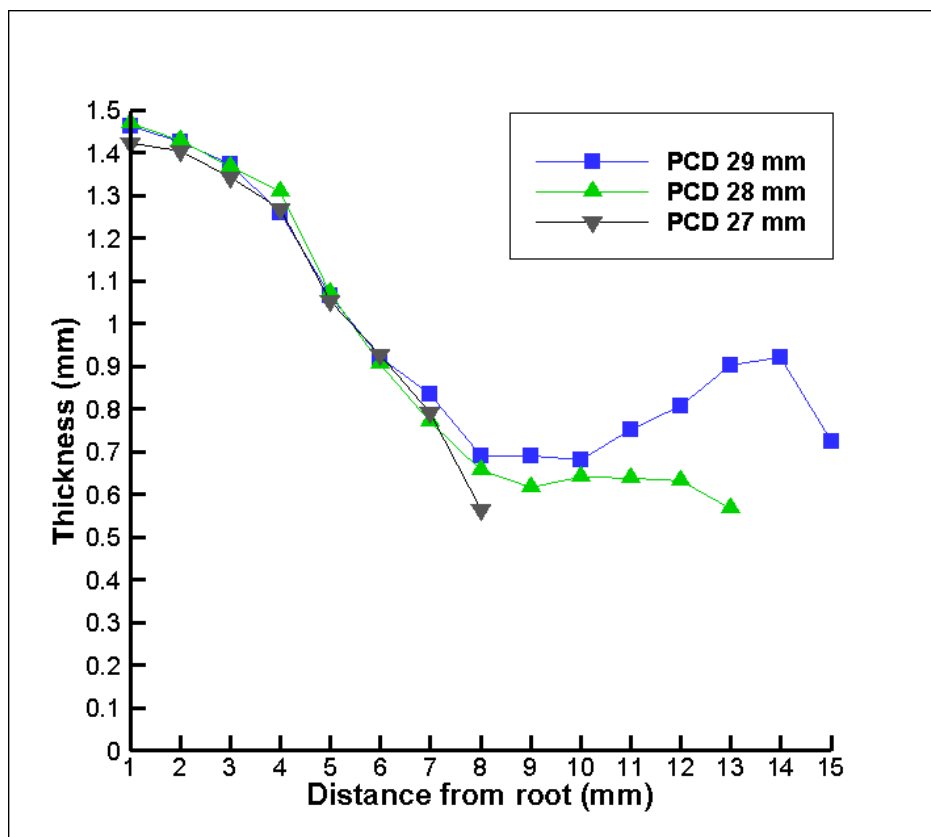


Figure 3.15 Thickness distribution on flanges formed with the multistage strategy

The same can be observed in the thickness distribution of the flanges formed (from a common precut hole diameter of 32 mm) by the two strategies. The thickness distribution on these two flanges is shown in Fig.3.16. It is observed that excessive thinning in single-stage occurred in the zone with a distance of 3 mm to 8 mm from the root, whereas in multistage it occurred in the zone with a distance of 7 mm to 9 mm from the root. Also, uniform thinning was observed in the multistage compared to the single stage. The bulge formation could be

controlled by using an adaptive blank as discussed in the literature (Voswinckel, Bambach, and Hirt 2015). Moreover, it was observed that in single-stage and multistage SPIHF the flange wall with an inclination of 85° and 84° was formed respectively, hence it is evident that a straight flange with a 90° wall was not formed due to spring back. This error can be eliminated by overbending the flange by adding a tool pass (Besong et al. 2020).

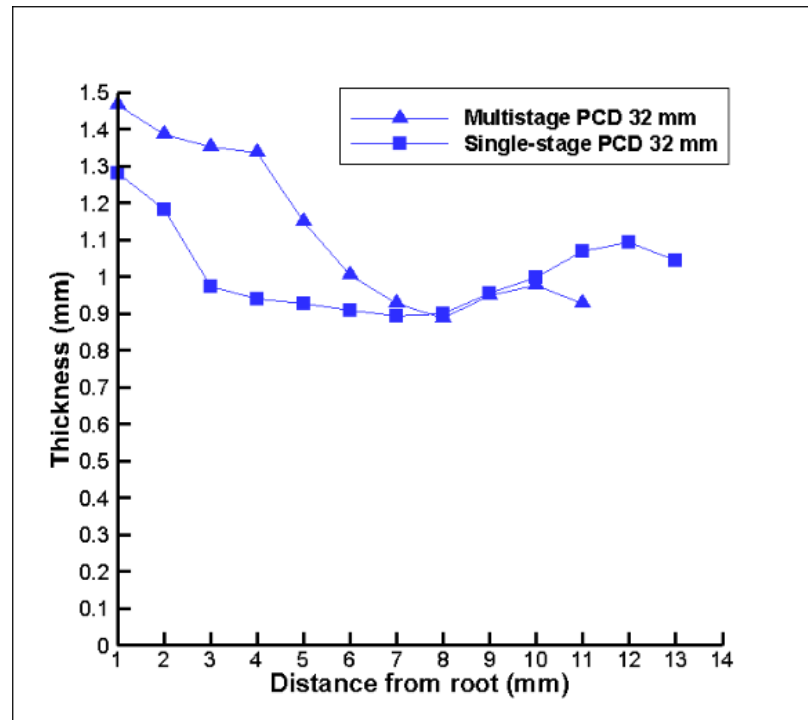


Figure 3.16 Thickness distribution of the flange formed by single-stage and multistage

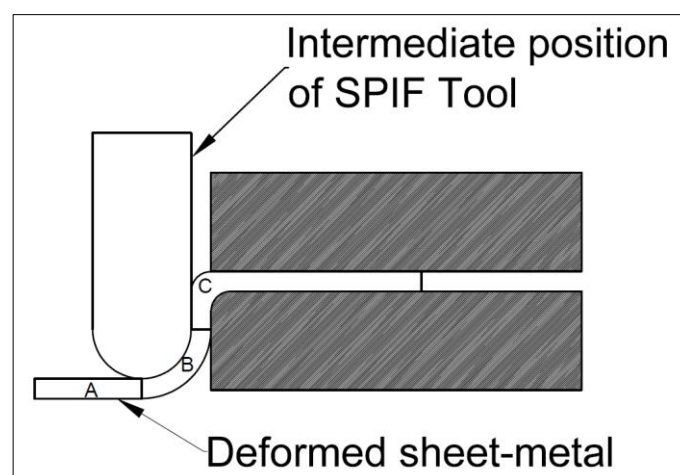


Figure 3.17 Schematic showing tool-sheet contact zones

Table 3.9 Time required for flange forming

Strategy	Time of pre-cut hole cutting	Dwell for application of lubricant	Flange forming time	Total time
Single-stage	2 Minutes, 37 Seconds	1 Minute	2 Minutes, 9 Seconds	5 Minutes, 46 Seconds
Multistage	2 Minutes, 37 Seconds	1 Minute	4 Minutes, 25 Seconds	8 Minutes, 2 Seconds

The time of flange forming was recorded on the VMC machine. The total time of the operation includes the time of cutting the pre-cut hole, the dwell time for applying the lubricant on the surface, and the forming time. It is shown in Table 3.9.

3.3 Summary

The LFR was experimentally found for AA1050 sheet metal and AA5052-H32 sheet metal. The effect of tool diameter on the LFR was evaluated by performing experiments using three different SPIF tools with different diameters (8 mm, 10 mm, and 12 mm). The effect of forming a strategy (single-stage/multistage) was analyzed. Moreover, the thickness distribution and geometry of the flange were evaluated. Following are the conclusions derived from the study.

- The use of the SPIF tool with a larger diameter resulted in increased formability and uniform thickness distribution. The tool T₁₂ formed a thicker and shorter flange compared to the flanges formed by T₈ and T₁₀.
- The FFL was derived by performing various SPIHF experiments, which was in good agreement with the theoretical FFL.
- The flange formed by the single-stage failed by plane strain condition because of high longitudinal strain. The flange formed by multistage failed by bidirectional stretching. The thickness distribution remained uniform in the multi-stage method.
- The multi-stage strategy offered 11% higher formability than the single-stage strategy but increased the time of operation to 105 %. There is a tradeoff between formability and operation time. It is feasible to perform high-speed SPIHF with a high feed rate in the single-stage SPIHF. The feed rate of 3000 mm/min was used and successful flanges were formed.

It is evident from the work presented in this chapter that the multistage strategy increases the time of operation by more than 100 %. Hence, the single-stage strategy of SPIHF should be implemented. To understand the effect of process parameters in the single-stage SPIHF, an experimental investigation has been carried out and presented in the next chapter.

Chapter 4 Effect of process parameters on formability in single-stage SPIHF of the cylindrical flange

In this chapter, the design of experiments for the study of the effect of process parameters in single-stage SPIHF of the cylindrical flange is discussed. The S/N ratio analysis of the parameters is presented. Moreover, the interactive effects of the parameters have been discussed.

4.1 Material and Experimental procedure

As discussed in the section 3.1, the preliminary experiments were carried out using AA1050 sheet metal whereas the further experimental study was carried out using AA5052-H32 sheet metal. The experiments to study the effect of parameters in single-stage SPIHF were carried out on the experimental setup described in section 3.1.2. The SPIF tool was moved on a helical path with the defined step depth, feed rate, and spindle speed to form cylindrical flanges. The pre-cut hole with a 36 mm diameter was used in all the experiments. Flanges with an internal diameter of 58 mm were formed. Hydraulic oil-68 was applied as a lubricant on the surface of the sheet before the forming process.

4.2 Preliminary experiments and their results

Preliminary experiments to understand the effect of process parameters were performed on AA1050 sheet with 1.5 mm thickness. The details are described in the following sections.

4.2.1 Effect of spindle speed

Preliminary experiments were performed to understand the effect of individual parameters. To check the effect of spindle speed on LFR, experiments were performed to form flanges of same diameter on the aluminium sheets with the same pre-cut hole diameter by varying the spindle speeds. Three levels of the spindle speed were selected (500 rpm, 1000 rpm and 1500

rpm). The details of the experiments are shown in table 4.1. The procedure for the same is shown in Fig.4.1.

Table 4.1 Experimental details to study the effect of spindle speed

Spindle speed	500-1500
Feed rate	300 mm/min
Step depth	0.5 mm
Tool diameter	10 mm

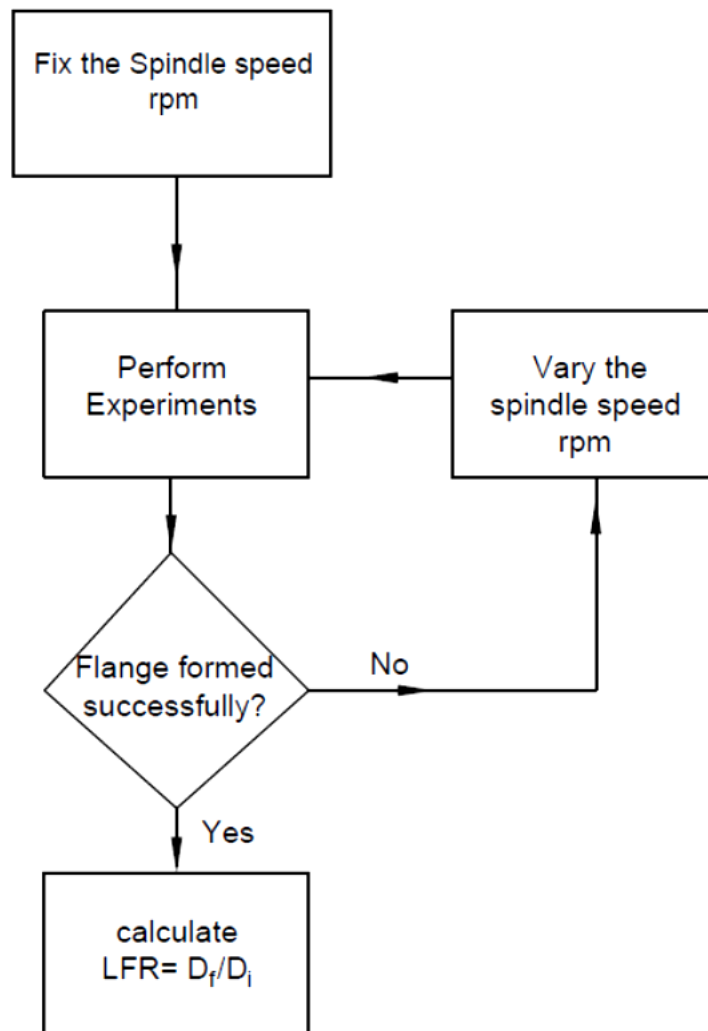


Figure 4.1 Procedure to study the effect of spindle speed on LFR

The results of the experiments are shown in table 4.2. It was observed that for a spindle speed of 500 rpm, the LFR of 1.70 was obtained. It was similar to the LFR obtained by a non-rotating tool as discussed in section 3.3. Hence, it was concluded that there was no effect of tool rotation speed on the LFR withing the range of 0 to 500 rpm. However, when the spindle speed of 1000 rpm was used, the LFR decreased to 1.65. Upon, observing the sheet surface during the forming process, it was visible that due to the increased spindle speed, the wear of the sheet increased. The lubricant oil carried the metal dust particles worn out from the aluminum sheet. Moreover, the sheet surface was visibly rough compared to the sheet surface of the flange formed with the spindle speed of 500 rpm. Further, in the experiments performed with the spindle speed of 1500 rpm, the LFR decreased to 1.61. The reason behind the reduced LFR was the excessive wearing of the aluminum sheet which resulted in early excessive thinning.

Table 4.2 Effect of spindle speed on LFR

Sr.No.	Spindle speed (RPM)	Precut hole diameter (mm)	Result
1	500	36	Success
2	500	35	Success
3	500	34	Success
4	500	33	Failure
5	1000	36	Success
6	1000	35	Success
7	1000	34	Failure
8	1500	37	Success
9	1500	36	Success
10	1500	35	Failure

4.2.2 Effect of feed rate

To study the effect of feed rate, experiments were performed by keeping the other process parameters constant and varying the feed rate value for the same precut hole diameter (34 mm). The experimental details are shown in table 4.3.

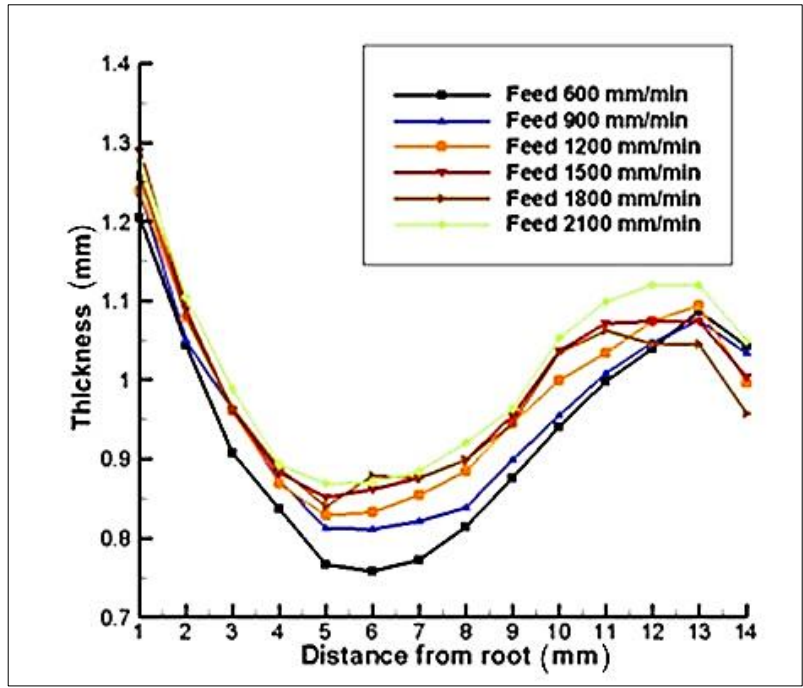
Table 4.3 Experimental details to study the effect of feed rate

Spindle speed	0 rpm
Feed rate	600 to 2100 mm/min (steps of 300)
Step depth	0.5 mm
Tool diameter	10 mm

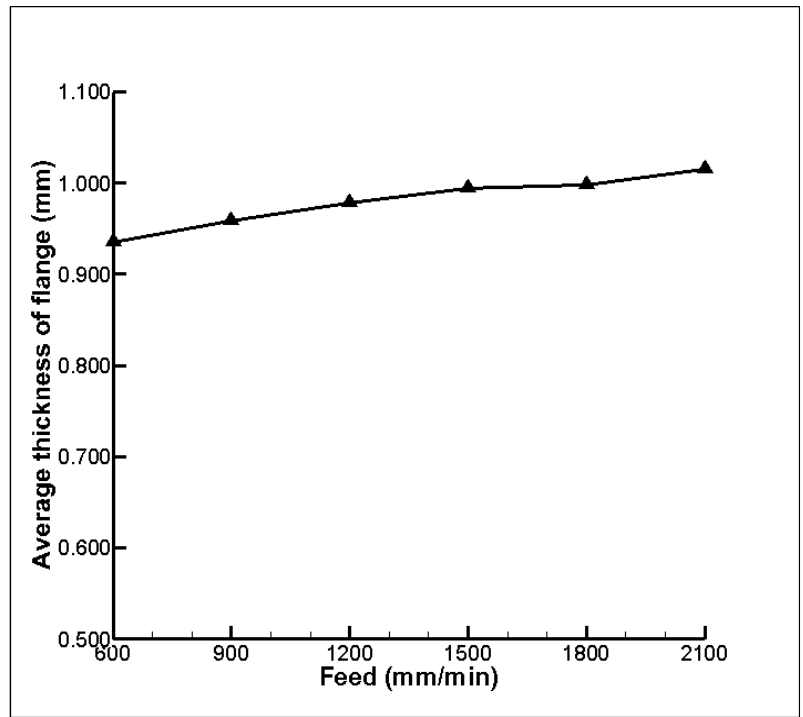
The feed rate did not have any effect on the LFR and all the flanges were formed successfully without failure. However, there was a minor effect on the thickness of the flange. The formed flanges are shown in Fig.4.2. The thickness distribution on the formed flanges is shown in Fig.4.3. It was observed that the flanges formed with different feed rates have similar thickness distribution, however the thinning on the flanges was different. With increased feed rate the thinning of the flange decreased. The average thickness of the flange was a little higher when a higher feed rate was used. However, this difference is very small. Hence, it could be concluded that the feed rate did not have any major influence on the formed flanges other than the reduction of the operation time. The results were similar to available literature about the effect of feed rate in SPIF (Mulay et al. 2017; Baruah, Pandivelan, and Jeevanantham 2017; Pereira Bastos, Alves de Sousa, and Fernandes Ferreira 2016). Moreover, the feed rate may have interactive effects while using a rotating tool, which should be analyzed further.



Figure 4.2 Flanges formed with different feed rate



(a)



(b)

Figure 4.3 (a) Thickness distribution, and (b) average thickness on formed flanges with the different feed rates

4.2.3 Effect of step depth

Experiments were performed to study the effect of step depth by keeping the other process parameters constant and varying the step depth value for the same pre-cut hole diameter (34 mm). The experimental details are shown in table 4.4. The formed flanges are shown in Fig.4.4.

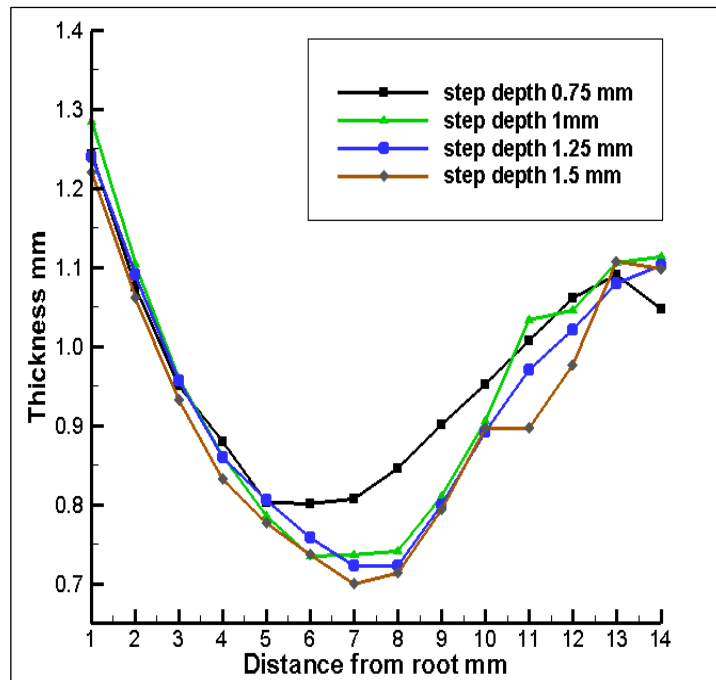
Table 4.4 Experimental details to study the effect of step depth

Spindle speed	0 rpm
Feed rate	300 mm/min
Step depth	0.75 to 1.5 mm (Steps of 0.25)
Tool diameter	10 mm

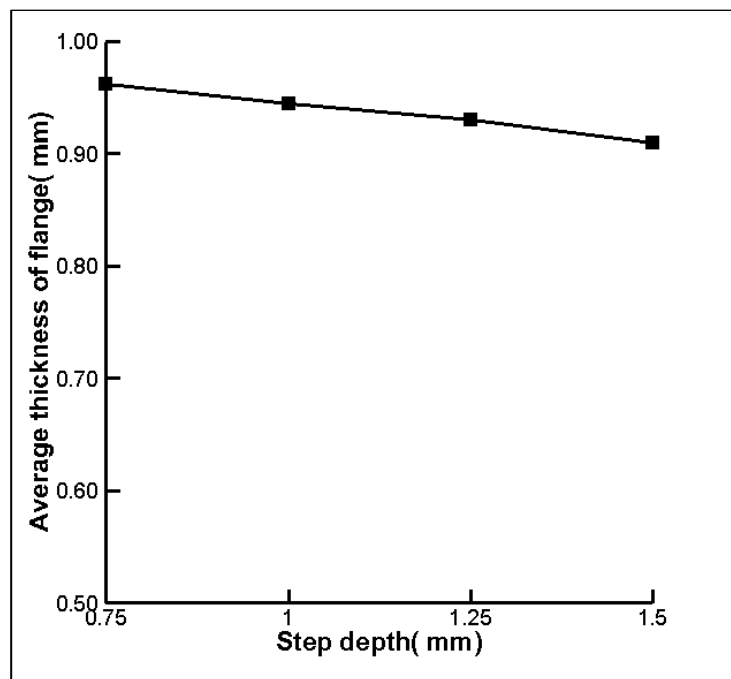
The thickness distribution on the flanges and the average thickness of the flanges are shown in Fig.4.5. It was observed that there was no effect of step depth on the LFR for the range considered in this study. The thickness distribution on the flanges (Fig.4.5(a)) was similar. However, the average thickness of the flanges varied a little, but the difference was very less as observed in Fig.4.5(b).



Figure 4.4 Flanges formed with different step depth



(a)



(b)

Figure 4.5 (a) Thickness distribution and (b) average thickness of formed flanges with different step depth

The results of the preliminary experiments provided a basic understanding of the individual effect of the process parameters on the formability of AA1050 sheet metal. Now, a further experimental study is performed on an aluminum alloy AA5052-H32 to analyse the effect of process parameters and their interactive effects. The same has been discussed in the following sections.

4.3 Study of the effect of process parameters in single-stage SPIHF of cylindrical flange formed using AA5052-H32 sheet metal

To study the effect of process parameters, it was required to design the experiments. It would be time taking task to perform the full factorial experiments and would require more resources. Hence, the design of experiment was required to get the results with a smaller number of experiments.

4.3.1 Design of Experiments by Taguchi Method

4.3.1.1 Taguchi's Parameter Design Approach

Two types of factors affect the product's functional characteristic in the parameter design: control factors and noise factors. The control factors are the factors which can be controlled, for example, selection of material, spindle speed, feed rate etc. The noise factors are the factors which are difficult to control, or some of them are impossible to control. There are three types of noise factors: outer noise, inner noise and between product noise. The noise factors are responsible for the degradation in the performance of the product. Therefore, the parameter design is intended to find the control factor values by which the effect of the noise can be minimized or removed. Ultimately, the parameter design makes the product robust.

To test the different levels of each of the control factors, design of experiments techniques is used. In the Taguchi's Design, orthogonal arrays are used to systematically analyse the control factors. There are different orthogonal arrays i.e., L4, L9, L12, L18, and L27. The appropriate orthogonal array should be selected based on the number of control factors and number of levels of each control factor. Typically, either 2 or 3 levels of the control factors

are selected. The experiments should be performed accordingly and the mean response and standard deviation may be approximated for each run by using the following equations.

$$\text{Mean response: } \bar{y} = \frac{1}{n} \sum_{i=1}^n y_i \quad , \quad \text{Standard Deviation: } S = \sqrt{\frac{\sum_{i=1}^n (y_i - \bar{y})^2}{n-1}}$$

The preferred parameter settings are then determined through analysis of the “signal-to-noise”. The (SN) ratio where factor levels that maximize the appropriate SN ratio are optimal. There are three standard types of SN ratios depending on the desired performance response.

- Smaller the better (for making the system response as small as possible):

$$SN_s = -10 \log \left(\frac{1}{n} \sum_{i=1}^n y_i^2 \right)$$

- Nominal the best (for reduction in the variability):

$$SN_T = 10 \log \left(\frac{\bar{y}^2}{S^2} \right)$$

- Larger the better (for increasing the system response):

$$SN_L = -10 \log \left(\frac{1}{n} \sum_{i=1}^n \frac{1}{y_i^2} \right)$$

A graphical approach is used to analyze the data after the calculation of the SN ratios for each experiment. The SN ratios and the average responses are plotted for each factor against each of its levels. The analysis of the graphs is then carried out by picking the winner. To do so, the factor level which maximize the value of the SN ratio is selected and the mean is brought to the target.

4.3.1.2 Design of Experiment to study the effect of process parameters in single-stage SPIHF

To study the effect of process parameters in single-stage SPIHF, three levels of each parameter (step depth, feed, spindle speed) have been selected. The L9 orthogonal array of the Taguchi method has been followed for the design of experiments. Preliminary experiments on AA5052-H32 sheets were performed to find the appropriate range of the process parameter values. The initial values were selected based on a literature review. As per the results discussed in section 4.2.2, there was no detrimental effect of feed rate and hence, it was intended to use high feed rate values (3000 mm/min) to decrease the forming

time. However, it was assumed that there must be an interactive effect when high spindle speed, high feed rate, and high step depth would be used. After performing the preliminary experiments, it was observed that the flange surface was damaged by the combination of high values of the three process parameters as shown in Fig.4.6.



Figure 4.6 Damaged surface of AA5052-H32 sheet due to high values of process parameters

It was observed that due to high step depth (more than 1 mm) with a high feed rate (3000 mm/min), the tool required to deform the sheet at a higher depth within less time. The tool faced high resistance due to the depth and at the same time, it was pushed at a high speed. So, the tool remained in contact with the deforming portion of the sheet for more time. Moreover, the tool rotation was also high (1200 rpm), hence the friction increased during the contact period. This situation resulted in excessive heating of the aluminum sheet and ultimately it was worn out. The forming was stopped after observing the fumes and damage on the aluminum sheet.

Based on the preliminary experiments, the range of the process parameter values was defined. It was decided to consider a spindle speed of 0 to 1000 rpm, feed rate of 1000 to 3000 mm/min, and step depth of 0.25 to 0.75 mm. Further, it was decided to consider three levels of each parameter to cover the whole range. The final values of the parameters which were considered for the design of experiments are shown in Table 4.5. The final set of experiments was defined based on L9 orthogonal array and is shown in Table 4.6.

Table 4.5 Process parameters and their values

Forming Factor	Unit	Level 1	Level 2	Level 3
Spindle speed	RPM	0	500	1000
Feed rate	mm/min	1000	2000	3000
Step depth	mm	0.25	0.5	0.75

Table 4.6 Set of experiments as per L9 orthogonal array

Experiment Number	Spindle Speed (RPM)	Feed (mm/min)	Step Depth (mm)
1	0	1000	0.25
2	0	2000	0.5
3	0	3000	0.75
4	500	1000	0.5
5	500	2000	0.75
6	500	3000	0.25
7	1000	1000	0.75
8	1000	2000	0.25
9	1000	3000	0.5

To analyze the formability, it was required to define the responses. The thickness of the flange, and the height of the flange was considered as the responses. Moreover, to analyse the surface quality of the formed flange, the surface roughness on the inner surface of the flange was also considered as a response. The thickness of the flange was measured along the axial direction at an interval of 1 mm by a digitally pointed anvil micrometer with 0.001 mm least count. To represent the thinning of the flange, the minimum thickness on each flange was considered as a response. The height of the flange was measured by a vernier height gauge with a least count of 0.01 mm at four places and the average height was considered as a response. The surface roughness (Ra) was measured in the axial direction on the inner surface of the flange by the surface roughness tester as mentioned in section 3.1.6.

The experiments were performed as per the defined orthogonal array and measurements were taken. The results are discussed in the following section.

4.3.2 Results and Discussion

The cylindrical flanges formed by the single-stage SPIHF process are shown in Fig.4.7.

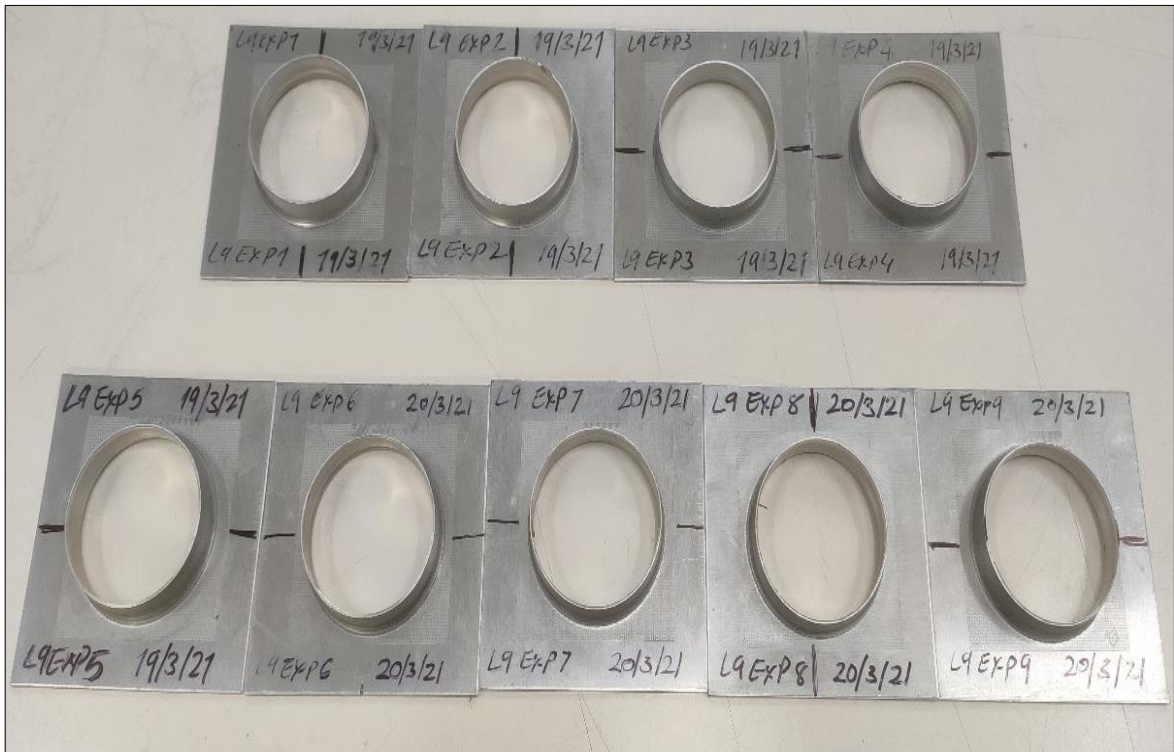


Figure 4.7 Flanges formed as per the L9 orthogonal array

The effect of process parameters was evaluated by S/N ratio analysis and the results are discussed below.

4.3.2.1 Effect of process parameters on thickness, height, and surface roughness

The measured values of the responses are shown in Table 4.7. These values were then used to evaluate the main effects of the process parameters S/N ratio analysis using MINITAB software. The thickness of the flange and height of the flange were regarded as “larger the better” whereas surface roughness was regarded as “smaller the better”. The main effect plots are shown in Fig.4.8 to Fig.4.10.

Table 4.7 Summary of the responses of the flanges formed

Experiment No.	Process parameters			Responses		
	Spindle Speed (RPM)	Feed (mm/min)	Step Depth (mm)	Thickness (mm)	Height of flange (mm)	Surface Roughness Ra (μm)
1	0	1000	0.25	0.943	13.86	0.23
2	0	2000	0.5	1.016	13.11	0.26
3	0	3000	0.75	1.014	12.93	0.25
4	500	1000	0.5	0.991	13.28	0.27
5	500	2000	0.75	0.984	12.98	0.28
6	500	3000	0.25	0.927	13.92	0.19
7	1000	1000	0.75	0.959	13.22	0.25
8	1000	2000	0.25	0.948	13.92	0.19
9	1000	3000	0.5	0.96	13.21	0.32

4.3.2.2 Thickness and height of the flange

It is observed in Fig.4.8 and Fig.4.9 that higher thickness with less height was achieved by a spindle speed of 0 rpm (non-rotating tool). The thickness reduced and the height increased when the spindle speed was increased. This can be attributed to the heat generation due to the rotating tool. As per the literature, more heat generation takes place due to the tool rotating at a higher speed which increases the temperature on the flange surface (Khalatbari et al. 2015). The increased temperature results in the material softening (Gohil and Modi 2021) and higher stretching of the material takes place. High stretching of the material reduced the thickness of the flange and increased the height of the flange.

It is observed from the main effect plot in Fig.4.8 that the highest thickness was achieved with the feed rate of 2000 mm/min, but the thickness was reduced with the feed rate of 3000 mm/min. Hence, no trend was observed in the results of thickness. It suggests that there was an interaction between the process parameters. It was also observed in the literature (Khalatbari et al. 2015) that the spindle speed (tool rotation speed) has high interaction effects with other parameters. Moreover, it is observed in Fig.4.9 that there is a little decrease in the

height of the flange when a high feed rate was used, however, the difference was very small. The results are in line with the results of the preliminary experiment discussed in section 4.2.2, which shows that high feed rate results in a thicker flange. Overall, it can be concluded that for the range of feed rates considered, there is no substantial effect of the feed rate in the SPIHF.

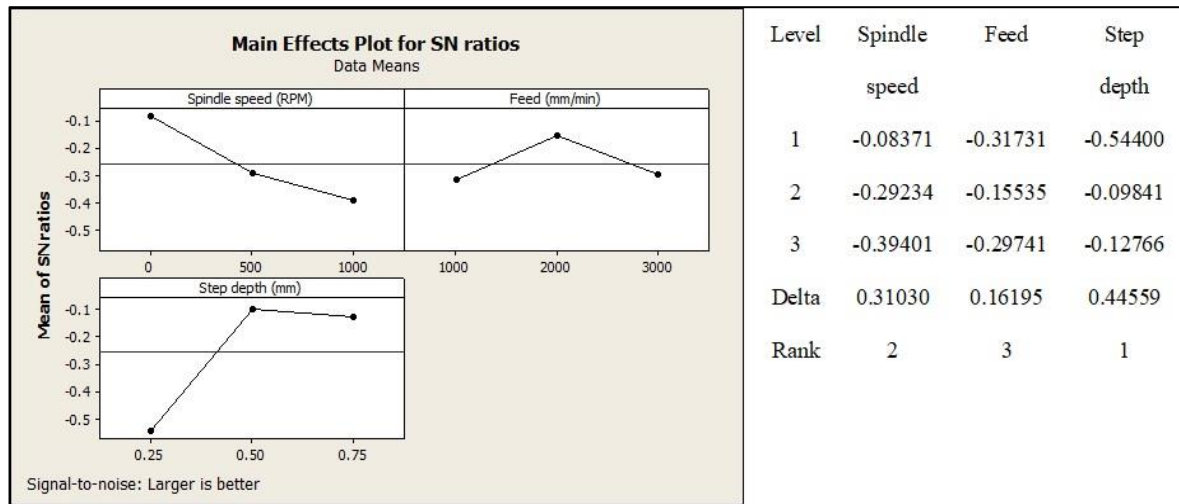


Figure 4.8 Main effect plots- Thickness of flange

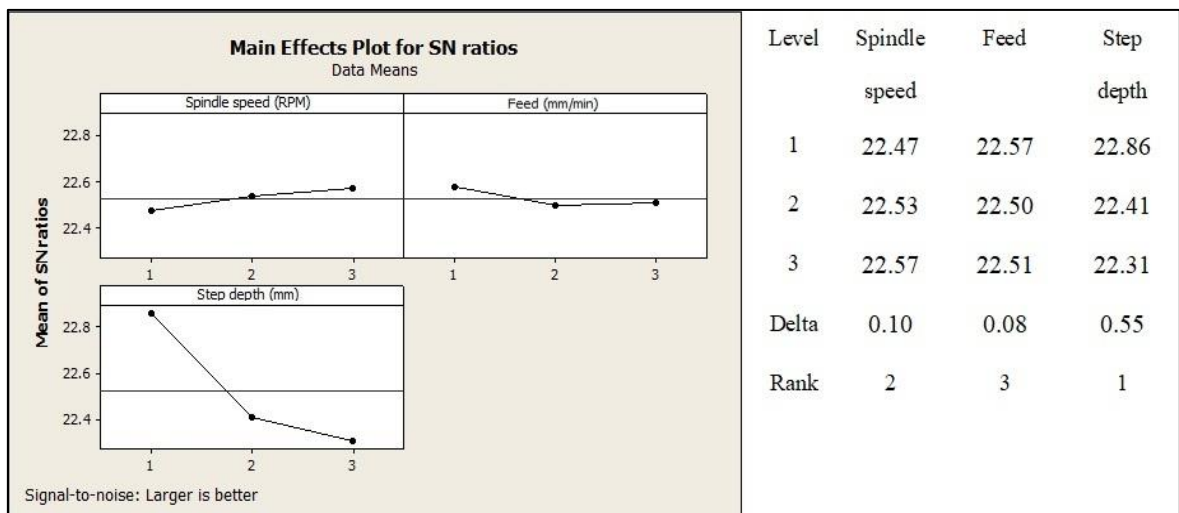


Figure 4.9 Main effect plots- Height of flange

It is observed in the main effect plots of step depth in Fig.4.8 that the flange with more thickness was formed when high step depth was used. The reason behind this was that the high step depth caused increased force on the sheet as well as a larger contact area between

the tool and the sheet. Hence, bending was the dominating deformation mechanism and not the stretching, which formed thick flanges. On the other side, if the stretching is less, the height of the flange should be less. That means the flange should be thick and short. The same was observed and it is visible in the Fig.4.9 also. Similar results were observed in the literature (Su et al. 2021) about SPIF of conical shape. It was observed that higher step depth resulted in less thinning rate and smaller wall angle.

4.3.2.3 Surface roughness

The main effect plots of surface roughness are shown in Fig.4.9. From the main effect plot of spindle speed (Fig.4.10), it is observed that there is no substantial effect of the spindle speed on the surface roughness of the flange for the range of spindle speed considered in this study. This is in line with the literature (Durante et al. 2009). However, from Table 4.7, it is observed that with a spindle speed of 1000 rpm and feed rate of 3000 mm/min were used, the roughness increased a little. This result can be correlated with the discussion presented in section 4.3.1 which shows possible interaction between high spindle speed and high feed rate.

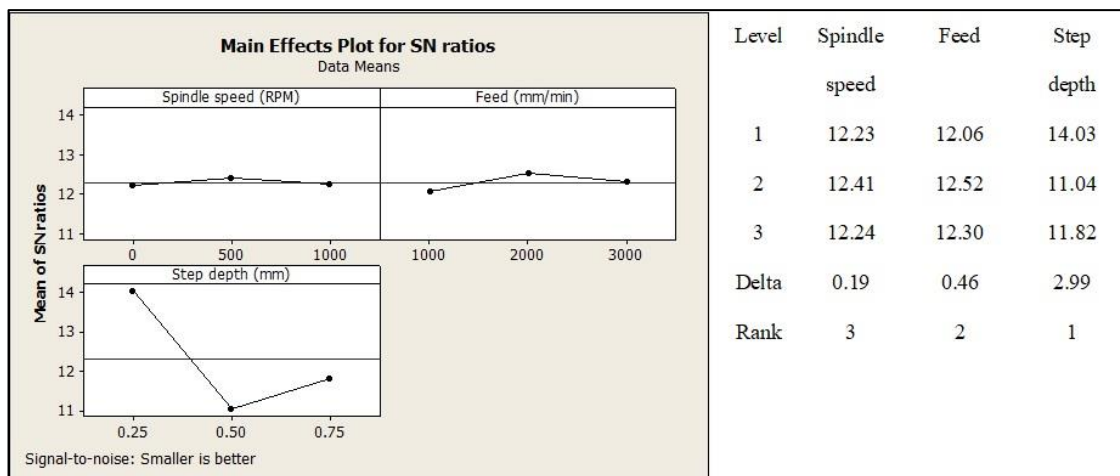


Figure 4.10 Main effect plots- Surface roughness

Further, it is observed in the main effect plot of feed rate for surface roughness that a high feed rate reduces the surface roughness slightly. However, the effect is not substantial. The most effective parameter affecting the surface finish is the step depth as visible in the main effect plot in Fig.4.10. The higher step depth increased the surface roughness because it

caused increased waviness whereas smaller step depth results in uniform stretching and better finishing, a similar discussion is presented by (Kumar et al. 2019; Jeswiet et al. 2005).

4.3.2.4 Interactive effects of parameters

The best values of each parameter for each response and the most effective parameters are tabulated in Table 4.8. Higher thickness can be achieved by a non-rotating tool with a feed rate of 2000 mm/min and a step depth of 0.5 mm. Higher height can be achieved by a tool rotating with 1000 rpm, a feed rate of 1000 mm/min, and a step depth of 0.25 mm. A better surface finish can be achieved by a tool rotating with 500 rpm, a feed rate of 2000 mm/min, and a step depth of 0.25 mm. Moreover, for all three responses i.e., the thickness of the flange, height of the flange, and surface roughness, the most effective parameter is the step depth. Hence, it is clear that the step depth is the most effective parameter to the flange quality in single-stage SPIHF of the cylindrical flange.

Table 4.8 Best values and most effective parameters

Response	Best values			Most effective parameter
	Spindle Speed (RPM)	Feed (mm/min)	Step Depth (mm)	
Thickness of flange	0 (No rotation)	2000	0.5	Step depth
Height of flange	1000	1000	0.25	Step depth
Surface roughness Ra	500	2000	0.25	Step depth

The interaction plots are plotted to check for the interactions between the parameters and are shown in Fig.4.11 to Fig.4.13. It is observed on the interaction plot of the thickness of the flange that there was a substantial interaction effect between ‘spindle speed and feed rate’ as well as ‘feed rate and step depth’. As per the plots, the thickness decreases under the combined effect of high spindle speed and high feed rate. This confirms the discussion presented in section 4.3.1 about the interactive effect between the two parameters. Higher

thickness was obtained with the non-rotating tool and high feed rate which is again showing the same trend as observed in the preliminary experiments as discussed in section 4.2.2. There was very low interaction between ‘spindle speed and step depth’. Thicker flanges were formed when higher step depth was introduced for all the values of the spindle speed. This is because of the high amount of bending and less stretching of the sheet in the flange forming with higher step depth. Moreover, the higher step depth can result in more wearing of the sheet but it is dependent on the other two process parameters.

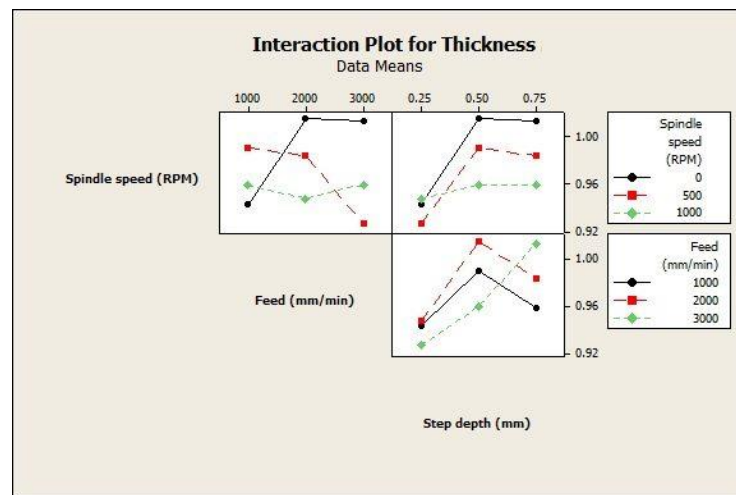


Figure 4.11 Interaction plots- Thickness of flange

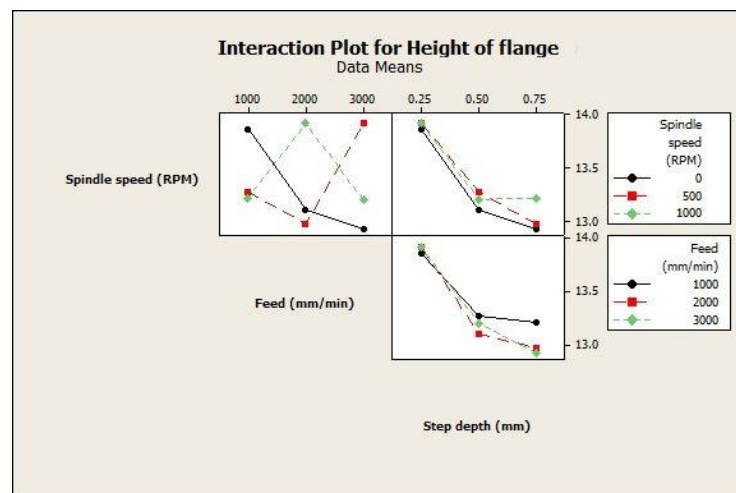


Figure 4.12 Interaction Plot for Height of the flange

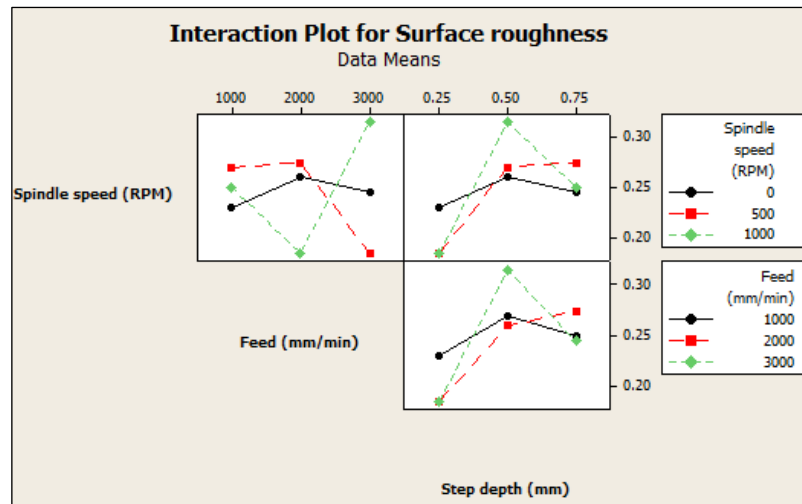


Figure 4.13 Interaction plot for surface roughness

The following observations are derived from the interaction plot of ‘spindle speed and feed rate’ for surface roughness (Fig.4.13). The feed rate has little effect on the surface roughness with the non-rotating tool. In the case of the rotating tool, a better surface finish was obtained when a low spindle speed (500 rpm) with a high feed rate was implemented. Further, the surface finish deteriorated when the high spindle speed (1000 rpm) with a high feed rate was implemented which is again confirming the results and discussion of preliminary experiments. At last, it is observed in the interaction plots of ‘spindle speed and step depth’ as well as ‘feed rate and step depth’ that higher spindle speed and feed rate with low step depth form a better surface.

4.4 Summary

An experimental study was carried out to analyze the effect of process parameters on the formability of the flange. The experiments were designed as per the L9 orthogonal array with three levels of each parameter (Spindle speed, Feed rate, and Step depth). The thickness of the flange, the height of the flange, and the surface roughness of the inside surface of the flange were considered as responses. The results were analyzed based on the S/N ratio analysis. The process parameters (spindle speed, feed, and step depth) had a major impact on the quality of the formed flanges. The most effective parameter was the step depth. The higher value of step depth reduced the forming time; however, the surface finish of the flange deteriorated, and the amount of stretching was reduced. So, it is recommended to use low

step depth to get better flange quality. Moreover, the spindle speed and feed rate had a high interactive effect on the responses. The combination of higher values of both deteriorated the quality of the flange. Finally, it can be concluded that to reduce the forming time in the SPIHF, a high feed rate with a low rotational tool speed should be used.

The study of formability in SPIHF of the cylindrical flange is presented in chapter 3 and this chapter. As per the results, it is recommended to form flanges in single-stage to reduce the operation time. Also, as discussed earlier, it is important to study the formability of different shapes of the flanges. The study on the formability of square flange in multi-stage SPIHF is available in the literature, however, no work is reported on the square flange forming with the single-stage method. Hence, in this work, the study on single-stage SPIHF of the square flange is carried out and presented in the next chapter.

Chapter 5 Formability in single-stage SPIHF of square flange

In this chapter, the study on formability in single-stage SPIHF of square flange has been presented. The experimental procedure to form square flanges in single-stage SPIHF has been described. LFR for the square flange forming has been discussed and an equation has been proposed. Also, the details of experiments conducted to analyze the effect of tool rotation and pre-cut hole corner radius on the formability of square flange has been presented. The results of the experimental study are analyzed and discussed.

5.1 Materials and Methods

To analyze the formability in square hole flanging using SPIHF, experiments were performed on AA5052-H32 sheet material with 1.5 mm thickness. The mechanical properties of the material are described in section 3.1.1.

5.1.1 Experimental procedure to form square flange using single-stage SPIHF

The methodology of single-stage SPIHF of cylindrical flange can be applied to form the square flange in which the SPIF tool can be traversed on the required square shape path. In this case, the pre-cut hole shape will be a square with rounded corners. The multistage method of forming the square flange by SPIHF can be used (Silva, Bay, and Martins 2016; Cristino et al. 2015), in which the flanges were formed by increasing the wall angle in each stage. In this work, the square flanges were formed by single-stage method in which the tool was traversed on the path as shown in Fig.5.1. The step depth was given after completion of each square loop. The tool was fed in the downward direction until the straight wall flange was formed or the sheet failed. As the path was a square shape, the corner radius of the formed flange remained same as the radius of the SPIF tool.

The flanges were formed with AA5052-H32 sheet material of 100 x 100 mm and 1.5 mm thickness. The sheet was held between the top and bottom plate, which had a square opening

at the center as shown in Fig.5.2. In the beginning of the forming process, a square pre-cut hole of predefined length and corner radius was made by an end mill cutter. The SPIF tool was then traversed to form square flange of 56 mm.

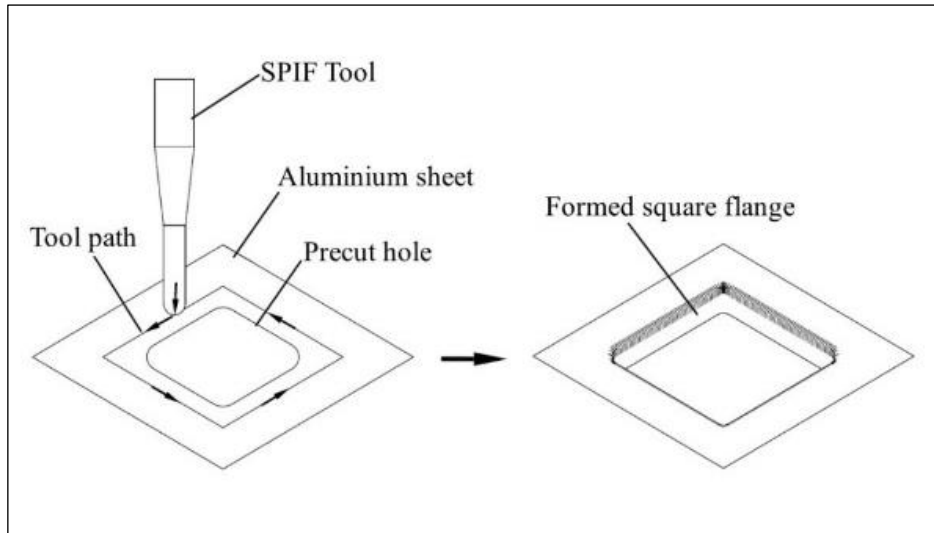


Figure 5.1 Tool path followed to form square flange in single-stage by SPIHF

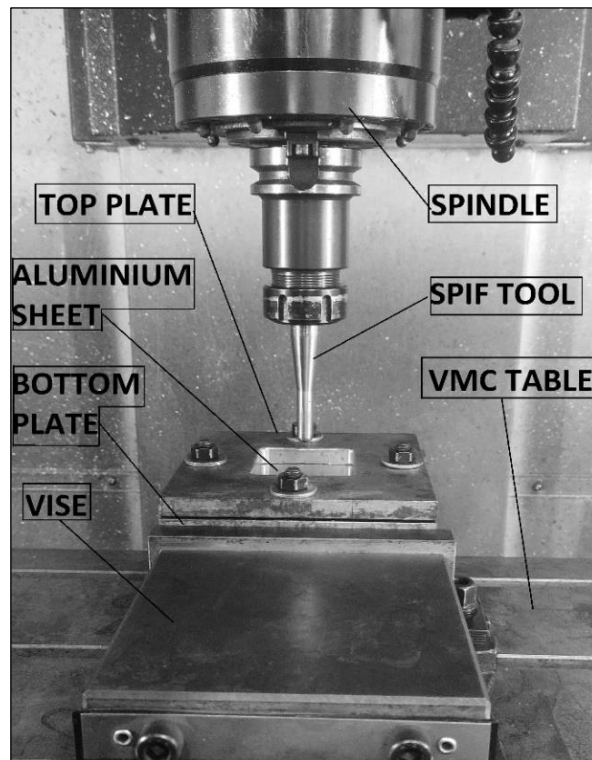


Figure 5.2 Experimental setup for SPIHF of square flange

5.1.2 Limit Forming Ratio in single-stage SPIHF of square flange

The term ‘Limit Forming Ratio’ (LFR) is used to describe the forming limit in hole flanging, which is the ratio of final flange diameter to the precut hole diameter. The formability in square hole flanging was indicated by the possible wall angle to form, and the thickness reduction (Cristino et al. 2015). The length and corner radius of pre-cut hole and the final flange were considered to analyze the results. However, it is possible to define the LFR in the similar manner as used in the cylindrical flanging. The definition of the term will help to simplify the indication of formability. To define the LFR for square hole flanging, it is required to consider the length (l_p) and corner radius (r_p) of pre-cut square hole, together with the length (l_f) and corner radius (r_f) of final flange square. In this work, the LFR is defined as a ratio of the perimeter of the final square flange to the perimeter of the initial precut square hole which can be calculated by using equation (5.1). The terms used in the equation are shown in fig.5.3.

$$\text{LFR}_{\text{square}} = \frac{4l_f + 2\pi r_f}{4l_p + 2\pi r_p} \quad (5.1)$$

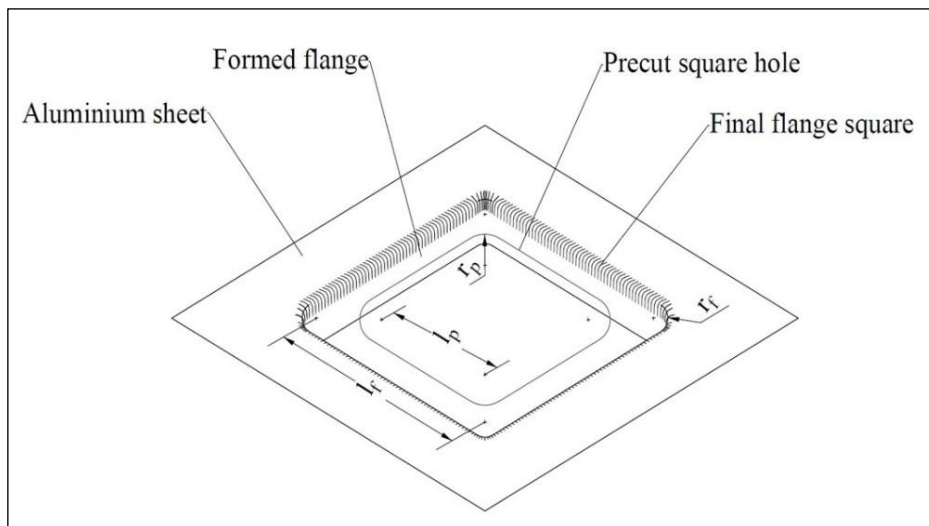


Figure 5.3 Terminology used to define LFR in forming of square flange

From the results discussed in section 4.2.1, it is clear that there is adverse effect of tool rotation on the LFR. Hence, experiments with a non-rotating tool and a rotating tool were performed separately to check the extent of the effect in square flange forming.

5.2 Results and Discussion

The results of the experiments performed to study the formability are presented and analyzed in this section.

5.2.1 Failure of square flange and the critical zone

In the preliminary experiments performed to form square flange by single-stage SPIHF, it was observed that higher strains were generated at the round corner and lower strains at the straight wall. The dominating deformation mode at the straight wall was bending and only a little stretching occurred. The merging of the round corner and straight wall undergone high stretching in the circumferential direction. The crack on the failed flanges appeared in this zone as shown in Fig.5.4 and it is defined as the “critical zone”. This is similar to what is observed in the multi-stage square SPIHF(Cristino et al. 2015). On the flange formed from PSL 44 mm with a non-rotating tool, the failure took place in the critical zone with biaxial stretching. In the experiments performed to plot the FFL (discussed in section 3.2.2.1), it was observed that the flange failed with a biaxial stretching condition when a rotating tool was used for forming the sheet with a PSL of 46 mm and corner radius of 6 mm. However, when the corner radius was increased to 8 mm, the strain condition changed to uniaxial tension. This suggested that the deformation behavior in single-stage square SPIHF changes if the corner radius is varied.

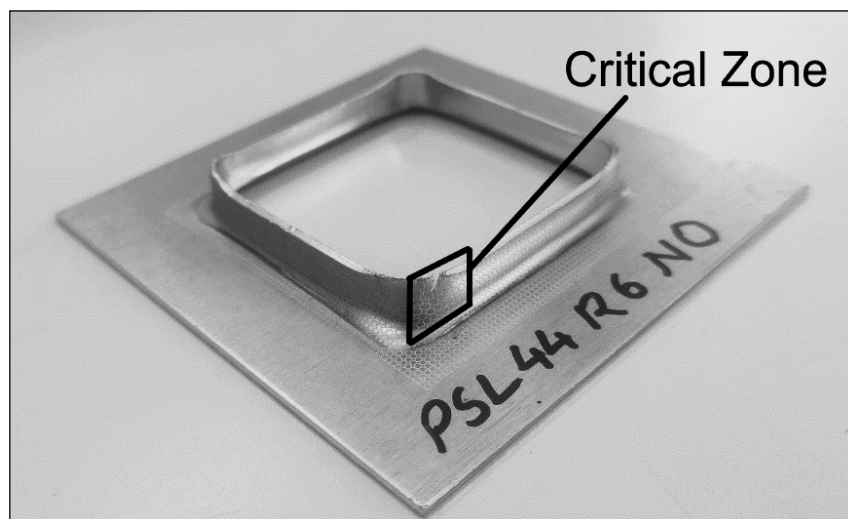


Figure 5.4 Critical zone on the square flange formed by SPIHF process

5.2.2 Formability with a non-rotating tool

Various experiments were performed to find the LFR in single-stage square SPIHF. In all the experiments, a non-rotating tool with 10 mm diameter, a step depth of 0.2 mm and a feed rate of 1000 mm/min were used. The experiments were performed by varying the Precut Square Length (PSL) to form a successful straight square flange without failure. The precut square hole corner radius of 6 mm was used in all experiments. The hole with the least PSL formed into a successful straight flange was considered to calculate the LFR.

Initially the flange forming was attempted with a PSL of 43mm, however the successful flange forming did not take place and the sheet failed before a straight flange was formed. Now, it was evident that to form the straight flange, it was required to increase the PSL. Hence further experiments were performed by increasing the PSL with an increment of 1 mm till successful flange formation took place. The results are shown in Table 5.1.

Table 5.1 Results of experiments performed to find LFR

Sr.No.	Pre-cut hole Square Length	Result
1	43	Failure
2	44	Failure
3	45	Success
4	46	Success

The least PSL formed into a straight flange without failure was 45 mm. The flanges with PSL 44 mm and 45 mm are shown in Fig.5.5.

To analyze the strain in the critical zones, the highest deformation on the circle grid were measured as explained in section 3.1.5. The values were superimposed on the major-minor strain space with the FFL obtained earlier. The critical zones of the flanges and the strain distribution is shown in Fig.5.6. A crack was observed on the flange with PSL 44 mm with an opening to the edge of the flange. The strain distribution of the same flange indicates that there was a near equibiaxial stretching in the lower zone of the flange. However, there was more circumferential stretching than the longitudinal stretching near the edge of the flange.

Hence, in this zone the deformation took place with a near plane strain condition. Ultimately, the flange failed due to high circumferential strain which caused the vertical opening of the crack. It can also be observed from Fig.5.6 that the maximum strain value on the flange is above the FFL which shows that the limiting strain is crossed. This is the indication of the failure of the flange.



Figure 5.5 Failed and successfully formed flange by single-stage SPIHF

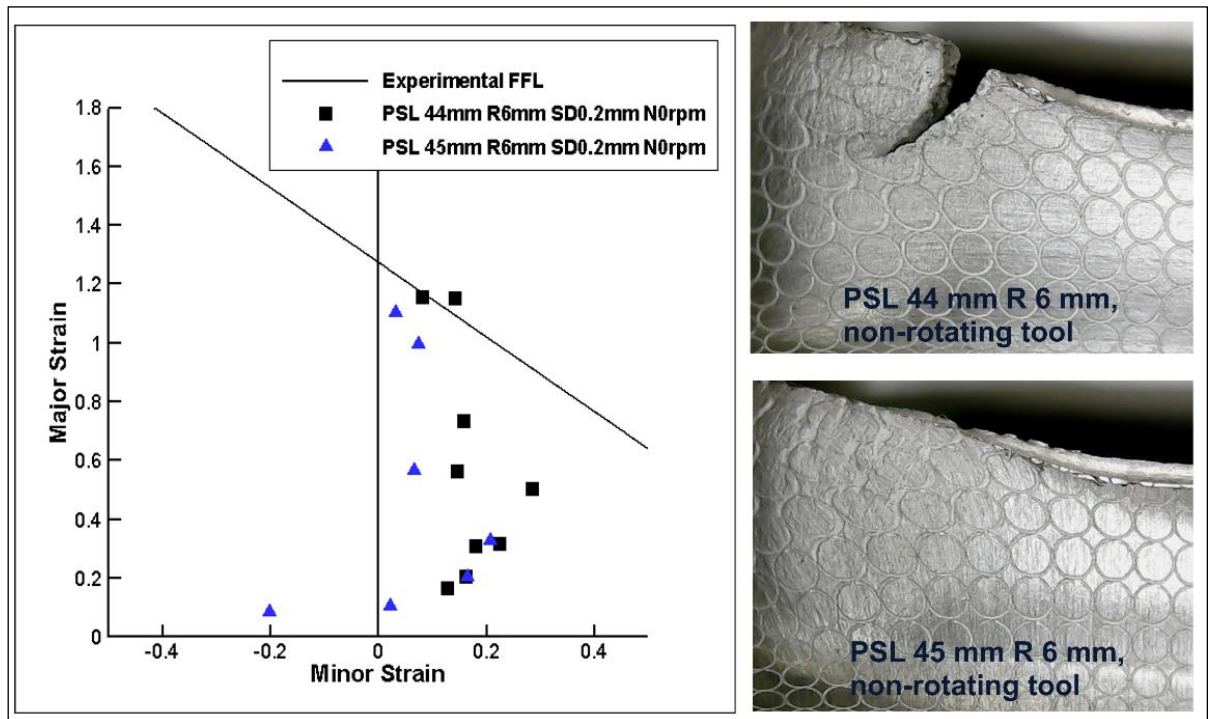


Figure 5.6 Strain distribution and critical zones of the flanges (PSL 44mm and PSL 45mm)

The strain distribution on the flange with PSL 45 mm is found to be near plane strain deformation in the zone close to the root and the edge of the flange. Equibiaxial stretching took place in the middle zone. Moreover, the highest strain point is below the FFL which indicates that the flange did not fail. The PSL 45 mm with a 6 mm corner radius is the critical pre-cut hole dimension, so the $LFR_{\text{non-rotating tool}}$ is 1.26 (as per the equation 5.1).

5.2.3 Formability with a rotating tool

To analyze the formability of Aluminium 5052 sheet metal in SPIHF with a rotating tool, experiments were performed with a SPIF tool rotating at 1000 rpm, the speed was decided based on the results of the preliminary experiments as discussed in section 4.3.1. The other experimental conditions were kept similar to what is discussed in the first paragraph of previous section. The formed square flanges are shown in Fig.5.7.

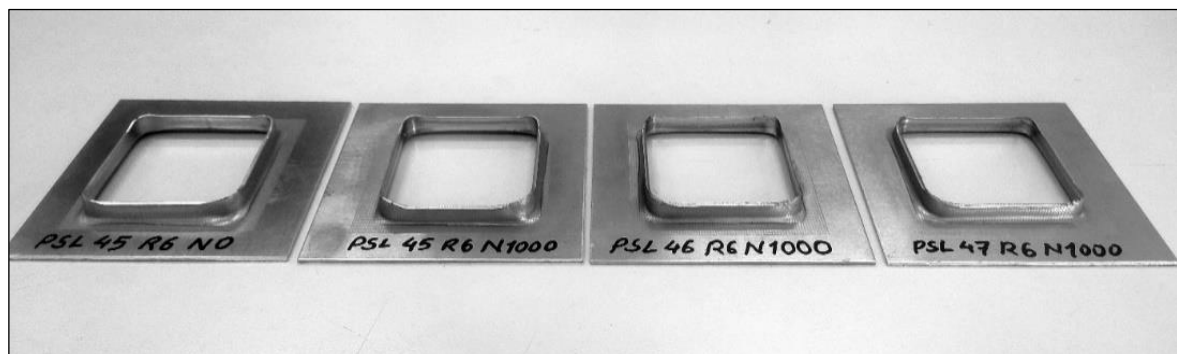


Figure 5.7 Flanges formed with a rotating SPIF tool

The critical zones of the flanges and the strain plot are shown in Fig.5.8. It was observed that when the rotating tool was used to form flanges from the PSL 45 mm, the strain value in the critical zone increased beyond the forming limit. Two factors were responsible for the increase in the strain, one of them was the wearing of the aluminum material due to tool rotation. The other factor was the high shear strain and heating caused by the tool rotation, which increased the stretching of the material in circumferential direction. Ultimately, the combined effect resulted into the vertical crack formation at the edge.

The experiments were then performed on the sheets with PSL 46 mm using the rotating tool with 1000 rpm. It was observed that, the flange was stretched with biaxial strain in the lower

zone. In the upper zone of the flange, the strain condition changed to plane strain and then to uniaxial tension. The flange could bear more strain compared to the one with PSL 45 mm. However, the strain values crossed the forming limit and the flange failed with a vertical crack near the edge. Hence, further experiments were performed on the sheets with PSL 47 mm. The strain condition in the lower zone of the flange remained in the drawing mode. The middle zone was deformed with plane strain mode and in the upper zone, the stretching with uniaxial tension took place. The highest strain values were just below the forming limit and hence a flange without crack was formed.

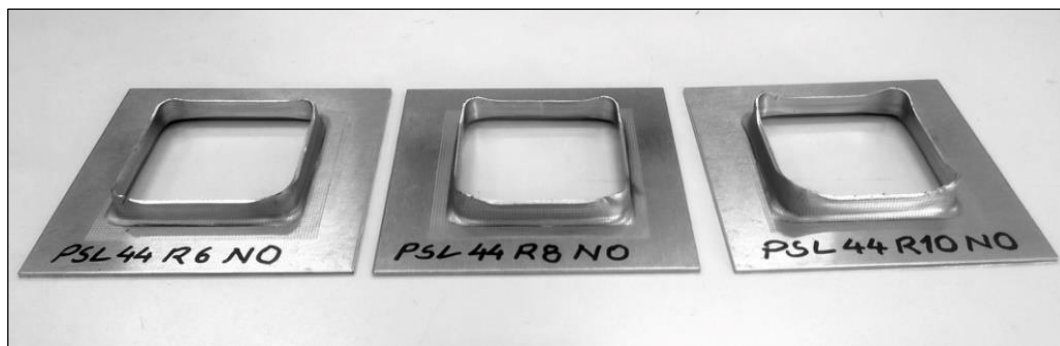


Figure 5.8 Square flanges formed from pre-cut square hole with PSL 44 mm and corner radius of 6,8 and 10 mm

It is evident from the discussion presented above that the critical PSL value is different for the flanges formed using a non-rotating tool and a rotating tool. In the case of the rotating-tool, the critical PSL was 47 mm with a corner radius of 6 mm. So, the $LFR_{\text{rotating-tool}}$ of 1.20 was obtained which is less than the LFR obtained with the non-rotating tool. This shows that the formability decreased when the rotating tool was used.

5.2.4 Effect of corner radius on Limit Forming Ratio

From the experiments performed to obtain the FFL, it was observed that the corner radius of the pre-cut square hole also affects the formability. Experiments were performed to form the square flange by varying the corner radius, to analyze its effect on the formability. It was decided to vary the corner radius in attempt to form a flange without crack by using the highest PSL which resulted into the failed flange in the experiments discussed in section 5.3.2.

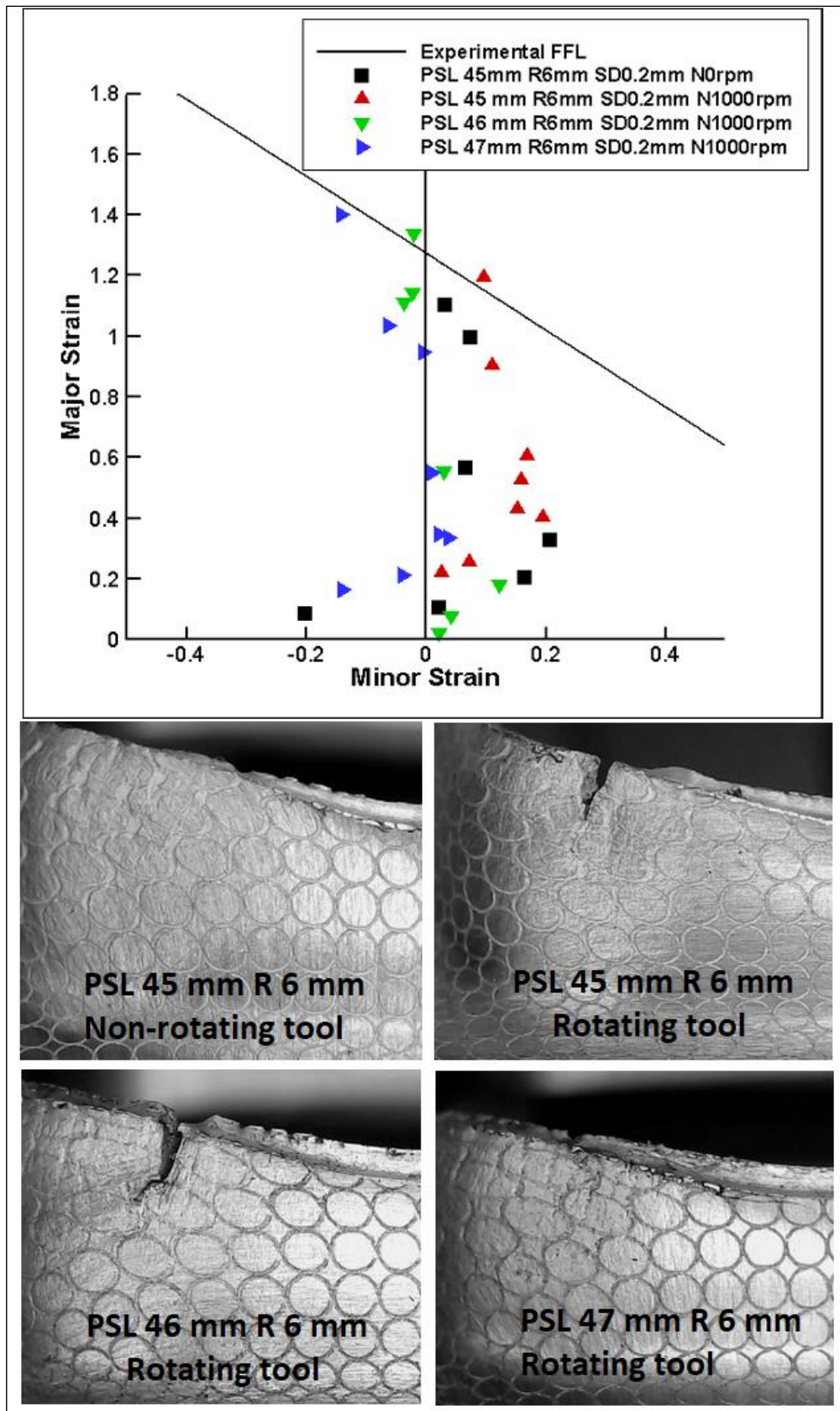


Figure 5.9 Strain distribution and critical zones of the flanges formed using rotating tool

According to the results, sheet with a square pre-cut hole of PSL 44 mm and corner radius 6 mm was selected. Now, experiments were performed considering the same PSL but with different corner radius i.e., 6 mm, 8 mm and 10 mm. The formed flanges are shown in Fig.5.9.

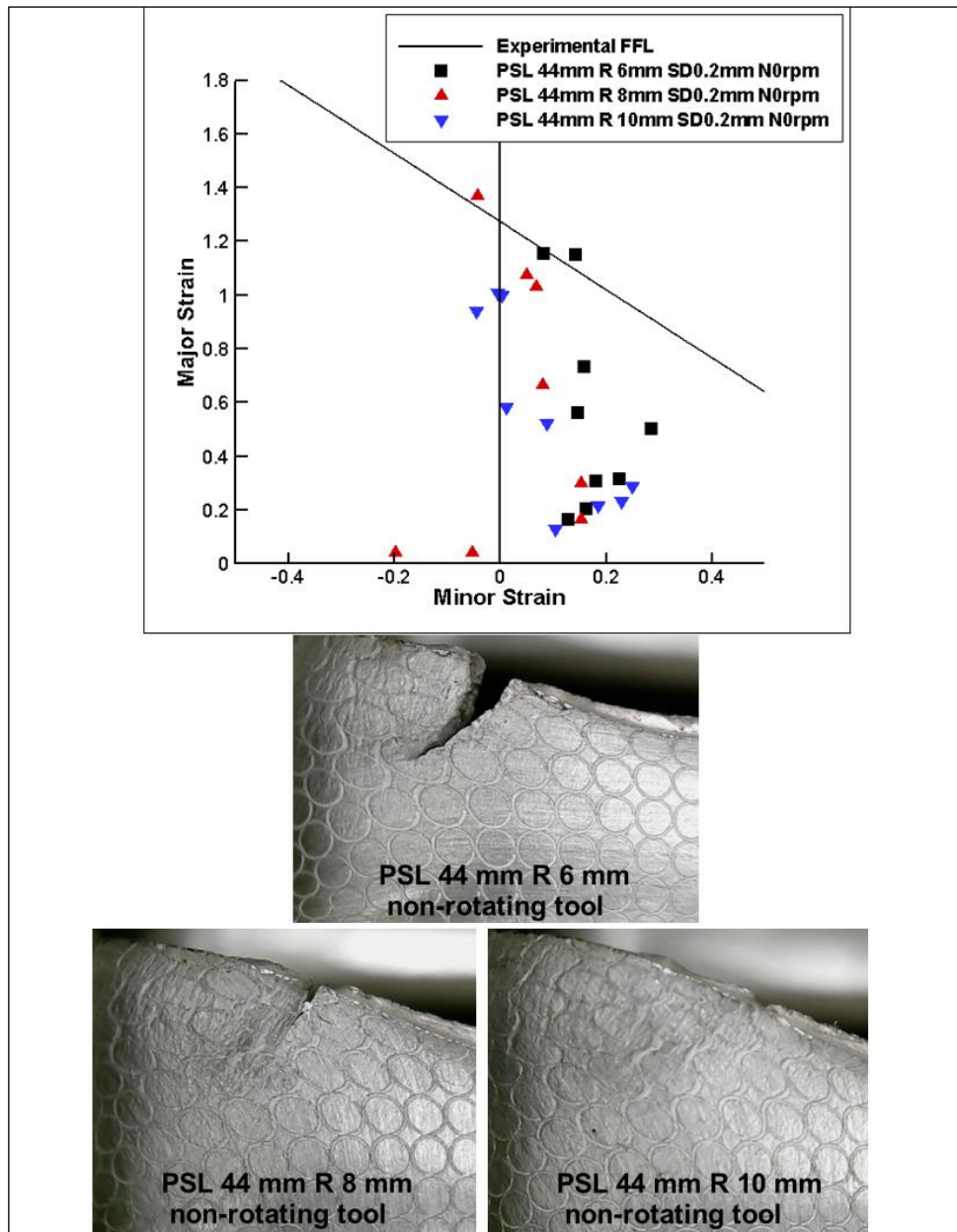


Figure 5.10 Flanges formed from pre-cut square holes with different corner radius and strain distribution on them

The strain distribution and the critical zones of these flanges are shown in Fig.5.10. It was observed that high biaxial stretching took place on the flange with PSL 44 mm and R 6 mm.

In the upper zone of the flange, the material was stretched with near plane strain condition and the strain values crossed the forming limit. Hence, the flange failed.

The next experiment was performed on a sheet with a pre-cut square hole of 44 mm length and 8 mm corner radius. It was observed on this flange that biaxial stretching took place in the middle zone but in the upper zone the strain condition was near plane strain. Further near the edge, high uniaxial tension took place in the circumferential direction and the strain values crossed the forming limit. Clearly, this flange was able to stretch more compared to the previous one but ultimately failed near the edge. Further, experiment was performed on a sheet with PSL of 44 mm and corner radius of 10 mm. It was observed that the flange experienced high bidirectional stretching in the middle zone and near plane strain stretching in the upper zone. The maximum strain values remained below the forming limit and hence no crack was observed on the flange. The LFR of 1.35 is obtained by changing the corner radius to 10 mm, which was 1.26 for the corner radius of 6 mm. These results indicate that the formability increased with increase in the corner radius of the pre-cut square hole. Larger corner radius reduces the stress concentration in the corner area and the stress is distributed along the radius which reduces the strain and increases formability. The deformation mode has shifted from biaxial stretching to plane strain (Fig.5.10). However, the limitation here is the less geometric accuracy. Because of the increased pre-cut hole corner radius, the height of the flange at corner increases. This introduces variation in the height of the flange, so the geometric inaccuracy increased.

5.3 Summary

The feasibility of SPIHF to form square flanges in a single-stage was analyzed. A Series of experiments were performed on AA5052-H32 sheets with 1.5 mm thickness to form the flanges with the non-rotating and rotating tool, and by varying the pre-cut hole corner radius. The following conclusions are derived from the experimental study.

- To describe the flange formability in square hole flanging, Limit Forming Ratio was defined as a ratio of the final flange perimeter to the initial pre-cut hole perimeter.
- In the square hole flange forming, the fracture took place at the merging area of the flange wall and the round corner, this zone is defined as the critical zone. Moreover, the crack

appeared near the flange edge and it was vertical, which shows that the fracture was because of circumferential stress. The material in the critical zone was overstretched when pre-cut hole square length was less than the critical value.

- The LFR with non-rotating tool was 1.26 whereas with rotating tool it was 1.20. The study was carried out at a single tool rotation speed. The effect may vary at a different tool rotation speed, which can be further analyzed.
- The increase in the pre-cut square hole corner radius increased the flange formability which showed that the geometry of the pre-cut hole and the final shape of the flange affected the formability even for the same material.

This work presented in this chapter shows that it is possible to form square flanges with single-stage SPIHF. Further, it is required to improve the mechanical properties of the aluminum flange to widen up the applications of the same. An attempt in this direction was made which is presented in the next chapter.

Chapter 6 Improvement in microhardness of AA5052-H32 material using an eccentric tool in single-stage SPIHF

In this chapter, an experimental study on improvement in the microhardness of AA5052-H32 material using an eccentric tool in single-stage SPIHF has been presented. The tool axis was eccentric to the spindle axis and hence when rotated it induced low frequency vibrations. The grain structure of the formed flanges with a non-rotating tool, a rotating tool and the newly proposed tool are presented and discussed. Moreover, the surface texture and microhardness measurements of these flanges are also presented.

6.1 Experimental Procedure

The single-stage square SPIHF experiments were performed on a 3-axis Vertical Machining Center (VMC). The experimental setup is shown in Fig.6.1. It comprised a top plate and a bottom plate to hold the aluminum sheets. The plates were having a square opening of 60 mm at the center. A SPIF tool of 10 mm diameter was used to deform the aluminum sheets.

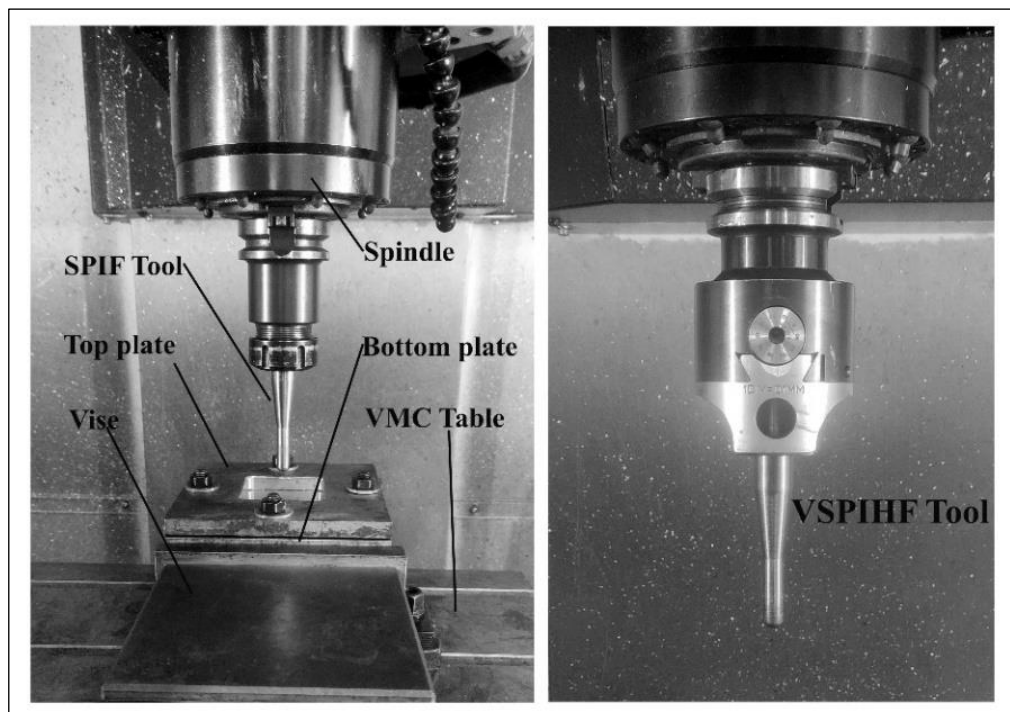


Figure 6.1 Experimental setup of square SPIHF and VSPIHF tool

To induce low-frequency vibrations during the flange forming, the SPIF tool was held in a micro boring head with a facility to offset the tool rotation axis with the axis of the spindle. This tool is called the Vibration assisted Single Point Incremental Hole Flanging (VSPIHF) tool. The scale with an accuracy of 0.01 mm using the micro boring head. To study grain refinement in SPIHF, Experiments were performed in three conditions, 1) with a non-rotating SPIF tool, 2) with a SPIF tool rotating at 1000 rpm, and 3) with a VSPIHF tool having offset of 0.25mm rotating at 1000 rpm.

The hole flanging process was performed in two steps, cutting a precut hole using an end mill cutter, and then the SPIF/ VSPIHF tool traversed on a path as shown in Fig 6.2 (a) to form the square flange. The VSPIHF tool was 0.25 mm offset to the spindle axis and hence the tool movement was with intermittent contact and no-contact positions as shown in Fig 6.2(b). A step depth of 0.2 mm and a feed rate of 1000 mm/min was used for all the experiments. The tool rotation speed of 1000 rpm was used for the experiments performed by the rotating tool and VSPIHF tool. Based on the values of spindle speed and feed rate it is considered that, in one revolution the tool makes a single impact on the sheet. Hence, during the VSPIHF process, vibrations with a low frequency of 16.66 Hz were introduced. In all experiments, hydraulic oil-68 was applied on the sheet surface for lubrication before the hole-flanging process. Sheets with the same precut square length of 48 mm were used.

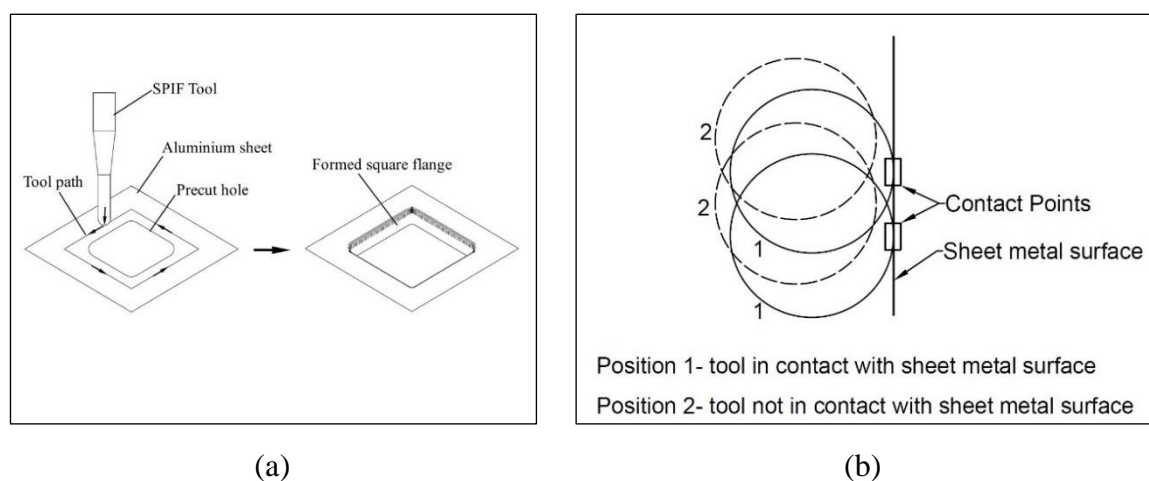
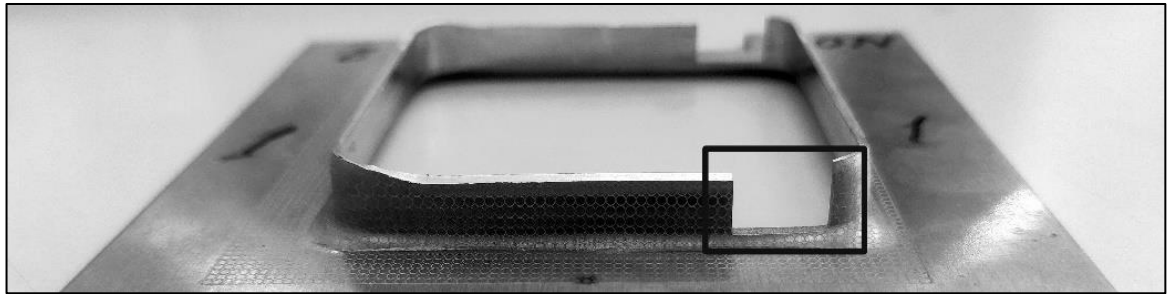


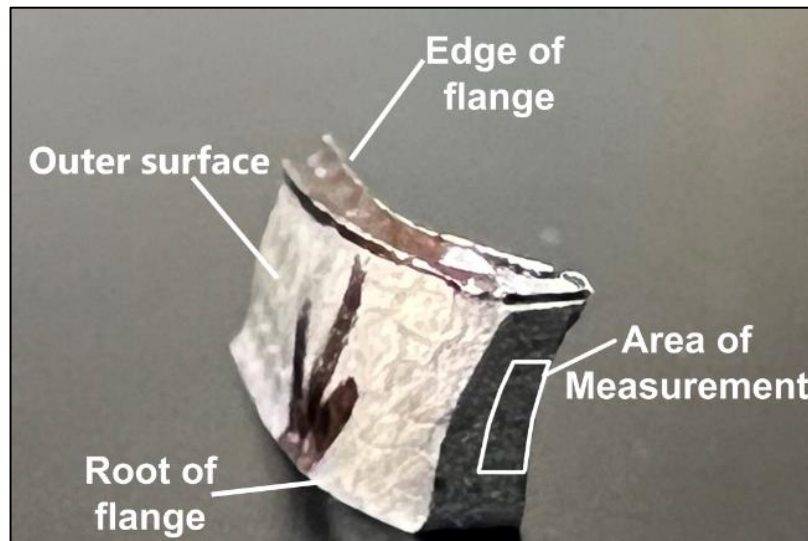
Figure 6.2 (a) Tool path for square flange forming (b) effective tool path in VSPIHF

All measurements were carried out at the critical zone of the square flange. The critical zone was at the junction of the round corner and the straight wall as discussed in previous chapter

and in the work presented by (Cristino et al. 2015). After flange forming, samples of 10 mm x 10 mm were cut by wire cutting method for EBSD measurements as shown in Fig 6.3(a). The EBSD measurements were carried out along the thickness of the flange at a sample area near the inside surface of the flange as shown in Fig 6.3(b).



(a)



(b)

Figure 6.3 (a) EBSD sample location, (b) Measurement area on the sample

To study the deformation behavior, a circle grid (with circles of 1 mm diameter) was marked on the sheets with laser engraving. The circles deformed to elliptical shape due to the deformation of sheet during flange forming. To measure the strain values, the major axis and minor axis of the ellipses were measured with an image analyzer software. Moreover, measurements were taken on the formed flanges to analyze the effect of the VSPIHF tool on the height, thickness, and surface roughness of the flange. The height of the flanges was

measured by a vernier height gauge. The Thickness of the formed flanges was measured by a pointed anvil digital micrometer at the critical zone of the square flange. Finally, the surface roughness was measured on the internal surface of the flange. Moreover, magnified images of the internal surface were taken to understand the tool-sheet contact pattern and its effect on the surface texture. The material characterization was done as explained in the section 3.1.1 and the FFL was obtained as explained in section 3.2.2.1 in chapter 3. The experimentally obtained FFL was considered as a failure limit in this study.

6.2 Results and Discussion

6.2.1 Microstructure

The grain boundary maps were captured by EBSD tests with a step size of 0.15 μm for, a) the non-deformed sheet, b) the flange formed without tool rotation, c) the flange formed with tool rotation, and d) the flange formed by VSPIHF tool which are shown in Fig.6.4(a), Fig.6.4(b), Fig.6.4(c) and Fig.6.4(d) respectively.

A non-uniform grain distribution is observed in the microstructure of the non-deformed sheet as shown in Fig.6.4(a). The average grain size was 28.268 μm . The flange forming by the non-rotating SPIF tool takes place with material stretching and bending. The tool surface remains in contact with the aluminium sheet surface continuously throughout the forming process. Thus, the surface-to-surface contact increases heat, and the deformation of the heated surface affects the microstructure. The grains are elongated in the material stretching direction as shown in Fig.6.4(b). The average grain size of 20.237 μm was observed which shows a refinement by 29% compared to the average grain size of as received aluminium sheet. Moreover, the area fraction of the large grains decreased to 0.124 from 0.197.

The microstructure of the flange formed with the rotating tool is shown in Fig.6.4(c), the average grain size in this microstructure is 12.902 μm , which shows a reduction of 56% compared to the as-received sheet. In the flange forming with the rotating SPIF tool, there is a high relative motion between the tool and the aluminum sheet. Although, the coefficient of friction decreases with the rotation of the tool, the variation of the temperature increases (Durante et al. 2009). The stretching and bending of the heated sheet, with high relative

motion between sheet and tool results in fine and elongated grains. Although grain refinement is observed here, a few dispersed bigger grains remain in the structure. The flanges in the current work were formed by the single-stage strategy, hence the work hardening may be less compared to what can be obtained by the multistage strategy. In the multistage process, the bending of a sheet in the initial stage results in ultrafine grains, and the subsequent stages result in elongated grains and work hardening (Shrivastava and Tandon 2019).

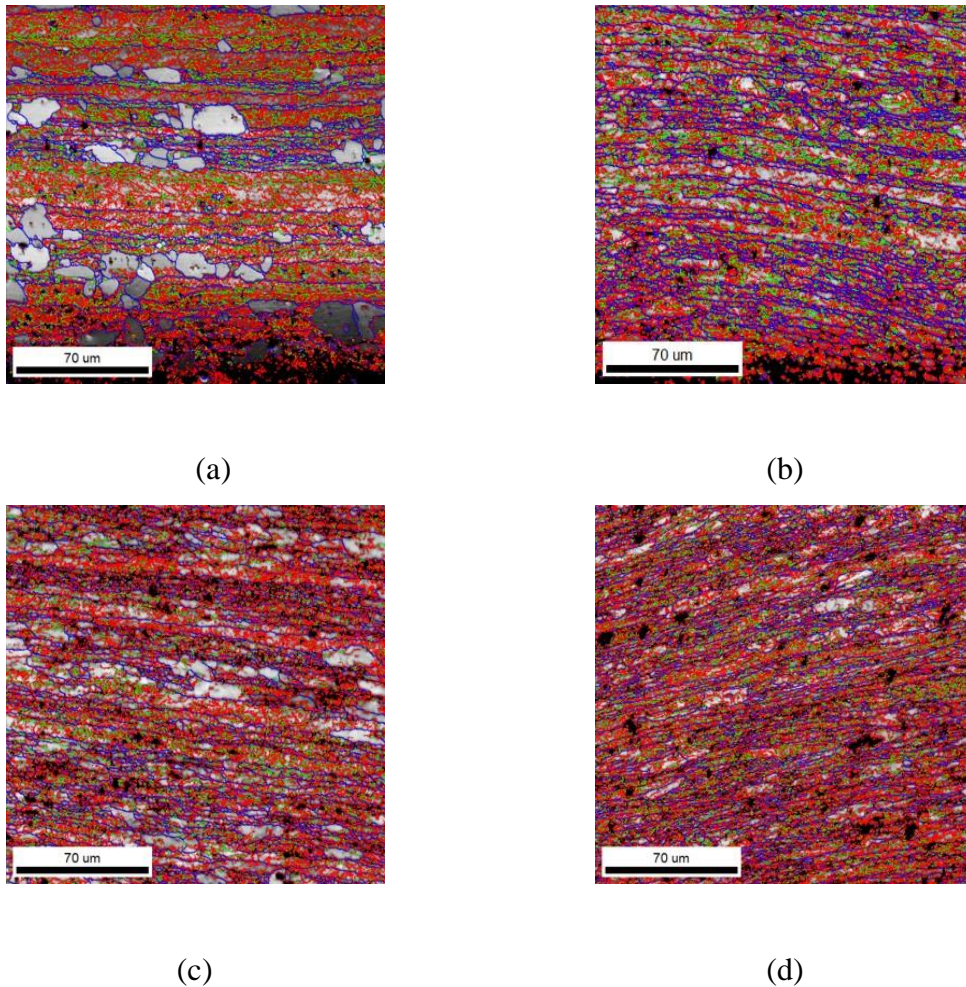


Figure 6.4 Microstructures from EBSD tests for (a) non-deformed sheet (b) flange formed without tool rotation (c) flange formed with tool rotation (d) flange formed by VSPIHF

The microstructure of the flange formed by VSPIHF is shown in Fig.6.4(d). It is observed that a fine-grain microstructure is obtained by the use of the novel tool. The offset of the tool axis with the spindle axis generates the alternate contact pattern as discussed in section 2. The tool motion results in a fine hammering action on the sheet material. The dislocations in

the microstructure move due to the impact of the tool which results in a concentration of dislocations and generates grain boundaries. Ultimately, the refinement of grains took place and a fine-grain microstructure is formed. A reduction of 72 % was observed in the average grain size. Moreover, the area fraction of large grains reduced to 0.028.

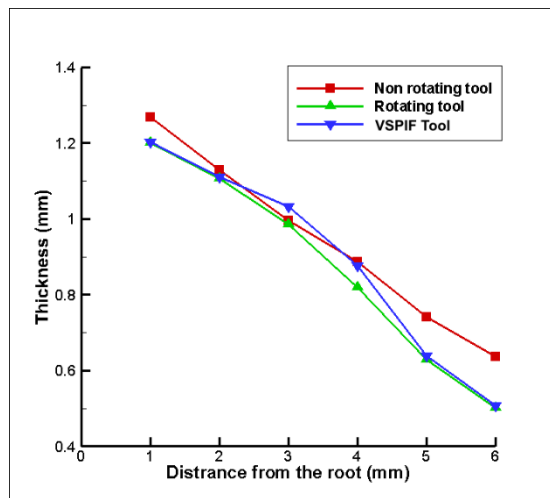
6.2.2 Thickness and height of flange

The thickness distribution on the flanges and height of the flanges formed without tool rotation, with tool rotation and VSPIHF tool are plotted in Fig.6.5(a) and (b) respectively considering the average values of the readings taken from the two repetitive experiments for each tooling condition (non-rotating, rotating and VSPIHF). The thickness and height values are tabulated in table 6.1. It is observed that the thickness on the flange formed without tool rotation is higher than the other two flanges. As explained above, heating of sheet increases because of the rotating tool. The shear force due to rotating tool in the heated zone increases thinning. Moreover, it was observed during the experiments that the rotating tool caused wear of sheet material and it was removed in form of metal dust which was carried away by the lubricant as shown in Fig.6.6.

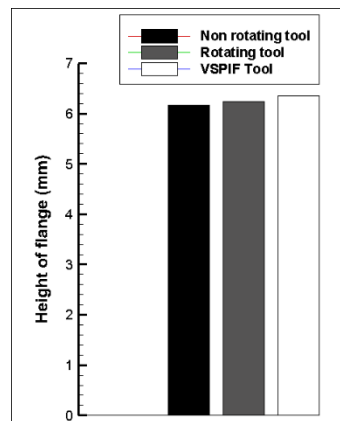
The strain distribution in the critical zone of the flange from the root towards the edge is shown in Fig.6.7. The points were obtained by measuring the circles in the critical zone with the highest deformation. It was observed that biaxial stretching takes place at the mid-zone of the flange whereas, near plane strain mode of deformation was observed near the edge of the flange. The strain plot reveals that the rotating tool caused higher biaxial stretching than the non-rotating tool and a little higher than the VSPIHF tool. Hence, more thinning occurred by rotating SPIF tool than the VSPIHF tool.

During the VSPIHF process, the tool had a contact-no-contact pattern as discussed earlier. Because of this pattern, the tool was not continuously in contact with the sheet material and hence, wearing was less. The strain distribution shows a little less biaxial stretching at the middle of the flange as compared to the rotating tool. This effect is visible in the thickness distribution. It is observed that the thickness on the flange was a little higher than the thickness on the flange formed with tool rotation. Moreover, more stretching due to tool rotation affects the height of the flange as observed in Fig.6.5(b). The height of the flange achieved by the non-rotating tool, rotating tool, and VSPIHF tool was 6.16 mm, 6.24 mm,

and 6.36 mm respectively. The height of the flange formed with rotating tool is a little higher than the flange formed by the non-rotating tool, which again shows that there was more stretching in the former.



(a)



(b)

Figure 6.5 (a) Thickness distribution on the flanges, (b) height of the flanges

Table 6.1 Thickness along the flange

Distance form root (mm)	1	2	3	4	5	6
Thickness on flange formed by non-rotating tool	1.26	1.129	0.995	0.887	0.741	0.637
Thickness on flange formed by rotating tool	1.201	1.106	0.986	0.82	0.629	0.501
Thickness on flange formed by VSPIHF tool	1.145	1.111	1.032	0.876	0.638	0.508

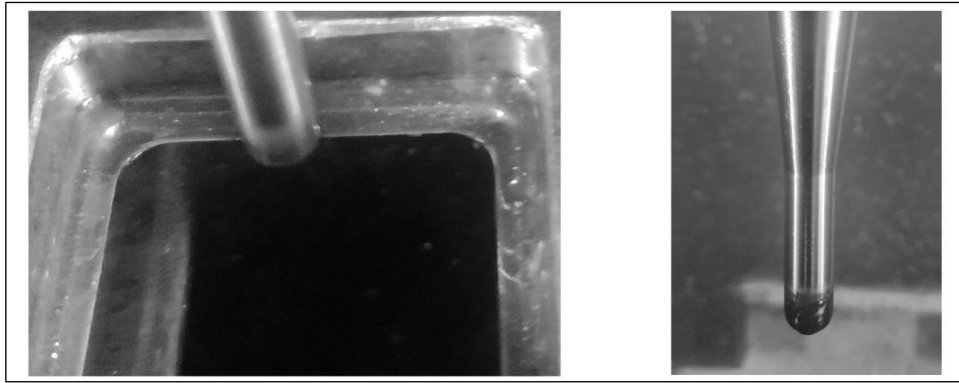


Figure 6.6 Metal dust visible on the sheet and the tool head

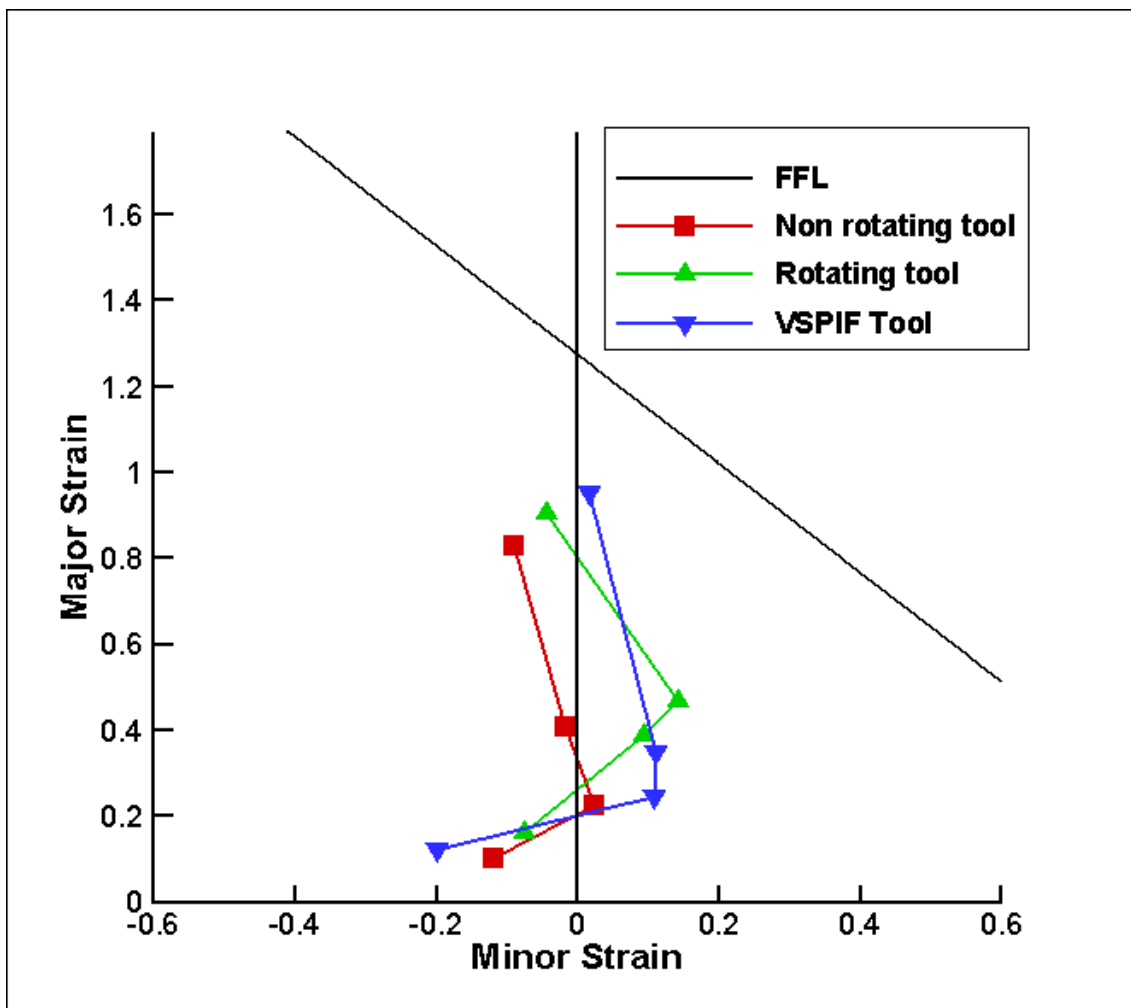
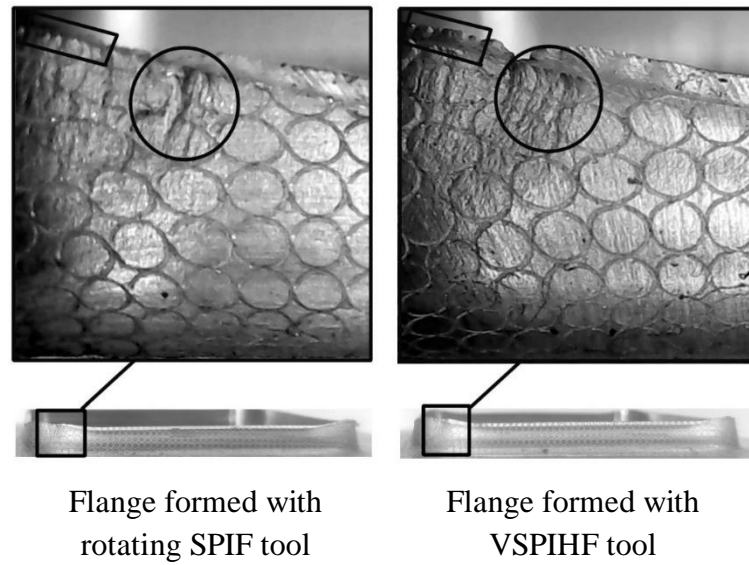


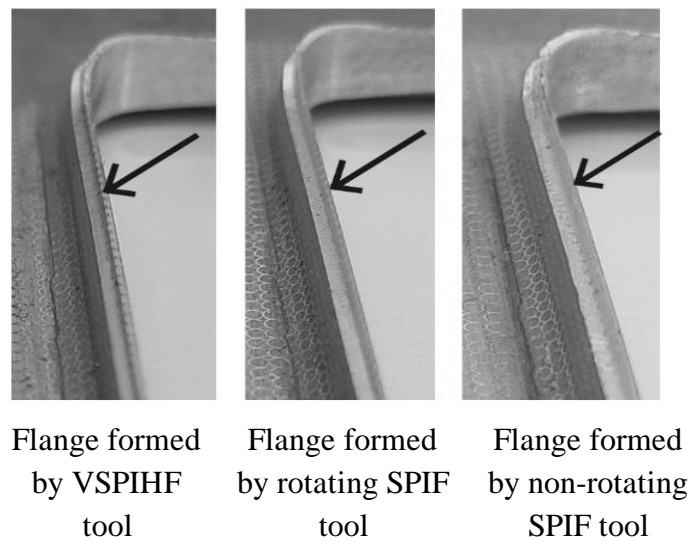
Figure 6.7 Strain distribution on the flanges

The use of the VSPIHF tool resulted in a little higher flange height as compared to what is obtained by using the rotating tool. This can be understood from Fig.6.8(a). It is visible that

due to repeated impacting of the tool, more but shallow stretch marks are observed on the outer surface whereas the rotating SPIF tool generates deep stretch marks due to higher stretching. Moreover, it was observed that the rotating tool and VSPIHF tool stretched the material on the inner surface near the edge, hence the edge deformation took place. Due to the hammering action in VSPIHF, the edge bending was little higher as visible in Fig.6.8(b). Hence, the flange height increased, however it was not substantial.



(a)



(b)

Figure 6.8 (a) Stretch marks in the critical zone of the flanges, (b) edge bending

6.2.3 Surface roughness and microhardness

To view the surface texture on the flange surface, images were captured with 50X magnification; the area near the edge on the inner surface of the flanges are shown in Fig.6.9.

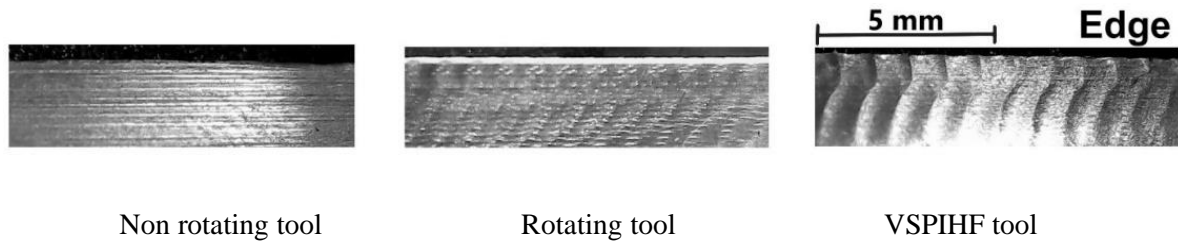


Figure 6.9 Surface texture of the flanges

The surface roughness on the internal surface along the tool feed direction was measured, and three readings were taken on each flange surface to get accurate results. The flange surface formed with a non-rotating tool shows thin horizontal marks i.e., in the tool motion direction, no vertical tool marks are visible. The rotating tool softens the material and leaves vertical marks on the surface as visible in the image. The alternate impact motion of the tool in VSPIHF generated deep marks on the surface as visible in the image, due to which, the roughness is more than the case of rotating tool. The average surface roughness on the three flanges is $0.215\ \mu\text{m}$, $0.269\ \mu\text{m}$, and $0.338\ \mu\text{m}$ respectively which shows an increase in surface roughness when the rotating tool and VSPIHF tool were used, it is consistent with the surface texture discussed above.

Table 6.2 Microhardness of the flanges

Sr. No.	Flange forming condition	Microhardness (HV)
1	Not formed- as received sheet	79.67
2	Flange formed with a non-rotating tool	99.57
3	Flange formed with a rotating tool	114.70
4	Flange formed with VSPIHF tool	128.30

The microhardness on the internal surface of each flange was measured with HV0.2. The load of 200 gf was applied with a dwell time of 10 seconds. Five readings were taken for all samples and the average values are considered. The results are shown in Table 6.2. The use

of the rotating tool and VSPIHF resulted in higher microhardness. The highest hardness was achieved on the flange formed by the VSPIHF method which can be attributed to strain hardening and grain refinement.

6.3 Summary

A new methodology of single point incremental hole flanging was proposed to achieve grain refinement on aluminium sheet material. The grain structure on the sheets formed by a non-rotating tool, a rotating tool and the proposed VSPIHF tool has been studied. Moreover, the effect of the proposed tool on thickness, height and surface roughness of the flanges have been analyzed. The findings are summarized as follows.

- The grain structure of the aluminium material was affected in the SPIHF process. The tool rotation resulted in uniform grain distribution and grain refinement. The use of VSPIHF tool generated tool rotation induced vibrations. An impacting action on the material was observed which broke the existing grains and resulted in more uniform grain distribution with refinement.
- The thickness and height of the flange was affected by the use of rotating SPIF tool and VSPIHF tool. The rotating tool increased the thinning of the material. Moreover, the strain plots suggested that high biaxial stretching occurred at the mid height of the flange when the rotating tool was used. The use of VSPIHF tool reduced the thinning, however the reduction was not substantial.
- The internal surface of the flange which was in contact with the forming tool had a greater effect on its texture because of the type of tool used. Rotating tool increased the surface roughness because of the surface damage due to wearing of material. A pattern of continuous deep marks was observed when the VSPIHF tool was used which also resulted into increase in the surface roughness of the material.
- The use of VSPIHF tool results into increased microhardness of the aluminium material which was in line with the refinement of the grains.

The overall results suggest improvement in the grain structure and increase in the hardness of the aluminium material by use of VSPIHF tool. However, the study was carried out at a single tool rotation speed. Further, the effect of different frequency of the vibrations induced by the VSPIHF tool can be explored which may also result into a better surface quality.

References

- Al-Ghamdi, Khalid A., and G. Hussain. "Stress Gradient Due to Incremental Forming of Bonded Metallic Laminates." *Materials and Manufacturing Processes*, vol. 32, no. 12, 2017, pp. 1384–90, <https://doi.org/10.1080/10426914.2017.1339315>.
- Ambrogio, G, et al. *A Force Measuring Based Strategy for Failure Prevention in Incremental Forming*. 2006, pp. 413–16, <https://doi.org/10.1016/j.jmatprotec.2006.04.076>.
- Ambrogio, G., et al. "Formability of AZ31 Magnesium Alloy in Warm Incremental Forming Process." *International Journal of Material Forming*, vol. 2, no. SUPPL. 1, 2009, pp. 5–8, <https://doi.org/10.1007/s12289-009-0434-8>.
- Ashkenazi, Dana. "How Aluminum Changed the World: A Metallurgical Revolution through Technological and Cultural Perspectives." *Technological Forecasting and Social Change*, vol. 143, no. April, 2019, pp. 101–13, <https://doi.org/10.1016/j.techfore.2019.03.011>.
- Bagudanch, I., et al. "Polymer Incremental Sheet Forming Process: Temperature Analysis Using Response Surface Methodology." *Materials and Manufacturing Processes*, vol. 32, no. 1, 2017, pp. 44–53, <https://doi.org/10.1080/10426914.2016.1176191>.
- Bambach, Markus, et al. "A New Process Design for Performing Hole-Flanging Operations by Incremental Sheet Forming." *Procedia Engineering*, vol. 81, no. October, 2014, pp. 2305–10, <https://doi.org/10.1016/j.proeng.2014.10.325>.
- Baruah, Angshuman, et al. "Optimization of AA5052 in Incremental Sheet Forming Using Grey Relational Analysis." *Measurement: Journal of the International Measurement Confederation*, vol. 106, 2017, pp. 95–100, <https://doi.org/10.1016/j.measurement.2017.04.029>.
- Basak, Shamik, et al. "Parameter Optimization and Texture Evolution in Single Point Incremental Sheet Forming Process." *Proceedings of the Institution of Mechanical Engineers, Part B: Journal of Engineering Manufacture*, vol. 234, no. 1–2, 2020, pp. 126–39, <https://doi.org/10.1177/0954405419846001>.
- Besong, Lemopi Isidore, Johannes Buhl, Ismail Ünsal, et al. "Development of Tool Paths for Multi-Axis Single Stage Incremental Hole-Flanging." *Procedia Manufacturing*, vol. 47, no. 2019, 2020, pp. 1392–98, <https://doi.org/10.1016/j.promfg.2020.04.290>.
- Besong, Lemopi Isidore, Johannes Buhl, and Markus Bambach. "Investigations on Hole-Flanging by Paddle Forming and a Comparison with Single Point Incremental Forming." *International Journal of Mechanical Sciences*, vol. 164, no. April, 2019, p.

105143, <https://doi.org/10.1016/j.ijmecsci.2019.105143>.

- Borrego, M., et al. “Experimental Study of Hole-Flanging by Single-Stage Incremental Sheet Forming.” *Journal of Materials Processing Technology*, vol. 237, 2016, pp. 320–30, <https://doi.org/10.1016/j.jmatprotec.2016.06.026>.
- Borrego, Marcos, et al. “Hole-Flanging of AA7075-O Sheets: Conventional Process versus SPIF.” *Procedia Manufacturing*, vol. 50, no. 2019, 2020, pp. 236–40, <https://doi.org/10.1016/j.promfg.2020.08.044>.
- Cao, Tingting, et al. “Investigation on a New Hole-Flanging Approach by Incremental Sheet Forming through a Featured Tool.” *International Journal of Machine Tools and Manufacture*, vol. 110, 2016, pp. 1–17, <https://doi.org/10.1016/j.ijmachtools.2016.08.003>.
- Centeno, G., et al. “Hole-Flanging by Incremental Sheet Forming.” *International Journal of Machine Tools and Manufacture*, vol. 59, 2012, pp. 46–54, <https://doi.org/10.1016/j.ijmachtools.2012.03.007>.
- Centeno, Gabriel, et al. “Critical Analysis of Necking and Fracture Limit Strains and Forming Forces in Single-Point Incremental Forming.” *Materials and Design*, vol. 63, 2014, pp. 20–29, <https://doi.org/10.1016/j.matdes.2014.05.066>.
- Ceretti, Elisabetta, et al. “Experimental and Simulative Results in Sheet Incremental Forming on CNC Machines.” *Journal of Materials Processing Technology*, vol. 152, no. 2, 2004, pp. 176–84, <https://doi.org/10.1016/j.jmatprotec.2004.03.024>.
- Chen, Xia, et al. “Investigation of Factors Affecting the Formability of Metallic Sheets in Dieless Incremental Hole-Flanging.” *International Journal of Advanced Manufacturing Technology*, vol. 103, no. 5–8, 2019, pp. 2609–20, <https://doi.org/10.1007/s00170-019-03459-x>.
- Cristino, V. A., et al. “Fracture in Hole-Flanging Produced by Single Point Incremental Forming.” *International Journal of Mechanical Sciences*, vol. 83, 2014, pp. 146–54, <https://doi.org/10.1016/j.ijmecsci.2014.04.001>.
- Cristino, V. A.M., et al. “Towards Square Hole-Flanging Produced by Single Point Incremental Forming.” *Proceedings of the Institution of Mechanical Engineers, Part L: Journal of Materials: Design and Applications*, vol. 229, no. 5, 2015, pp. 380–88, <https://doi.org/10.1177/1464420714524930>.
- Cristino, Valentino A.M., et al. “Hole-Flanging of Metals and Polymers Produced by Single Point Incremental Forming.” *International Journal of Materials and Product Technology*, vol. 50, no. 1, 2015, pp. 37–48, <https://doi.org/10.1504/IJMPT.2015.066865>.

- Cui, Z., and L. Gao. "Studies on Hole-Flanging Process Using Multistage Incremental Forming." *CIRP Journal of Manufacturing Science and Technology*, vol. 2, no. 2, 2010, pp. 124–28, <https://doi.org/10.1016/j.cirpj.2010.02.001>.
- Dai, Kun, et al. "CNC Incremental Sheet Forming of an Axially Symmetric Specimen and the Locus of Optimization." *Journal of Materials Processing Technology*, vol. 102, no. 1, 2000, pp. 164–67, [https://doi.org/10.1016/S0924-0136\(00\)00423-4](https://doi.org/10.1016/S0924-0136(00)00423-4).
- Davarpanah, Mohammad Ali, and Rajiv Malhotra. "Formability and Failure Modes in Single Point Incremental Forming of Metal-Polymer Laminates." *Procedia Manufacturing*, vol. 26, 2018, pp. 343–48, <https://doi.org/10.1016/j.promfg.2018.07.042>.
- Duflou, J. R., et al. "Process Window Enhancement for Single Point Incremental Forming through Multi-Step Toolpaths." *CIRP Annals - Manufacturing Technology*, vol. 57, no. 1, 2008, pp. 253–56, <https://doi.org/10.1016/j.cirp.2008.03.030>.
- Durante, M., et al. "The Influence of Tool Rotation on an Incremental Forming Process." *Journal of Materials Processing Technology*, vol. 209, no. 9, 2009, pp. 4621–26, <https://doi.org/10.1016/j.jmatprotec.2008.11.028>.
- Essa, Khamis, and Peter Hartley. "An Assessment of Various Process Strategies for Improving Precision in Single Point Incremental Forming." *International Journal of Material Forming*, vol. 4, no. 4, 2011, pp. 401–12, <https://doi.org/10.1007/s12289-010-1004-9>.
- Eyckens, P., et al. "The Significance of Friction in the Single Point Incremental Forming Process." *International Journal of Material Forming*, vol. 3, no. SUPPL. 1, 2010, pp. 947–50, <https://doi.org/10.1007/s12289-010-0925-7>.
- Filice, L., et al. "Analysis of Material Formability in Incremental Forming." *CIRP Annals - Manufacturing Technology*, vol. 51, no. 1, 2002, pp. 199–202, [https://doi.org/10.1016/S0007-8506\(07\)61499-1](https://doi.org/10.1016/S0007-8506(07)61499-1).
- Fiorotto, M., et al. "Preliminary Studies on Single Point Incremental Forming for Composite Materials." *International Journal of Material Forming*, vol. 3, no. SUPPL. 1, 2010, pp. 951–54, <https://doi.org/10.1007/s12289-010-0926-6>.
- Formisano, A., et al. "Negative and Positive Incremental Forming: Comparison by Geometrical, Experimental, and FEM Considerations." *Materials and Manufacturing Processes*, vol. 32, no. 5, 2017, pp. 530–36, <https://doi.org/10.1080/10426914.2016.1232810>.
- Gandla, Praveen Kumar, et al. "Effect of Pre-Cut Hole Diameter on Deformation Mechanics in Multi-Stage Incremental Hole Flanging of Deep Drawing Quality Steel." *Archives of Civil and Mechanical Engineering*, vol. 21, no. 1, 2021, pp. 1–23,

<https://doi.org/10.1007/s43452-020-00156-5>.

- Gohil, Ashish, and Bharat Modi. "Review of the Effect of Process Parameters on Performance Measures in the Incremental Sheet Forming Process." *Proceedings of the Institution of Mechanical Engineers, Part B: Journal of Engineering Manufacture*, vol. 235, no. 3, 2021, pp. 303–32, <https://doi.org/10.1177/0954405420961215>.
- Guzmán, Carlos Felipe, et al. "Study of the Geometrical Inaccuracy on a SPIF Two-Slope Pyramid by Finite Element Simulations." *International Journal of Solids and Structures*, vol. 49, no. 25, 2012, pp. 3594–604, <https://doi.org/10.1016/j.ijsolstr.2012.07.016>.
- Hirsch, Jürgen. "Recent Development in Aluminium for Automotive Applications." *Transactions of Nonferrous Metals Society of China (English Edition)*, vol. 24, no. 7, 2014, pp. 1995–2002, [https://doi.org/10.1016/S1003-6326\(14\)63305-7](https://doi.org/10.1016/S1003-6326(14)63305-7).
- Hirt, G., et al. "Forming Strategies and Process Modelling for CNC Incremental Sheet Forming." *CIRP Annals - Manufacturing Technology*, vol. 53, no. 1, 2004, pp. 203–06, [https://doi.org/10.1016/S0007-8506\(07\)60679-9](https://doi.org/10.1016/S0007-8506(07)60679-9).
- Holmberg, Stefan, et al. "Evaluation of Sheet Metal Formability by Tensile Tests." *Journal of Materials Processing Technology*, vol. 145, no. 1, 2004, pp. 72–83, <https://doi.org/10.1016/j.jmatprotec.2003.07.004>.
- Huang, You Min, and Kuo Hsiung Chien. "The Formability Limitation of the Hole-Flanging Process." *Journal of Materials Processing Technology*, vol. 117, no. 1–2, 2001, pp. 43–51, [https://doi.org/10.1016/S0924-0136\(01\)01060-3](https://doi.org/10.1016/S0924-0136(01)01060-3).
- Hussain, G., L. Gao, et al. "Empirical Modelling of the Influence of Operating Parameters on the Spifability of a Titanium Sheet Using Response Surface Methodology." *Proceedings of the Institution of Mechanical Engineers, Part B: Journal of Engineering Manufacture*, vol. 223, no. 1, 2009, pp. 73–81, <https://doi.org/10.1243/09544054JEM1259>.
- Hussain, G., H. R. Khan, et al. "Guidelines for Tool-Size Selection for Single-Point Incremental Forming of an Aerospace Alloy." *Materials and Manufacturing Processes*, vol. 28, no. 3, 2013, pp. 324–29, <https://doi.org/10.1080/10426914.2012.700151>.
- Hussain, Ghulam. "Experimental Investigations on the Role of Tool Size in Causing and Controlling Defects in Single Point Incremental Forming Process." *Proceedings of the Institution of Mechanical Engineers, Part B: Journal of Engineering Manufacture*, vol. 228, no. 2, 2014, pp. 266–77, <https://doi.org/10.1177/0954405413498864>.
- Isik, K., et al. "Formability Limits by Fracture in Sheet Metal Forming." *Journal of Materials Processing Technology*, vol. 214, no. 8, 2014, pp. 1557–65,

<https://doi.org/10.1016/j.jmatprotec.2014.02.026>.

- Jeswiet, J., F. Micari, et al. "Asymmetric Single Point Incremental Forming of Sheet Metal." *CIRP Annals - Manufacturing Technology*, vol. 54, no. 2, 2005, pp. 88–114, [https://doi.org/10.1016/S0007-8506\(07\)60021-3](https://doi.org/10.1016/S0007-8506(07)60021-3).
- Jeswiet, J., E. Hagan, et al. "Forming Parameters for Incremental Forming of Aluminium Alloy Sheet Metal." *Proceedings of the Institution of Mechanical Engineers, Part B: Journal of Engineering Manufacture*, vol. 216, no. 10, 2002, pp. 1367–71, <https://doi.org/10.1243/095440502320405458>.
- Kacem, A., et al. "Failure Prediction in the Hole-Flanging Process of Aluminium Alloys." *Engineering Fracture Mechanics*, vol. 99, 2013, pp. 251–65, <https://doi.org/10.1016/j.engfracmech.2012.12.018>.
- Khalatbari, H., et al. "High-Speed Incremental Forming Process: A Trade-Off between Formability and Time Efficiency." *Materials and Manufacturing Processes*, vol. 30, no. 11, 2015, pp. 1354–63, <https://doi.org/10.1080/10426914.2015.1037892>.
- Kim, T. J., and D. Y. Yang. "Improvement of Formability for the Incremental Sheet Metal Forming Process." *International Journal of Mechanical Sciences*, vol. 42, no. 7, 2000, pp. 1271–86, [https://doi.org/10.1016/S0020-7403\(99\)00047-8](https://doi.org/10.1016/S0020-7403(99)00047-8).
- Kim, Y. H., and J. J. Park. "Effect of Process Parameters on Formability in Incremental Forming of Sheet Metal." *Journal of Materials Processing Technology*, vol. 130, no. 131, 2002, pp. 42–46, [https://doi.org/10.1016/S0924-0136\(02\)00788-4](https://doi.org/10.1016/S0924-0136(02)00788-4).
- Kobayashi, S., et al. "A Theory of Shear Spinning of Cones." *Journal of Manufacturing Science and Engineering, Transactions of the ASME*, vol. 83, no. 4, 1961, pp. 485–94, <https://doi.org/10.1115/1.3664573>.
- Kumar, Ajay, et al. "Parametric Effects on Formability of AA2024-O Aluminum Alloy Sheets in Single Point Incremental Forming." *Journal of Materials Research and Technology*, vol. 8, no. 1, 2019, pp. 1461–69, <https://doi.org/10.1016/j.jmrt.2018.11.001>.
- Kumar, Ajay, and Vishal Gulati. "Experimental Investigation and Optimization of Surface Roughness in Negative Incremental Forming." *Measurement: Journal of the International Measurement Confederation*, vol. 131, no. August, 2019, pp. 419–30, <https://doi.org/10.1016/j.measurement.2018.08.078>.
- Laugwitz, M., et al. "Development of Tooling Concepts to Increase Geometrical Accuracy in High Speed Incremental Hole Flanging." *International Journal of Material Forming*, vol. 11, no. 4, 2018, pp. 471–77, <https://doi.org/10.1007/s12289-017-1356-5>.

- Lee, Jong Sup, et al. "Evaluation of Hole Flangeability of Steel Sheet with Respect to the Hole Processing Condition." *Key Engineering Materials*, vol. 340-341 I, 2007, pp. 665–70, <https://doi.org/10.4028/www.scientific.net/kem.340-341.665>.
- Leszak, Edward. "Apparatus and Process for Incremental Dieless Forming." *Google.Com*, 1967, p. 19, <http://www.google.com/patents/US3549577>.
- Li, Yanle, William J. T. Daniel, et al. "Deformation Mechanics and Efficient Force Prediction in Single Point Incremental Forming." *Journal of Materials Processing Technology*, vol. 221, 2015, pp. 100–11, <https://doi.org/10.1016/j.jmatprotec.2015.02.009>.
- Li, Yanle, Zhaobing Liu, et al. "Simulation and Experimental Observations of Effect of Different Contact Interfaces on the Incremental Sheet Forming Process." *Materials and Manufacturing Processes*, vol. 29, no. 2, 2014, pp. 121–28, <https://doi.org/10.1080/10426914.2013.822977>.
- Liu, Zhaobing, et al. "Experimental Investigation of Mechanical Properties, Formability and Force Measurement for AA7075-O Aluminum Alloy Sheets Formed by Incremental Forming." *International Journal of Precision Engineering and Manufacturing*, vol. 14, no. 11, 2013, pp. 1891–99, <https://doi.org/10.1007/s12541-013-0255-z>.
- Liuru, Z., et al. "Study on Incremental Forming for the Fender of the Car." *Materials Research Innovations*, vol. 19, no. March, 2015, pp. S6105–07, <https://doi.org/10.1179/1432891715Z.0000000001435>.
- Liuru, Z., and Z. Yinmei. "A New Method for Multi-Pass Single-Point Incremental Forming of Vertical Wall Square Box with Small Corner Radius." *Materials Research Innovations*, vol. 19, no. May 2015, 2015, pp. S5543–45, <https://doi.org/10.1179/1432891714Z.0000000001148>.
- Lu, B., Y. Fang, et al. "Mechanism Investigation of Friction-Related Effects in Single Point Incremental Forming Using a Developed Oblique Roller-Ball Tool." *International Journal of Machine Tools and Manufacture*, vol. 85, 2014, pp. 14–29, <https://doi.org/10.1016/j.ijmachtools.2014.04.007>.
- Lu, B., H. Ou, et al. "Titanium Based Cranial Reconstruction Using Incremental Sheet Forming." *International Journal of Material Forming*, vol. 9, no. 3, 2016, pp. 361–70, <https://doi.org/10.1007/s12289-014-1205-8>.
- Lu, Haibo, et al. "Part Accuracy Improvement in Two Point Incremental Forming with a Partial Die Using a Model Predictive Control Algorithm." *Precision Engineering*, vol. 49, 2017, pp. 179–88, <https://doi.org/10.1016/j.precisioneng.2017.02.006>.
- Martínez-Donaire, A. J., M. Borrego, et al. "Analysis of the Influence of Stress Triaxiality on Formability of Hole-Flanging by Single-Stage SPIF." *International Journal of*

- Mechanical Sciences*, vol. 151, no. July 2018, 2019, pp. 76–84, <https://doi.org/10.1016/j.ijmecsci.2018.11.006>.
- Martínez-Donaire, A. J., F. J. García-Lomas, et al. “New Approaches to Detect the Onset of Localised Necking in Sheets under Through-Thickness Strain Gradients.” *Materials and Design*, vol. 57, 2014, pp. 135–45, <https://doi.org/10.1016/j.matdes.2014.01.012>.
- Martínez-Donaire, A. J., D. Morales-Palma, et al. “Numerical Explicit Analysis of Hole Flanging by Single-Stage Incremental Forming.” *Procedia Manufacturing*, vol. 13, 2017, pp. 132–38, <https://doi.org/10.1016/j.promfg.2017.09.019>.
- Meier, H., et al. “Increasing the Part Accuracy in Dieless Robot-Based Incremental Sheet Metal Forming.” *CIRP Annals - Manufacturing Technology*, vol. 58, no. 1, 2009, pp. 233–38, <https://doi.org/10.1016/j.cirp.2009.03.056>.
- Mirnia, M. J., et al. “An Investigation into Thickness Distribution in Single Point Incremental Forming Using Sequential Limit Analysis.” *International Journal of Material Forming*, vol. 7, no. 4, 2014, pp. 469–77, <https://doi.org/10.1007/s12289-013-1143-x>.
- Mohanty, Swagatika, et al. “Robot-Assisted Incremental Sheet Metal Forming under the Different Forming Condition.” *Journal of the Brazilian Society of Mechanical Sciences and Engineering*, vol. 41, no. 2, 2019, <https://doi.org/10.1007/s40430-019-1581-6>.
- Montanari, L., et al. “A New Approach for Deformation History of Material Elements in Hole-Flanging Produced by Single Point Incremental Forming.” *International Journal of Advanced Manufacturing Technology*, vol. 69, no. 5–8, 2013, pp. 1175–83, <https://doi.org/10.1007/s00170-013-5117-4>.
- . “On the Relative Performance of Hole-Flanging by Incremental Sheet Forming and Conventional Press-Working.” *Proceedings of the Institution of Mechanical Engineers, Part L: Journal of Materials: Design and Applications*, vol. 228, no. 4, 2014, pp. 312–22, <https://doi.org/10.1177/1464420713492149>.
- Morales-Palma, D., et al. “Preliminary Investigation on Homogenization of the Thickness Distribution in Hole-Flanging by SPIF.” *Procedia Manufacturing*, vol. 13, 2017, pp. 124–31, <https://doi.org/10.1016/j.promfg.2017.09.101>.
- Morales-Palma, Domingo, et al. “Optimization of Hole-Flanging by Single Point Incremental Forming in Two Stages.” *Materials*, vol. 11, no. 10, 2018, <https://doi.org/10.3390/ma11102029>.
- Mugendiran, V., and A. Gnanavelbabu. “Analysis of Hole Flanging on AA5052 Alloy by Single Point Incremental Forming Process.” *Materials Today: Proceedings*, vol. 5, no. 2, 2018, pp. 8596–603, <https://doi.org/10.1016/j.matpr.2017.11.557>.

- Mulay, Amrut, et al. "Experimental Investigations into the Effects of SPIF Forming Conditions on Surface Roughness and Formability by Design of Experiments." *Journal of the Brazilian Society of Mechanical Sciences and Engineering*, vol. 39, no. 10, 2017, pp. 3997–4010, <https://doi.org/10.1007/s40430-016-0703-7>.
- Najm, Sherwan Mohammed, et al. "Parametric Effects of Single Point Incremental Forming on Hardness of AA1100 Aluminium Alloy Sheets." *Materials*, vol. 14, no. 23, 2021, <https://doi.org/10.3390/ma14237263>.
- Oleksik, Valentin, et al. "Experimental Study on the Surface Quality of the Medical Implants Obtained by Single Point Incremental Forming." *International Journal of Material Forming*, vol. 3, no. SUPPL. 1, 2010, pp. 935–38, <https://doi.org/10.1007/s12289-010-0922-x>.
- Pandre, Sandeep, et al. "Processing of DP590 Steel Using Single Point Incremental Forming for Automotive Applications." *Materials and Manufacturing Processes*, vol. 36, no. 14, 2021, pp. 1658–66, <https://doi.org/10.1080/10426914.2021.1942903>.
- Park, Jong Jin, and Yung Ho Kim. "Fundamental Studies on the Incremental Sheet Metal Forming Technique." *Journal of Materials Processing Technology*, vol. 140, no. 1-3 SPEC., 2003, pp. 447–53, [https://doi.org/10.1016/S0924-0136\(03\)00768-4](https://doi.org/10.1016/S0924-0136(03)00768-4).
- Pereira Bastos, Ricardo N., et al. "Enhancing Time Efficiency on Single Point Incremental Forming Processes." *International Journal of Material Forming*, vol. 9, no. 5, 2016, pp. 653–62, <https://doi.org/10.1007/s12289-015-1251-x>.
- Petek, Aleš, and Karl Kuzman. "Backward Hole-Flanging Technology Using an Incremental Approach." *Strojnikski Vestnik/Journal of Mechanical Engineering*, vol. 58, no. 2, 2012, pp. 73–80, <https://doi.org/10.5545/sv-jme.2011.194>.
- Qin, Qin, et al. "Control and Optimization of Bulge Defect in Incremental Forming of Cu-Al Bimetal." *International Journal of Material Forming*, vol. 14, no. 6, 2021, pp. 1243–58, <https://doi.org/10.1007/s12289-020-01605-5>.
- "Sheet Metal Fabrication Services: Global Strategic Business Report." *Global Industry Analyst, Inc.*, vol. 4, no. 1, 2023, <https://www.researchandmarkets.com/reports/5141380/>.
- Shim, Myoung Sup, and Jong Jin Park. "The Formability of Aluminum Sheet in Incremental Forming." *Journal of Materials Processing Technology*, vol. 113, no. 1–3, 2001, pp. 654–58, [https://doi.org/10.1016/S0924-0136\(01\)00679-3](https://doi.org/10.1016/S0924-0136(01)00679-3).
- Shrivastava, Parnika, and Puneet Tandon. "Microstructure and Texture Based Analysis of Forming Behavior and Deformation Mechanism of AA1050 Sheet during Single Point Incremental Forming." *Journal of Materials Processing Technology*, vol. 266, no.

- November 2018, 2019, pp. 292–310, <https://doi.org/10.1016/j.jmatprotec.2018.11.012>.
- Silva, M. B., N. Bay, et al. “Hole-Flanging by Single Point Incremental Forming.” *Materials Forming and Machining: Research and Development*, Elsevier Ltd., 2016, <https://doi.org/10.1016/B978-0-85709-483-4.00002-8>.
- Silva, M. B., T. M. Martinho, et al. “Incremental Forming of Hole-Flanges in Polymer Sheets.” *Materials and Manufacturing Processes*, vol. 28, no. 3, 2013, pp. 330–35, <https://doi.org/10.1080/10426914.2012.682488>.
- Silva, M. B., P. Teixeira, et al. “On the Formability of Hole-Flanging by Incremental Sheet Forming.” *Proceedings of the Institution of Mechanical Engineers, Part L: Journal of Materials: Design and Applications*, vol. 227, no. 2, 2013, pp. 91–99, <https://doi.org/10.1177/1464420712474210>.
- Silva, M. B., M. Skjoedt, et al. “Revisiting the Fundamentals of Single Point Incremental Forming by Means of Membrane Analysis.” *International Journal of Machine Tools and Manufacture*, vol. 48, no. 1, 2008, pp. 73–83, <https://doi.org/10.1016/j.ijmachtools.2007.07.004>.
- Silva, M. B., M. Skjoedr, et al. “Single-Point Incremental Forming and Formability-Failure Diagrams.” *Journal of Strain Analysis for Engineering Design*, vol. 43, no. 1, 2008, pp. 15–35, <https://doi.org/10.1243/03093247JSA340>.
- Skjoedt, M., N. Bay, et al. “Multi Stage Strategies for Single Point Incremental Forming of a Cup.” *International Journal of Material Forming*, vol. 1, no. SUPPL. 1, 2008, pp. 1199–202, <https://doi.org/10.1007/s12289-008-0156-3>.
- Skjoedt, M., M. B. Silva, et al. “Strategies and Limits in Multi-Stage Single-Point Incremental Forming.” *Journal of Strain Analysis for Engineering Design*, vol. 45, no. 1, 2010, pp. 33–44, <https://doi.org/10.1243/03093247JSA574>.
- Stachowicz, F. “Estimation of Hole-Flange Ability for Deep Drawing Steel Sheets.” *Archives of Civil and Mechanical Engineering*, vol. 8, no. 2, 2008, pp. 167–72, [https://doi.org/10.1016/S1644-9665\(12\)60203-9](https://doi.org/10.1016/S1644-9665(12)60203-9).
- Su, Chunjian, et al. “Effects of Forming Parameters on the Forming Limit of Single-Point Incremental Forming of Sheet Metal.” *International Journal of Advanced Manufacturing Technology*, vol. 113, no. 1–2, 2021, pp. 483–501, <https://doi.org/10.1007/s00170-020-06576-0>.
- Toros, Serkan, et al. “Review of Warm Forming of Aluminum-Magnesium Alloys.” *Journal of Materials Processing Technology*, vol. 207, no. 1–3, 2008, pp. 1–12, <https://doi.org/10.1016/j.jmatprotec.2008.03.057>.

- Vahdati, Mehdi, et al. "An Analytical Model to Reduce Spring-Back in Incremental Sheet Metal Forming (ISMF) Process." *Advanced Materials Research*, vol. 83–86, 2010, pp. 1113–20, <https://doi.org/10.4028/www.scientific.net/AMR.83-86.1113>.
- Voswinckel, Holger, et al. "Improving Geometrical Accuracy for Flanging by Incremental Sheet Metal Forming." *International Journal of Material Forming*, vol. 8, no. 3, 2015, pp. 391–99, <https://doi.org/10.1007/s12289-014-1182-y>.
- Yan, Zhou, et al. "Multistage Tool Path Optimisation of Single-Point Incremental Forming Process." *Materials*, vol. 14, no. 22, 2021, <https://doi.org/10.3390/ma14226794>.
- Yang, C., et al. "Dieless Incremental Hole-Flanging of Thin-Walled Tube for Producing Branched Tubing." *Journal of Materials Processing Technology*, vol. 214, no. 11, 2014, pp. 2461–67, <https://doi.org/10.1016/j.jmatprotec.2014.05.027>.
- Yoganjaneyulu, G., et al. "Investigation on the Fracture Behavior of Titanium Grade 2 Sheets by Using the Single Point Incremental Forming Process." *Journal of Manufacturing Processes*, vol. 35, no. June, 2018, pp. 197–204, <https://doi.org/10.1016/j.jmapro.2018.07.024>.
- Young, D., and J. Jeswiet. "Wall Thickness Variations in Single-Point Incremental Forming." *Proceedings of the Institution of Mechanical Engineers, Part B: Journal of Engineering Manufacture*, vol. 218, no. 11, 2004, pp. 1453–59, <https://doi.org/10.1243/0954405042418400>.
- Zhang, Huan, et al. "Dieless Double-Sided Incremental Hole-Flanging with Different Toolpath Strategies." *ASME 2016 11th International Manufacturing Science and Engineering Conference, MSEC 2016*, vol. 1, 2016, pp. 1–8, <https://doi.org/10.1115/MSEC20168829>.
- Zheng, Kailun, et al. "A Review on Forming Techniques for Manufacturing Lightweight Complex—Shaped Aluminium Panel Components." *International Journal of Lightweight Materials and Manufacture*, vol. 1, no. 2, 2018, pp. 55–80, <https://doi.org/10.1016/j.ijlmm.2018.03.006>.

Publications from this research

International Journal Publications

- Rudreshkumar Makwana, Bharat Modi, Kaushik Patel, Single-stage single point incremental square hole flanging of AA5052 material, *Materials and manufacturing Processes*, Vol.38, Issue-6, 680-691, 2023. DOI: [10.1080/10426914.2022.2136377](https://doi.org/10.1080/10426914.2022.2136377)
- Makwana,R., Modi, B., Patel, K., Experimental study on single point incremental hole flanging of Aluminium 5052 material, *Advances in Materials and Processing Technologies*, 2023. DOI: [10.1080/2374068X.2023.2280295](https://doi.org/10.1080/2374068X.2023.2280295)
- Makwana,R., Modi, B., Patel, K., In-process grain refinement on AA5052-H32 sheet metal in single-stage single point square hole flanging, *Manufacturing Letters*, Elsevier, Vol.35, 232-238, 2023.DOI: [10.1016/j.mfglet.2023.08.028](https://doi.org/10.1016/j.mfglet.2023.08.028)

Papers presented at International Conference

- Rudreshkumar Makwana, Bharat Modi, & Kaushik Patel, In-process grain refinement on AA5052-H32 sheet metal in single-stage single point square hole flanging, 51st SME North American Manufacturing Research Conference, Rutgers University, New Brunswick, New Jersey, USA, 12-16 June 2023.
- Rudresh Makwana, B.A.Modi, K.M.Patel, Single stage and Multi stage Hole Flanging using Single Point Incremental Forming, International Conference on Progressive Research in Industrial & Mechanical Engineering, NIT Patna, India, 5-7 August 2021.
- Rudreshkumar Makwana, Bharat Modi, Kaushik Patel, Effect of feed and step depth in hole flanging using single point incremental forming, International Conference on Advances in Physical Science and Materials, SNS College of Technology, Coimbatore, India, 13-14 August 2020. Published in *Journal of Physics: Conference Series*, Vol.1706, 2020.

- Rudresh Makwana, B.A.Modi, K.M.Patel, Experimental study on effect of tool diameter on thickness, height and geometric accuracy of flange in hole flanging using single point incremental forming, Nirma University International Conference on Engineering, Nirma University, Ahmedabad, Gujarat, India, 21-22 November 2019. Published in Technologies for Sustainable Development - Proceedings of the 7th Nirma University International Conference on Engineering, NUICONE 2019.